2019

School of Engineering
Howard College Campus
Durban

WET AND DRY DESULPHURIZATION TECHNOLOGIES: MODELLING AND SIMULATION

By:

Hiren Mavalall

MSc Chemical Engineering
2019

A dissertation submitted in the School of Engineering
University of Kwa-Zulu Natal
Durban
In the fulfilment of the requirements of the degree of Master of Science in Engineering

DECLARATION

The work presented in this dissertation was undertaken at the School of Engineering, University of KwaZulu-Natal, Howard College Campus in Durban, South Africa, from February 2018 until December 2019.

All work presented is this dissertation is original unless otherwise stated. It has neither in whole nor part been submitted previously to any other University or Institute as part of a degree.

I, Hiren Mavalall , declare that

1. The research reported in this thesis, except where otherwise indicated, is my original research.

2. This thesis has not been submitted for any degree or examination at any other university.

3. This thesis does not contain other persons‟ data, pictures, graphs or other information, unless specifically acknowledged as being sourced from other persons.

4. This thesis does not contain other persons' writing, unless specifically acknowledged as being sourced from other researchers. Where other written sources have been quoted, then:

a. Their words have been re-written but the general information attributed to them has been referenced

b. Where their exact words have been used, then their writing has been placed in italics and inside quotation marks, and referenced.

5. This thesis does not contain text, graphics or tables copied and pasted from the Internet, unless specifically acknowledged, and the source being detailed in the thesis and in the References sections.

_____

Hiren Mavalall

As the candidate’s supervisor hereby certify that I find this work to be suitable for submission for the degree of Master of Science in Chemical Engineering.

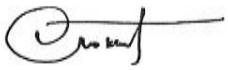

_____

Prof. David Lokhat

ACKNOWLEDGEMENTS

I would like to take this opportunity to acknowledge and show my deepest gratitude to the following who have all greatly contributed to the completion of this dissertation:

- Firstly, and fore mostly I would like to thank God and my family for giving me the strength, motivation and support to pursue my masters as well as in all other endeavours in life.
- My supervisors Prof David Lokhat, Prof Milan Carsky and Dr Suren Moodley for imparting on me their vast knowledge, support and guidance.
- Finally, to my close friends for their continued support and motivation throughout my life.

ABSTRACT

Energy demand continues to increase with population growth and economic development therefore numerous technologies have been proposed over the years to convert coal to electricity. Turbine cycles have received a great deal of interest in the last decade, especially the integration of the gasification with the gas turbine/steam turbine combined cycle (lGCC). The major components of a coal-based IGCC cycle are coal handling and gasification, sulphur removal, gas turbine cycle, steam turbine cycle. Sulphur removal processes are generally classified into amine absorption processes (wet-based systems), and hot desulphurization processes using metal oxide sorbents (dry-based systems). Amine absorption processes are proven commercially available technologies but are energy intensive. Hot desulphurization processes have a cost advantage over amine absorption processes, but the degree of long-term reliability is still to be proven. The main aim of this study was to compare the commercial operability and economic feasibility between an amine absorption process (using an MDEA-based amine solution) and two hot desulphurization processes (the first using a free zinc oxide sorbent and the second using a silica supported zinc oxide sorbent).

Aspen Plus simulation package was used to develop the simulation models. A coupled gasification and sulphur removal system was designed for each process. The gasifier model takes the processes of gasification into account i.e. coal drying, coal pyrolysis, char gasification and char combustion. A fluidized bed reactor was chosen to carry out the gasification due to its good temperature control. Fluidization behaviour and reaction kinetics for char gasification and combustion were included in the model. A coal flow rate of 84 tons/day was selected (a typical flowrate of coal processed in an industrial gasifier) with an operating pressure of 30 atm and 900°C. A built-in amine data package was used to calculate electrolyte capabilities and kinetic reactions in the liquid phase, of the amine absorption process. MDEA/H_2O was the amine solution used, due to its high affinity to sulphur compounds. This process required a pre-cooling and tar removal step prior to desulphurization and regeneration, and was achieved by a heat exchanger and a water spray tower respectively, at 30 atm. An absorber tower was used for desulphurization with operating temperatures between 40° and 60°C, and pressures around 55 atm. A distillation column was used for the regeneration process with operating temperatures between 110° and 120°C, and pressures around 1 atm. Multiple auxiliary units were set up along the process in order for process streams to meet process conditions. Pumps, compressors and turbines were added to cater for any pressure changes and heat exchangers along with its utility for any temperature changes. 10% of the regenerated amine solution was purged and remainder was recycled. For the hot desulphurization processes free zinc oxide sorbent and zinc oxide sorbent supported on silica. Fluidized bed reactor was chosen to carry out the desulphurization and regeneration, due to its good temperature control. Fluidization behaviour, elutriation characteristics and reaction kinetics from literature were incorporated in these models. Both the desulphurization and regeneration had an operating temperature of 550°C and 30 atm. Cyclone separators were used to separate solids carried over by the fluidized

beds. 90% of the regenerated free sorbent was purged and remainder was recycled, while 50% of the regenerated supported sorbent was purged with the remainder being recycled. A total annual cost (TAC) analysis was developed to compare the economic feasibility of each process, consisting of the capital and operating costs.

The intrinsic rate constant was regressed from available experimental data for the supported sorbent. The intrinsic kinetics obtained from the regression was found to be six orders of magnitude lower than that reported in the literature due to the low intrinsic rate constant extracted from the regression may not be a true reflection of the reaction behaviour, if mass transfer limitations through the product layer diffusion were significant. The intrinsic rate constant and product layer diffusion rate constant from literature were used to represented the kinetics for the supported sorbent in the simulation.

The hot desulphurization processes did not require pre-cooling or a tar removal step, which made these processes more thermally efficient than the amine absorption process. The amine absorption unit had a lower purge rate as compared to the hot desulphurization processes, resulting in better utilization of the Sulphur removing agent, therefore making the amine absorption process more effective. The capital cost for the amine absorption process was 105.657 mil.R, which was much higher than capital costs for the hot desulphurization processes (32.633 mil.R and 22.403 mil.R for the free sorbent and supported sorbent processes respectively), due to the larger amounts of process equipment required for amine absorption. The operating cost for the amine absorption process was R63.943 mil.R/yr, which was much higher than TAC for the hot desulphurization processes (R38.038 mil.R/yr and 24.991 mil.R/yr for the free sorbent and supported sorbent processes respectively). This was due to the utility requirements present in the amine absorption process. The TAC for the amine absorption process was R99.162 mil.R/yr, which was much higher than TAC for the hot desulphurization processes (R48.916 mil.R/yr and 32.459 mil.R/yr for the free sorbent and supported sorbent processes respectively). It was concluded that hot desulphurization processes are economically less intensive than amine absorption processes with lower waste production, and supported sorbents provide cheaper and more effective operation than free metal oxide sorbents.

Table of Contents

List of Figures

List of Tables

Nomenclature

Symbols	Definitions	Units
a	Shape-voidage factor	-
A	Cross-sectional area	m^2
Ar	Archimedes number	-
b	Shape-voidage factor	-
d_p	Particle diameter	m
D	Diameter	m
D_{AB}	Molecular diffusivity of reactant gas A in bulk gas B	m^2/s
D_e	Effective diffusion coefficient of gaseous reactant in the product layer	m^2/s
D_e*	Effective diffusion coefficient of gaseous reactant through micro-pores	m^2/s
D_K	Knudsen diffusivity	m^2/s
g	Gravitational acceleration	m^2/s
H	Height	m
k’	Intrinsic rate constant	m/s
k_i*	elutriation coefficient for particle size i	kg/m^3
K	Kinetic factor	1/s
K_i	Elutriation rate constant	1/m
M	Mass	kg
MM	Molar mass	g/mol
N	Number of holes per area of a distributor plate	$holes/m^2$
p	pitch	m
P	Pressure	atm
Q	Volumetric flowrate	m^3/s
r_{pore}	Radius of pores in porous solids	m
R	Radius	m
Re	Reynolds number	-
Sg	Specific surface area of porous particle	m^2/kg
t	Time	s
T	Temperature	°C
TAC	Total Annual Cost	R/yr
TDH	Transport disengagement height	m
U	Gas velocity	m/s
U_b	Bubble velocity	m/s
V	Volume	m^3
V_b	Bubble volume	m^3

Greek Symbols	Definitions	Units
ε	Particle porosity	-
ϵ	Bed voidage	-
ϵ_b	Voidage form by bubbles	-
$\emptyset$	Particle shape factor	-
ρ	Density	kg/m^3
μ	Viscosity	Pa.s
ν	atomic and structural diffusion volumes	-

Subscripts	Definitions
agg	Agglomerate particle
b	Bed
c	Unreacted core
e	Elutriated solids
f	freeboard
mf	Minimum fluidization
0	Original condition
p	Particle
t	terminal

CHAPTER 1: INTRODUCTION

1.1) Motivation of research

Non-renewable energy will not deplete anytime soon, but patterns of energy use may vary (Basu, 2006) as energy demand continues to increase. The two main objectives of commercial power generation cycles, are improved efficiency and low costs (Atimtay & Harrison, 1998). Coal gasification has the potential of generating power more efficiently while meeting environmental regulations (Mokatab, et al., 2019). Turbine cycles have generated a large amount of interest recently, especially the integration of the gasification with the gas turbine/steam turbine combined cycle (lGCC) (Atimtay & Harrison, 1998). A IGCC cycle consists of coal handling, gasification and sulphur removal, gas turbine cycle, steam turbine cycle.

Coal handling is required to deliver the coal in a suitable form for gasification and includes unit operations such as grinding, coal cleaning, size screening, slurry preparation and transportation. Once fed into the gasifier, the coal fuel is contacted with an oxidizing agent (oxygen or air, in addition to steam, to produce a gas product consisting of hydrogen, carbon monoxide, carbon dioxide, and steam. Minor concentrations of other components present in coal in, such as sulphur, will end up in the coal gas as contaminants in the form of hydrogen sulphide, H_2S as contaminants (Atimtay & Harrison, 1998). Most of the contaminants will have to be removed prior to combustion in the gas turbine or prior to venting of the flue gases to the atmosphere.

Sulphur removal processes are generally classified into amine absorption processes (wet-based systems), and hot desulphurization processes (dry-based systems). Amine absorption processes operate typically around 20-120 °C (Mokatab, et al., 2019). They are based on wet scrubbing, physical or chemical absorption processes. These are proven commercially available, but are energy intensive (Mokatab, et al., 2019). Hot desulphurization processes operate above 400°C, and are based mostly on fast chemical reactions (Atimtay & Harrison, 1998) but the degree of long-term reliability is still debateable (Basu, 2006). Hot desulphurization processes use metal oxide sorbents, particularly zinc-based sorbents, and have improved sulphur sorption capacity when dispersed over an inert support material (Basu, 2006). These technologies are under development or in the early stages of commercialization. A basic comparison study is proposed to access the commercial viability of hot desulphurization processes (utilizing free and supported sorbents) against an amine absorption process.

1.2) Research Question

This research project aims to answer the following question:

Is hot desulphurization processes a better commercial alternative to amine absorption processes for coal gas treatment processes?

1.3) Aims

The overall aim is modelling, simulation and cost comparison between wet and drying desulphurization technologies for coal gasification gas. The sub-aims of this study consist of:

- Comparing the commercial operability between an amine absorption process (using a MDEA-based amine solution) and two hot desulphurization processes (the first using a free zinc oxide sorbent and the second using a silica supported zinc oxide sorbent).
- Comparing the economic feasibility of the hot desulphurization processes to that of an amine absorption process.

1.4) Objectives

To achieve the aim above, the following objectives had to be met:

- Conduct an in-depth literature review on the current methods of gas treatment.
- Identify the types of process equipment and materials required, and the operating conditions of the processes
- Set up the coupled processes (gasification with either amine absorption, hot desulphurization using free zinc oxide sorbents or hot desulphurization using supported zinc oxide sorbents) on Aspen Plus simulation software package.
- Use an amine data package provided on Aspen Plus to set up the amine absorption process.
- Incorporate kinetics and fluidization behaviour in fluidized bed reactor designs for gasification and hot desulphurization.
- Simulate each process and optimize operating conditions and process equipment sizes to meet the sales gas specification of less than 4 ppm of H_2S (Mokatab, et al., 2019) in the gas .
- Develop a costing method to determine the total annual cost (TAC) for each process, using Aspen Process Economic Analyser (APEA)
- Analyse and compare the operability and the economic feasibility of each process on a commercial scale.

1.5) Structure of the Dissertation

This dissertation consists of seven chapters and is structured to provide a comprehensive understanding of the research conducted. The contents of the chapters are as follows:

Chapter 1 provides a brief background and motivation to the research. The research questions, aims and objectives are also mentioned.

Chapter 2 consists of literature reviewed that is relevant to the study. Insight is given into the process equipment and operating conditions required for the gasification process as well as the gas treatment processes. Waste treatment options are investigated as well as kinetic modelling of gas-solid reactions.

Chapter 3 describes the simulation setup on Aspen Plus. Process equipment, process materials, auxiliary units and utilities are specified along with a simulation approach for each process.

Chapter 4 describes the modelling and regression performed to extract kinetic data from experimental data for a silica supported zinc oxide sorbent.

Chapter 5 provides an in-depth analysis on the optimization of process conditions and equipment sizes. Provides a full summary of all optimized conditions and total annual cost (TAC) for each process.

Chapter 6 states the main conclusions drawn from the comparative study between each processes. It states to what extent the research questions, aims and objectives were met and provides possible recommendations for future research on this study.

CHAPTER 2: LITERATURE REVIEW AND THEORETICAL FRAMEWORK

2.1) Gasification

Gasification processes convert solids into synthesis gases. The concept has been present in the history of mankind. The first fuel used by humans was wood, and is still a common fuel source presently. In its early history, wood was used in buildings, and in the form of charcoal for industrial processes amongst other things. During 1620 to 1720, densely populated areas around the world suffered a shortage of wood (Higman & van der Burgt, 2011). The obvious solution was coal with production of coal really taking off during the latter part of the eighteenth century at the home of the industrial evolution, England. Towards the end of the eighteenth century, gas production from coal by pyrolysis was implemented on an industrial scale (Higman & van der Burgt, 2011).

Today gasification technology has gathered some serious interest in terms of electricity generation. With increasing energy demands, gasification is seen as a means of enhancing the environmental acceptability of coal as well as increasing the overall efficiency of the conversion of chemical energy in the coal into electricity (Higman & van der Burgt, 2011). The three major types of gasification processes under development are the moving bed gasifier, the fluidized bed gasifier, and the entrained gasifier. Key features for each type of gasifier are shown on Table 2-1.

Function	Moving bed		Fluidized bed	Entrained flow
	Dry ash	Slagging		
Capacity potential	Low	High	Intermediate	High
Ability to handle caking coals with pretreatment	Moderate	Shown at 300-ton-per-day scale	Shown on small scale	Excellent
Temperature of operation	1100°-450°C	1550°-450°C	870°-1050°C	1650°-950°C
Temperature of control	Poor	Poor	Good	Moderate
Refractory problems	Moderate	Poor	Moderate	Poor
By-product tar formation	Yes	Yes	Possibly	Probably not
Ability to extract ash low in carbon	Moderate	Good	Moderate	Good
Ability to consume fine carbon particles	Poor	Good	Probably poor	Good

Table 2-1: Key features of coal gasifiers (Higman & van der Burgt, 2011)

The gasification of coal can be described in four processes: coal drying, coal pyrolysis, char gasification, and char combustion (Basu, 2006). A schematic of this process is shown on Figure 2-1.

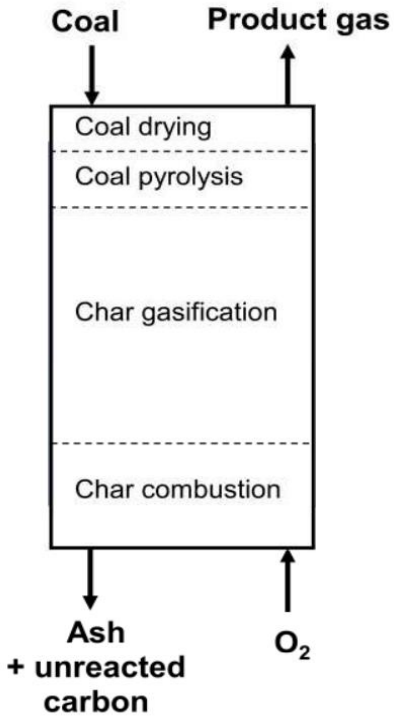

Figure 2-1: Schematic of coal gasification (Basu, 2006)

2.1.1) Coal Drying

The physical moisture present in the coal is released into the gas phase in the coal drying process as the temperature in the gasifier is usually high enough to vaporize all the bound water in the coal (Basu, 2006).

2.1.2) Coal Pyrolysis

Coal pyrolysis breaks down the coal to form CO, H_2, CO_2, H_2O, H_2S, N2, CH_4, tar, and char as shown by the following equation. Pyrolysis takes place at low temperatures (350-800°C) simultaneously with the heating up of coal particles (Basu, 2006)

$$Coal \rightarrow CO + H_2 + CO_2 + H_2O + H_2S + N_2 + CH_4 + tar + Char \qquad Eq\ (1)$$

2.1.3) Char gasification and Combustion

These are the reactions in the gasification of coal (Basu, 2006).

$$C + \frac{Z+2}{2Z+2} O_2 \rightarrow \frac{Z}{Z+1} CO + \frac{1}{Z+1} CO_2 \qquad Eq\ (2)$$

$$C + H_2O \rightarrow CO + H_2 \qquad Eq\ (3)$$

$$C + CO_2 \rightarrow 2CO \qquad Eq\ (4)$$

$$C + 2H_2 \rightarrow CH_4 \qquad Eq\ (5)$$

$$CO + H_2O \rightarrow CO_2 + H_2 \qquad Eq\ (6)$$

$$H_2 + 0.5O_2 \rightarrow H_2O \qquad Eq\ (7)$$

Where:

- $Z = \frac{[CO]}{[CO_2]} = 2500e^{-\frac{6249}{T}}$ *Eq (8)*

- [CO] and [CO_2] concentration of CO and CO_2 respectively
- T is the temperature in unit of K

2.2) Fluidization

Fluidization is a process in which solids behave as a fluid. Gas or liquid mediums are used to fluidize these solids. Fluidization on a commercial scale can be divided into two categories (Yang, 2003):

- physical operations, such as transportation, heating, absorption, mixing of fine powder, etc. and
- chemical operations, such as reactions of gases on solid sorbents and reactions of solids and gases

The fluidized bed is one of the best known contacting methods used in the processing industry (Yang, 2003). Its advantages include well mixing of particles, therefore producing negligible temperature gradients, and is employable on both large and small scale operations (Yang, 2003).

2.2.1) Fluidization Regimes

When solid particles are fluidized, the fluidized bed behaves differently as velocity, gas and solid properties are varied. There are a number of regimes of fluidization that present itself at various conditions and can be viewed on Figure 2-2.

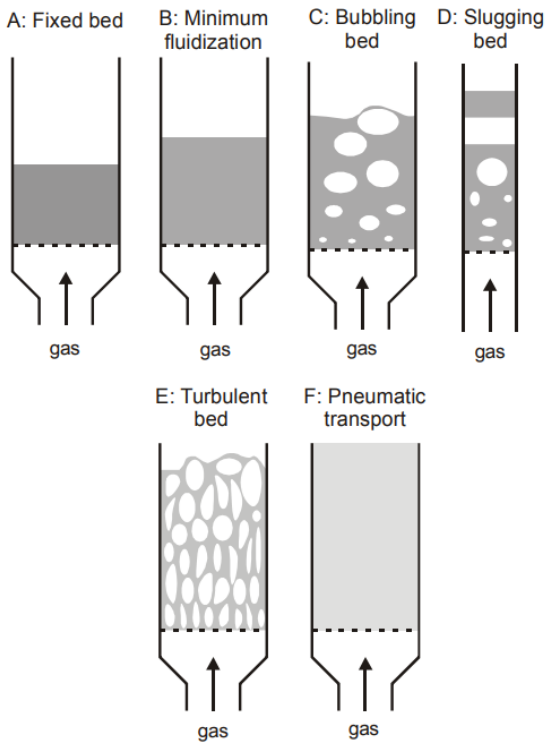

Figure 1-2: Representation of fluidized beds in different regimes (Yang, 2003)

When the flow of a gas passing through a bed of particles is increased continuously, a few particles vibrate, but still within the same height as the bed at rest. This is called a fixed bed as shown in CASE A of Figure 2-2. As the gas velocity increases, a point is reached where the drag force imparted by the upward moving gas equals the weight of the particles, and the voidage of the bed increases slightly: this is called minimum fluidization as shown in CASE B of Figure 2-2, resulting in a minimum fluidization velocity (U_{mf}). The formation of fluidization bubbles begins as the gas flow is further increased, creating a bubbling fluidized bed as shown in CASE C of Figure 2-2. As the velocity is increased further, the bubbles in the fluidized bed will grow and coalesce as they rise, therefore if the ratio of the bed height to the bed diameter high enough, the size of bubbles may become almost the same as diameter of the bed. This is called slugging as shown by CASE D of Figure 2-2. Fluidization at a high enough gas flow rate produces a superficial velocity that will exceed the terminal velocity of the particles, therefore the upper surface of the bed disappears and, instead of bubbles, one observes a turbulent motion of solid clusters and voids of gas of various sizes and shapes (Yang, 2003). Beds under these conditions are called turbulent beds as shown in CASE E of Figure 2-2. Eventually the fluidized bed becomes an entrained bed when the superficial velocity is increased further and amounts to pneumatic transport of solids as shown in CASE F of Figure 2-2.

2.2.2) Geldart's Classification of Particles

Not every particle can be fluidized. The behaviour of solid particles in fluidized beds depends mostly on their size and density (Yang, 2003). An observation by Geldart is shown on Figure 2-3.

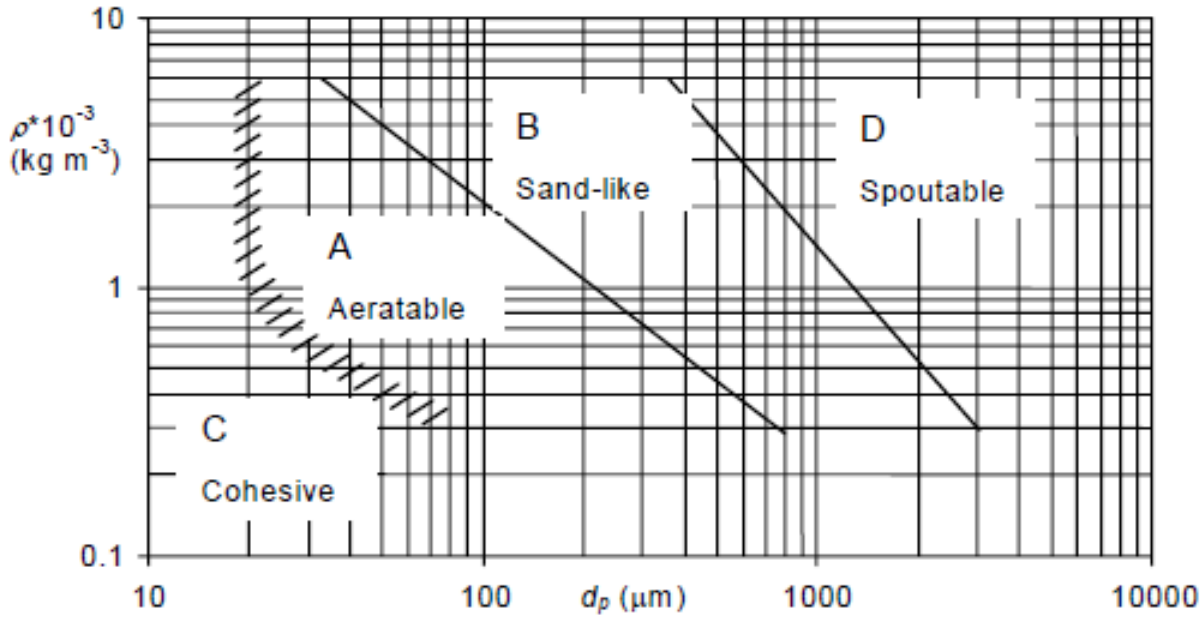

Figure 2-2:Diagram of the Geldart's classification of particles

The classification of each particle are categorized as follows:

- Group A particles have mean particle size less than 50 μm and/or low particle density (<~1.4 g/cm^3). These particles fluidize easily, under smooth fluidization at low superficial velocities without the formation of bubbles (Yang, 2003).
- Group B are sand-like particles with most particles of this group having size 150 μm to 500 μm and density from 1.4 to 4 g/cm^3 (Yang, 2003). Once the minimum fluidization velocity is exceeded for these particles, the excess gas appears in the form of bubbles. Glass beads and coarse sand are typically used group B materials (Yang, 2003).
- Group C materials are very fine powders and are difficult to fluidize due to interparticle forces being large (Yang, 2003). In small diameter beds, channelling occurs with the use of group C particles (Yang, 2003). Examples of group C materials are talc, flour and starch.
- Group D materials are very large or very dense (Yang, 2003). They are difficult to fluidize in deep beds. As velocity increases, a jet could be formed in the bed and material may blow out with the jet (Yang, 2003), therefore if the gas distribution is uneven, severe channelling can be expected (Yang, 2003). Roasting coffee beans, lead shot and some roasting metal ores are examples of group D materials.

2.2.3) Fluidization Velocity and Voidage

The superficial gas velocity at which the bed of powder is just fluidized, is normally called the minimum fluidization velocity (U_{mf}). The effect of pressure and temperature on the U_{mf}, are usually estimated using Ergun's equation or its variations, such as that suggested by (Wen & Yu, 1966) The Ergun equation can be written as:

$$\frac{\Delta P_B}{L} = \frac{150(1-\epsilon)^2 \mu U}{\emptyset^2 \epsilon^2 d_p^2} + \frac{1.75(1-\epsilon) U^2 \rho_f}{\epsilon^3 \emptyset d_p} \qquad \textit{Eq (9)}$$

At the minimum fluidization condition, the pressure drop across the bed can be expressed as

$$\frac{\Delta P}{L} = (\rho_s - \rho_f)(1 - \epsilon_{mf})g \qquad \textit{Eq (10)}$$

Equating these two equations, a quadratic equation with respect to $(Re)_{mf}$, can be obtained.

$$1.75a(Re)_{mf}^2 + 150b(Re)_{mf} = Ar \qquad \textit{Eq (11)}$$

Where

- $(Re)_{mf} = \frac{d_p U_{mf} \rho_f}{\mu}$ *Eq (12)*
- $Ar = \frac{d_p^3 \rho_f (\rho_s - \rho_f) g}{\mu^2}$ *Eq (13)*
- $a = \frac{1}{\emptyset \epsilon_{mf}^3}$; $b = \frac{1 - \epsilon_{mf}}{\emptyset^2 \epsilon_{mf}^3}$ *Eq (14)*

The shape-voidage factor has been approximated by (Wen & Yu, 1966) to be

$$a \cong 14 \, ; b \cong 11 \qquad \textit{Eq (15)}$$

The initial bubble size can be calculated from Davidson-Schuler equation for the volume of a bubble formed by a flowrate of gas q (m^3/s) (Geldart, 1985).

$$V_b = \frac{1.14 q^{1.2}}{g^{0.2}} \qquad \textit{Eq (16)}$$

Where:

- $q = \frac{U}{N}$ *Eq (17)*
- $V_b = \frac{\pi d_{eq}^3}{6}$ *Eq (18)*

U is the superficial gas velocity (m/s); N =number of holes per area (holes/m^2)

- *For square pitch* $N = \frac{1}{p^2}$ *Eq (19)*
- *For triangular pitch* $N = \frac{2}{\sqrt{3} p^2}$ *Eq (20)*

Where

- p = pitch (m), the distance between the centre of holes located on a distributor plate
- d_{eq} = the equivalent diameter of bubble with volume of V_b (m^3).

Therefore, d_{eq} (m) can be shown as;

$$d_{eq} = \sqrt[3]{\frac{6.84}{\pi}} \left(\frac{U^2}{g^{\frac{1}{3}} . N^2} \right)^{0.2} \qquad \textit{Eq (21)}$$

The rise velocity of a large spherical cap bubble can be described using a semi-empirical relation in terms of the volume-equivalent diameter as follows:

$$U_b = 0.711\sqrt{g.d_{eq}} \qquad \textit{Eq (22)}$$

A two-phase theory of fluidization was proposed by (Toomey & Johnstone, 1952) and developed by (Davidson & Harrison, 1963) in which it was assumed that all gas in excess of that needed for minimum fluidization passes through the bed as bubbles. The bubble flow rate in a fluidized bed Q_b (the rate at which bubble volume crosses any section A in the bed) is then approximately equal to the excess gas (Davidson & Harrison, 1963):

$$\frac{Q_b}{A} = U - U_{mf} \qquad \textit{Eq (23)}$$

With bubble velocity, the fraction of the bed area occupied by bubbles can be given as:

$$\epsilon_b = \frac{Q_b}{A.U_b} \qquad \textit{Eq (24)}$$

Assuming that the voidage of the particulate phase equals the voidage at minimum fluidization, hence all gas in excess of that needed for minimum fluidization passes through the bed as bubbles, the height (h) of the bed can be derived:

$$h - h_{mf} = \int_0^h \frac{Q_b}{A.U_b} dz \qquad \textit{Eq (25)}$$

If the assumption can be made that the bubble velocity is constant throughout the bed, the bed height can be estimated from:

$$\frac{h-h_{mf}}{h_{mf}} = \frac{U-U_{mf}}{U_b} \qquad \textit{Eq (26)}$$

The expansion of the bed then equals the fraction of the bed consisting of bubbles:

$$\epsilon_b = \frac{h-h_{mf}}{h} \qquad \textit{Eq (27)}$$

The mean voidage can then be calculated from

$$1 - \epsilon = (1 - \epsilon_b)(1 - \epsilon_{mf}) \qquad \textit{Eq (28)}$$

2.2.4) Transport Disengagement Height (TDH) and Elutriation

2.2.4.1) TDH

A fluidized bed can be divided into different vertical zones as shown in Firgure 4. The dense fluidized bed is found at the bottom and the freeboard above that (Yang, 2003). The main objective of the freeboard is to prevent large amounts of the bed material from being carried out by the gas. Experimental observations show that above the dense bed, the solids holdup gradually decreases until it becomes constant (Yang, 2003). The distance between this point and the surface of the dense fluidized

bed is called the Transport Disengagement Height (TDH).

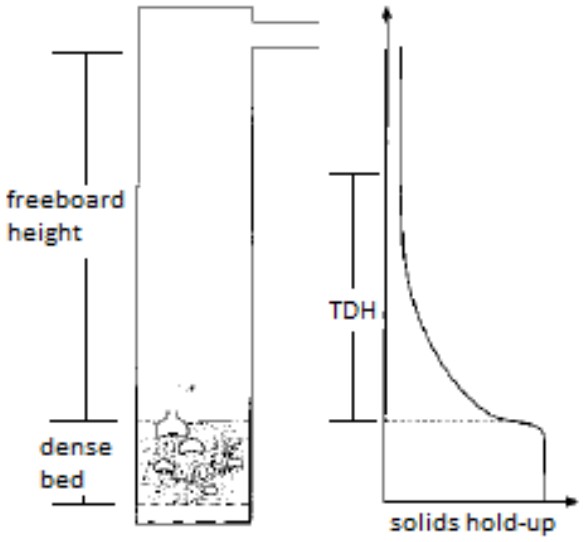

Figure 2-3: Schematic of a fluidized bed

TDH is an important design parameter for the design of a fluidized bed vessel. To reduce the carryover from a fluidized bed, the freeboard should have a height of at least the TDH (Yang, 2003). On the other hand, there is no additional advantage to increasing the height of the vessel beyond the TDH (Yang, 2003). There is no commonly accepted method for the calculation of the TDH, but there are several empirical correlations. Some of these correlations are found on Table 2-2.

Correlations for TDH	Reference
$TDH = 0.85U^{1.2}(7.33 - 1.2\log U)$	(Chan & Knowlton, 1984)
$TDH = 1000\frac{U^2}{g}$	(Fournol, et al., 1973)
$TDH = 18.2d_b$	(George & Grace, 1978)
$TDH = 13.8d_b$	(Fung & Hamdullahpur, 1993)

Table 2-2: TDH correlations

2.2.4.2) Elutriation

In fluidized beds the fluidizing gas velocity often exceeds the terminal velocity of the smaller particles (Yang, 2003). This results in elutriation of these fines from the bed even for a freeboard equal or higher than the TDH (Yang, 2003). The mass elutriated (M_{ie}) for a particular particle size and assuming no attrition or agglomeration of particles, can be expressed as follows (Yang, 2003).

$$M_{ie} = M_{io}(1 - e^{-K_i t}) \qquad \textit{Eq (29)}$$

Where M_{io} = mass of particle originally in the bed (kg); t = time; Ki = elutriation rate constant for particles of size i, and can be expressed as follows.

$$K_i = \frac{k_i^* A}{M_{io}} \qquad \textit{Eq (30)}$$

Where k_i*= elutriation coefficient; A = the cross-sectional area of the bed;

A correlation for the elutriation coefficient accounting for all sizes and densities of particles can be shown as

$$k_i^* = 0.011\rho_{si}\left(1 - \frac{U_{ti}}{U}\right)^2; \qquad U_{ti} < U \qquad \textit{Eq (31)}$$

$$k_i^* = 0; \qquad U_{ti} \geq U \qquad \textit{Eq (32)}$$

Where U_{ti} = terminal velocity of particle of size i; ρ_{si} = density of particle of size i. The terminal velocity can be expressed as

$$U_{ti} = \frac{0.153 g^{0.71} d_{pi}^{1.14} \left(\rho_{si} - \rho_f\right)^{0.71}}{\rho_f^{0.29} \mu^{0.43}} \qquad \textit{Eq (33)}$$

2.3) Gas Treatment

Synthesis Gas is made up of methane and light hydrocarbons but also contains minor amounts of acid gases (hydrogen sulfide (H_2S) and carbon dioxide (CO_2)) (Mokatab, et al., 2019). Synthesis gas with H_2S is called sour gas and without H_2S is called sweet gas (Mokatab, et al., 2019). Corrosion to gas processing equipment and pipelines can occur in the presence of sour gases. The main challenge in gas treatment is to remove sulphur components from sour gas to meet stringent emission standards. H_2S must be removed to meet the sales gas specification of 4 ppm (Mokatab, et al., 2019).

There are two types of sulphur removal processes i.e. dry and wet based processes. Wet methods are based on the removal of sour gases by physical absorption using physical solvents toward sour gases or by chemical reaction with the sour gases using a chemical alkaline solvent (alkanilamines) (Mokatab, et al., 2019). Dry based methods use either a physical-chemical phenomenon, in which impurities of the gas is trapped and removed physically or chemically by the surface of a selective solid, such as metal oxides (Mokatab, et al., 2019).

2.3.1) Wet based Sour Gas Removal

2.3.1.1) Alkanolamines

The common wet based methods for gas treating processes are the use of various alkanilamines, as they are well suited for application where low sour gas contents are required on treated gas (Mokatab, et al., 2019). In their earlier applications, monoethanolamine (MEA), and diethanolamine (DEA) were the common commercial amines as other amines such as diglycolamine (DGA) and diisopropanolamine (DIPA) gained commercial recognition later. In recent years, various methyldiethanolamine (MDEA) and specialty solvent blends were developed which takes advantage of the low energy characteristics of MDEA (Mokatab, et al., 2019).

These amines are compounds formed from ammonia (NH_3) by replacing one or more of the hydrogen atoms with another hydrocarbon group (Mokatab, et al., 2019) are categorized as primary, secondary

and tertiary, depending upon the degree of substitution of hydrogen atoms by organic groups (Mokatab, et al., 2019).

MDEA, a tertiary amine, is the most widely used gas treating agent today. Unlike primary and secondary amines, MDEA barely reacts with CO_2 (Mokatab, et al., 2019). This allows MDEA to selectively remove H_2S when treating a gas stream containing both H_2S and CO_2. Other advantages of a MDEA solvent over other solvents include low vapour pressure and solution losses, lower energy for solvent regeneration, low corrosiveness and resistance to degradation, therefore has greater multi-cycle capacity (Mokatab, et al., 2019). However, MDEA processes would require low absorption temperature to meet low H_2S specifications (Mokatab, et al., 2019).

2.3.1.2) Amine Process Description

The basic flow scheme of amine absorption processes has remained unchanged throughout the years. Typically, sour gas is fed to the amine absorber where the sulphur gas content is removed by an aqueous amine solution, producing a rich amine at the bottom and sweet gas from the top. This process occurs at pressures around 55 bar and temperatures between 40°C and 60°C (Mokatab, et al., 2019). The rich amine is brought down to atmospheric pressure and is heated before entering the regenerator (Mokatab, et al., 2019). The regenerator is a stripper/distillation column that operates at around atmospheric pressure and temperatures ranging from 80°C to temperatures less than 120°C (Mokatab, et al., 2019), producing a lean amine and a high sulphur gas. The lean amine is then cooled and pumped back to the absorber and the high sulphur gas is sent for further treating. A process flow schematic is shown on Figure 2-5.

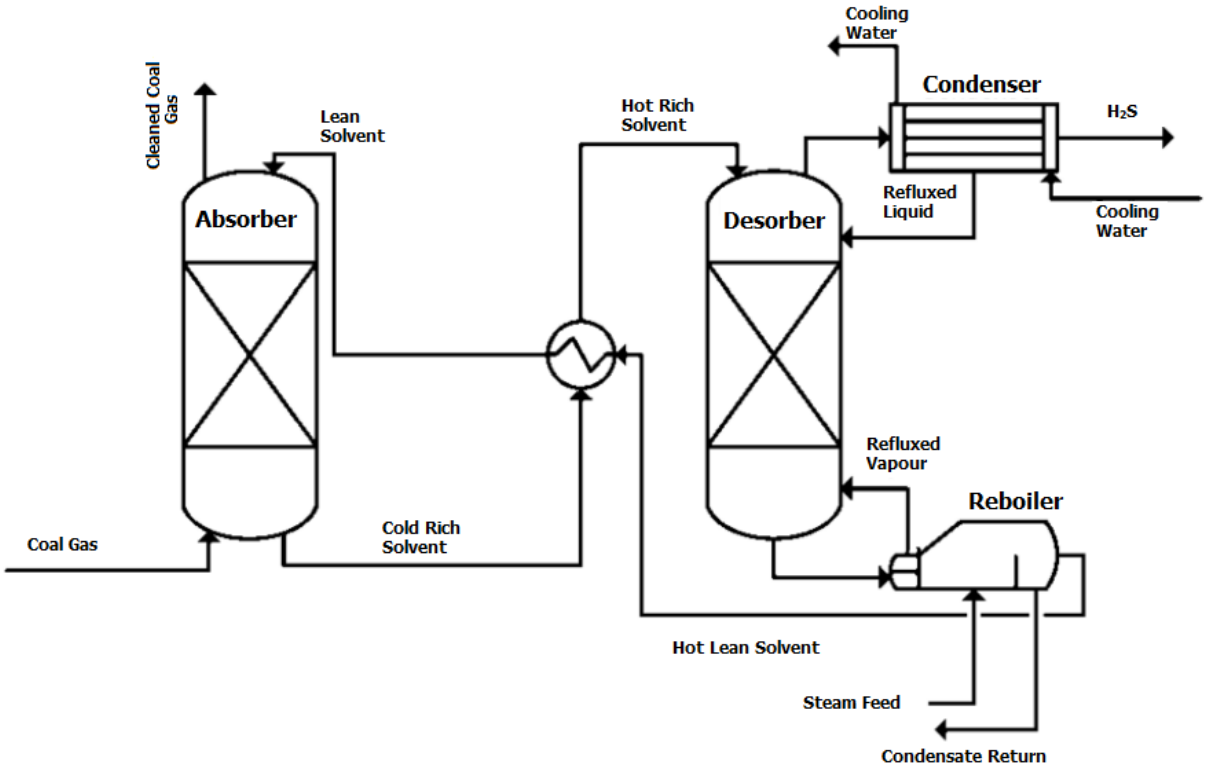

Figure 2-4: Schematic of an amine absorption process (Mokatab, et al., 2019)

2.3.2.3) Tar removal

Tar is formed as a by-product of the gasification process and mainly takes place on the pyrolysis stage (Nicolaou, 2016). Tar can defined as organic compounds produced under thermal or partial oxidation which are assumed aromatic, or as a mixture of condensable hydrocarbons which include single ring aromatics to PAHs (Nicolaou, 2016). Tar was defined as hydrocarbons with molecular weight around benzene (C6H6) (Bergman, et al., 2002). Tar removal methods separate into wet and dry cleaning techniques

2.3.2.3.1) Dry Cleaning Methods

These methods include catalytic cracking, thermal cracking and plasma cracking technologies that operate at high temperatures (Nicolaou, 2016). Greater process efficiencies are achieved are a pre-cooling stage of the synthesis gas is not required as these processes rely on cracking of the heavy hydrocarbon instead of using a liquid removal agent (Nicolaou, 2016).

2.3.2.3.2) Wet Cleaning Methods

Wet cleaning technologies are the most effective than dry cleaning methods and are therefore more commercially developed (Nicolaou, 2016). These methods apply the use of liquid scrubbers which have been used commercially for longer periods of time, as they provide easier ways to remove contaminants in the synthesis gas. (Nicolaou, 2016). Wet scrubbing technologies commonly used are; spray scrubbers, wet dynamic scrubbers, cyclonic spray scrubbers, impactor scrubbers, venturi scrubbers, and electrostatic scrubbers. A schematic for the above mentioned technologies are shown on Figure 2-6.

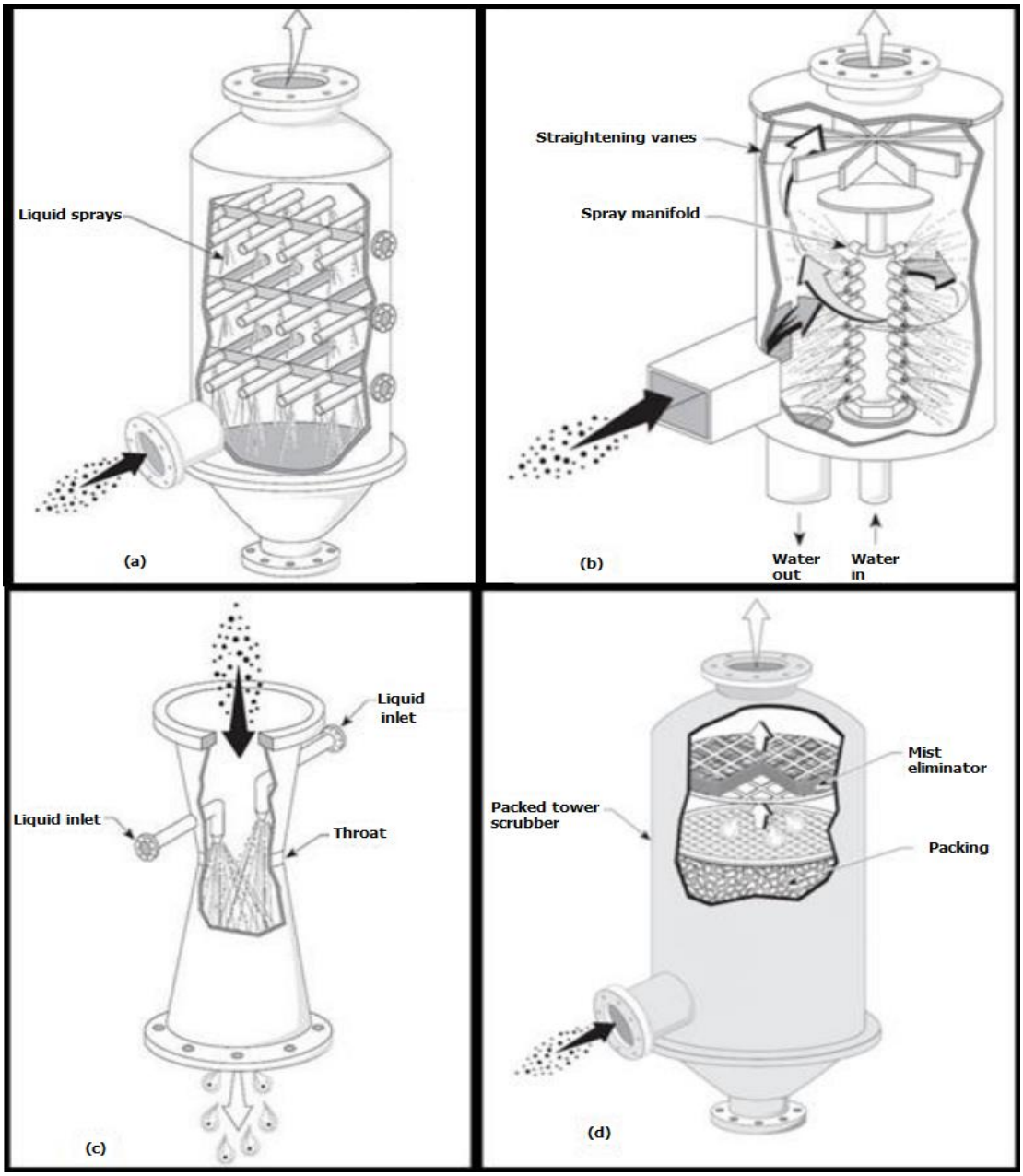

Figure 2-5: (a): Spray tower-(b): Cyclone Spray Chamber-(c): Venturi scrubber-(d): Packed bed scrubber (Nicolaou, 2016)

2.3.2) Dry based Sour Gas Removal

2.3.2.1) Metal oxides and reactions

Dry based processes meet sulphur specifications by removing a small quantity of H_2S from gas stream (Atimtay & Harrison, 1998). The process relies on the reaction of a metal oxide sorbent with H_2S to form a metal sulphide compound. The metal oxides can be regenerated with oxygen or air, producing the waste product (Atimtay & Harrison, 1998). These are high temperature processes that operate at temperatures above 300°C (Atimtay & Harrison, 1998), therefore the stability and selectivity of these sorbents are the main requirements. In general, the following reaction should be favourable:

$$MeO(s) + H_2S(g) \leftrightarrow MeS(s) + H_2O(g) \qquad Eq\ (34)$$

Where Me refers to any metal. Multiple researchers determined that Ba, Ca, Co, Cu, Fe, Mn, Mo, Sr, W, V, and Zn are thermodynamically feasible candidates for metal oxides sorbents and can be used in high temperature removal of acid gases. (Atimtay & Harrison, 1998). Metal oxides have generated great interest for sulphur removal as they possess a higher sorption capacity, ability to decrease H_2S concentrations to a lower level, better (thermo-) stability and less deactivation (Atimtay & Harrison, 1998).

Regeneration process is an oxidation reaction in which a sulphur atom is exchanged with an oxygen atom. Air is the most commonly used regenerating agent and is a very exothermic reaction (Atimtay & Harrison, 1998). The reaction can be seen below

$$MeS(s) + 1.5O_2(g) \leftrightarrow MeO(s) + SO_2(g) \qquad \textit{Eq (35)}$$

Metal oxides have received much attention as sorbents over the past years because of their desirable properties i.e. high sulphur capacity, ability to remove H_2S from coal derived fuel gas to levels of a few ppm, and the feasibility of regeneration with air (Atimtay & Harrison, 1998). Some of the most common sorbents are based on iron and zinc oxides, and are usually supported on other inert carriers such as zeolites (alumina or silica) to provide greater stability of sorbent (Atimtay & Harrison, 1998)

2.3.2.2) Sorbent Support

The main reasons for a the use of a sorbent support are stability of the sorbent phase, e.g., stabilization of small metal particles, as well as cost, i.e., dilution of an expensive sorbent component (Bailie, et al., 2001). The support allows for the dispersion of the active sorbent component (Bailie, et al., 2001). Zeolites are excellent sorbent supports due to the regularity of their pore structure, stability and high surface area. Due to well-defined pore sizes, theses sorbents can impose selectivity on the reaction products. This is done by restricting access of reactants to the active site, the formation of certain transition states, or the egress of certain products (Bailie, et al., 2001).

Zeolite frameworks are negatively charged, and are balanced by the presence of extra-framework cations such as Na+ or H+ (Bailie, et al., 2001). The cationic sites in zeolites can be substituted with metal cations, thus introducing the sorbent material into the structure. Further treatment is required to produce an active sorbent (Bailie, et al., 2001) therefore calcination and reduction are carried out on the metal cations to form active sites dispersed on the support (Bailie, et al., 2001), making zeolites a good option as supports for metal oxides.

The two main methods for introducing metal cations into zeolites are ion exchange and the incipient wetness technique (Bailie, et al., 2001). The treatment steps in these techniques play a vital role in determining the structure of the sorbent produced (Bailie, et al., 2001). The advantage of zeolites, is its ability to isolate metal atoms in the pores. This prevents sintering of the metal atoms, and would reduce the effective surface area during operation at high temperatures (Bailie, et al., 2001).

2.3.2.3) Gas-cleaning and gas-solid separation technologies

The necessity of for gas-cleaning is normally due to either technological requirements of a process (the gas or the dust, or both, are valuable or needed for further process) or environmental requirements when cleaning of effluents is needed to prevent outdoor or indoor air pollution (or explosion risks). Quite often, the two purposes of gas cleaning are combined because by cleaning the gases for environmental reasons a valuable product is recovered and that may at least partly offset the costs of dust control (Svarovsky, 1981).

Forces are applied to the particles in order to bring them to a collecting surface (Svarovsky, 1981). The principles of particle separation are usually classified according to the nature of the forces involved (Svarovsky, 1981). The forces may be:

- external forces due to fields of acceleration which are external to the gaseous suspension, such as gravity, electrostatic or magnetic forces; or
- internal forces due to fields or effects which take place within the suspension itself, e.g. inertial or centrifugal forces, diffusion, coagulation, electrostatic effects of charged particles, etc.

Gas-solid separation equipment generally combines two or more of these principles in one unit; the classification of equipment therefore does not necessarily follow the same pattern. The most common classification are split into four groups (Svarovsky, 1981), as follows:

1. aero-mechanical dry separators (with gravity and/or inertial effects prevailing)
2. aero-mechanical wet separators (scrubbers) (making use of diffusional and inertial effects)
3. electrostatic precipitators (depending on electrostatic and gravity forces)
4. filters (using inertial and diffusional effects)

Many gas-cleaning systems combine two or more of the above groups together either by using different equipment in series or by combining these in a single unit.

2.3.2.3.1) Aero-mechanical dry separators

The different types of gas cleaners in this category are shown below:

- Settling chambers: Settling chambers represent the simplest and often the cheapest way of removing coarse particles from gas streams (Svarovsky, 1981). The gas stream is allowed to expand into a large chamber where the gas velocity drops, thus giving time for the large particles to settle into the hoppers underneath (Svarovsky, 1981).
- Inertial separators: A sudden change of direction of gas flow caused by a baffle or a louvre is utilized in inertial separators; particles, due to their inertia, continue to move in the original direction and separate from the main gas stream (Svarovsky, 1981). Cyclones: Cyclones are now used in many different fields of technology, but are generally used in gas cleaning to separate of relatively coarse dusts (Svarovsky, 1981). The advantages of the use of cyclones include low running costs, relatively low capital cost (simple construction), reliability in use

and suitability for higher temperatures (Svarovsky, 1981). The inlet gas is brought tangentially into a cylindrical section and a strong vortex is created inside the cyclone body. Particles in the flow are subjected to centrifugal forces which move them radially out wards, towards the inside cyclone surface on which the solids separate.

- Fan collectors: fan collector is a combination of an induced-draught fan and a dust collector; they are sometimes referred to as "mechanical cyclones" because the vortex is here produced by a power-driven motor (Svarovsky, 1981). In use, the fan collectors usually combine separation and conveying. The dust-laden gas enters through the centre of the motor; on passage through the motor, the dust is centrifuged to the periphery of the spiral compartment where it is skimmed off with a small quantity of gas and passed into either a hopper or a secondary separator, which is almost invariably a cyclone (Svarovsky, 1981).

2.3.2.3.2) Aero-mechanical wet separators

The separation of particles from gases is achieved using scrubbers mixed with a liquid solvent, usually water (Svarovsky, 1981). Water being present plays a vital role in particle collection. Particles separate on collecting surfaces, in the form of water droplets or the surface of the scrubber therefore, particle re-entrainment is virtually eliminated, making scrubbers more efficient than the dry separators (Svarovsky, 1981).

2.3.2.3.3) Electrostatic precipitators

Electrostatic forces are applied to remove the solid or liquid particles trapped in a gas stream. Gas passes through an intense electrostatic field creating separation forces that are applied to the particles (Svarovsky, 1981). The disadvantages and limitations of electrostatic precipitators which stem from the fundamental principles of particle charging, particle migration velocities and particle behaviour on and after their arrival at the collecting electrodes (Svarovsky, 1981).

2.3.2.3.4) Filters

Gas filtration may be defined as the separation of particles from gases by passing a gaseous suspension through a porous, permeable medium which retains the particles (Svarovsky, 1981). Depending on where in the medium the particle will separate as follows:

- dust cake filtration: if the particles are deposited in the form of a cake on the upstream side of a relatively thin filter medium (in single-layer filters);
- depth filtration: in which particle deposition takes place inside the medium (in packed filters).

2.3.3) Sulphur recovery and handling

Acid gas is a mixture of hydrogen sulphide (H_2S), with minor concentrations of hydrocarbon gases and water vapour and is the by-product of these regeneration processes (Mokatab, et al., 2019). In the past, acid gases would be flared /incinerated, but now small amounts of acid gases is generally unacceptable due to growing environmental limitations (Mokatab, et al., 2019), which means that acid gas must be processed further or stored downhole.

Elemental sulphur is relatively nontoxic and chemically inert as compared to the H_2S. It can be stored, handled, transported in bulk and can be stockpiles when demands are low. (Mokatab, et al., 2019). The main use of elemental sulphur is for the production of sulphuric acid, to manufacture phosphate fertilizer (Mokatab, et al., 2019). Sulphur vapour exists as S_2, S_6, and S_8, with S_8 vapours being dominant at low temperatures, therefore as the temperature rises, S_8 is converted to S_6 and S_2 (Mokatab, et al., 2019).

2.3.3.1) Sulphur Recovery

Sulphur recovery refers to the conversion of H_2S to elemental sulphur. The original sulphur recovery process (Claus Process) was developed to recover sulphur as a by-product in the production of soda (Na_2CO_3) where elemental sulphur was produced by the partial oxidation of H_2S over a preheated sorbent bed (Mokatab, et al., 2019). This is described by the following exothermic reaction:

$$H_2S + \frac{3}{2}O \rightarrow \frac{1}{8}S_8 + H_2O \qquad \textit{Eq (36)}$$

The lack of temperature control was caused by the exothermic nature of the reaction therefore placing great limitations on the process (Mokatab, et al., 2019). A modification to the Claus process was made where The oxidation of 1/3 of the hydrogen sulphide to sulphur dioxide was carried out in a boiler, and the remaining 2/3 hydrogen sulphide reacted with the sulphur dioxide over a sorbent and has become the standard sulphur recovery technology (Mokatab, et al., 2019)

2.3.3.1.1) Modified Claus Process

The overall reaction in the modified Claus process, is carried out in two stages. In the first stage (thermal section), enough air is added to oxidize only one-third of the incoming H_2S to SO_2. This reaction is highly exothermic and is not limited by equilibrium.

$$H_2S + \frac{3}{2}O_2 \rightarrow \frac{1}{8}S_8 + H_2O \qquad \textit{Eq (37)}$$

In the reaction furnace the unburned H_2S in the acid gas reacts with the produced SO_2 to yield elemental sulphur vapour. This reaction is referred to as the Claus reaction and is shown below. This reaction is endothermic and is limited by equilibrium.

$$SO_2 + 2H_2S \leftrightarrow \frac{3}{2}S_2 + 2H_2O \qquad Eq\ (38)$$

The second stage was a catalytic step and contains three processes. The first is the preheater step which raises the temperature of the gas to avoid condensation of sulphur vapour in the pores of the sorbent. In the second step the hydrogen sulphide and sulphur dioxide are reacted over an activated alumina sorbent in a series of catalytic reactors. These reactions are both exothermic (Mokatab, et al., 2019), and are represented as follows:

$$2H_2S + SO_2 \leftrightarrow \frac{3}{6}S_6 + 2H_2O \qquad Eq\ (39)$$

$$2H_2S + SO_2 \leftrightarrow \frac{3}{8}S_8 + 2H_2O \qquad Eq\ (40)$$

In the third step a condenser is used to remove liquid sulphur therefore shifting the equilibrium so that further reaction may take place in the next catalytic reactor (Mokatab, et al., 2019). A typical modified Claus process flow schematic is shown on Figure 2-7.

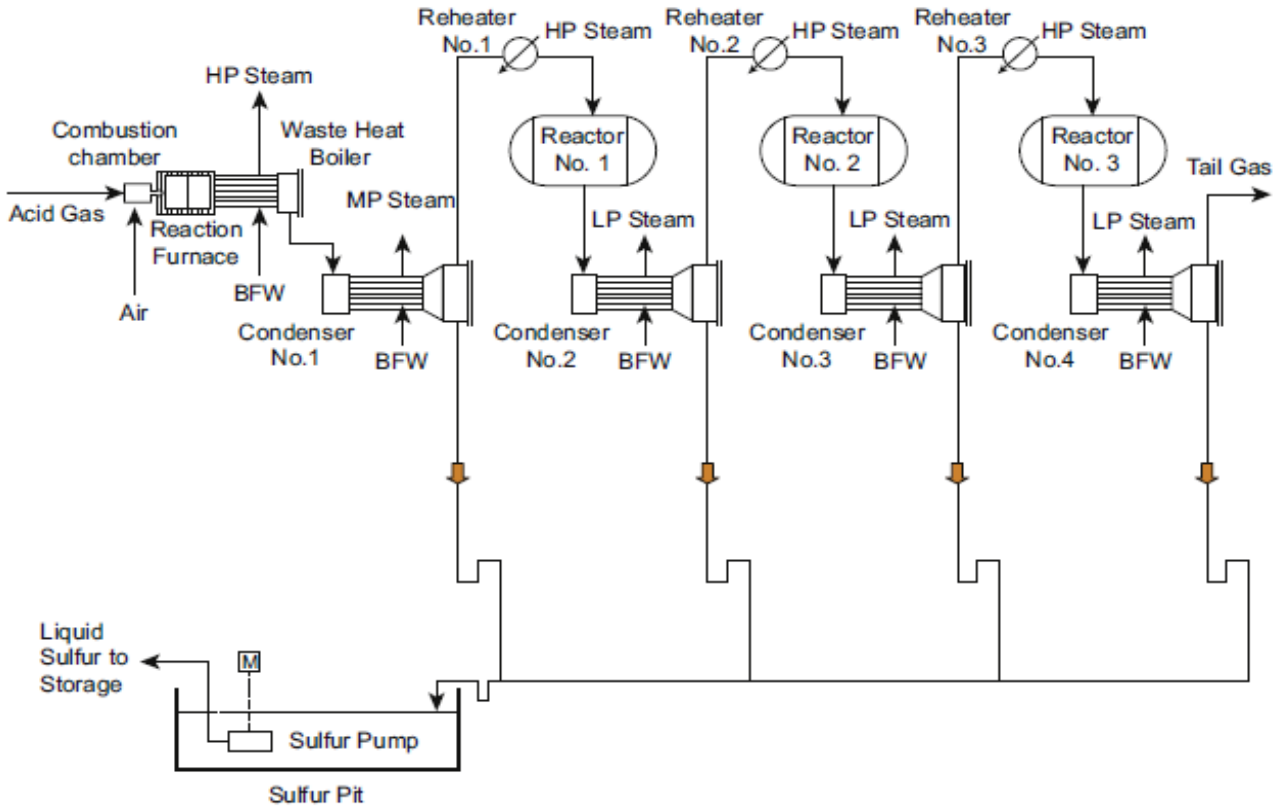

Figure 2-6: Schematic of a Modified Claus process (Mokatab, et al., 2019)

2.3.3.2) Tail Gas Clean-up

Gas from a Claus unit generally contains small amounts of sulphur compounds therefore leading to the development of Claus tail gas clean-up processes in order to remove the residual sulphur species to

meet emissions regulations (Mokatab, et al., 2019). Tail gas clean-up processes can be categorized into three groups as follows:

- Reduction processes, which produces H_2S from sulphur compounds present in the tail gas. This is achieved by hydrogenation (Mokatab, et al., 2019).
- SO_2 scrubbing makes use of an amine-based solution to covert the Claus tail gas streams into a SO_2 rich stream (Mokatab, et al., 2019). The enriched SO_2 stream may be recycled to the Claus unit for conversion to elemental sulphur, if the emissions limit is not met (Mokatab, et al., 2019).
- Sulphur recovery can be increased by adding multiple catalytic stages.

2.3.3.3) Sulphur Storage and Handling

Liquid sulphur can be shipped by tank trucks, by railcars or by pipeline. The solid forms are preferred as it provides greater ease of handling and transporting (Mokatab, et al., 2019). A short-term storage block could be utilized during emergencies and sulphur residue from these blocks can be melted down and recovered (Mokatab, et al., 2019)

2.4) Water Treatment Technologies

Water treatment technologies can be categorized into three groups: Physical Methods, Chemical Methods, and Energy Intensive Methods (Cheremisinoff, 2002). In physical methods of wastewater filtration plays a dominant role (Cheremisinoff, 2002). Chemical methods rely on the chemical interactions of the contaminants, and the application of chemicals that either aid in the separation of contaminants from water, or assist in the destruction or neutralization of harmful effects associated with contaminants (Cheremisinoff, 2002). Energy intensive technologies include electrochemical techniques, which are applied to drinking water applications (Cheremisinoff, 2002).

2.5) Gas solid modelling

2.5.1) Selection of a model

Every conceptual picture or model for reaction processes comes with its mathematical rate equation. If a model is chosen then the rate equation must be excepted, and vice versa, therefore if a model represents the actual behaviour of the system, then its rate expression will predict the actual kinetics more accurately, and a model will be useless if differs widely from reality.

The solid in question are free metal oxides and supported metal oxides. They are generally found in powdered form and are the primary reactant. They can be compressed into various shapes, examples include cylindrical and spherical pellets. These pellets can be described as porous solids. Taking the abovementioned comments into consideration, a rate model can be described as follows

2.5.2) Reaction Rate Expression

A model consisting of two parts can be used. The first that is adopted is the shrinking-core model. Figure 2-8 gives a visual representation of the model.

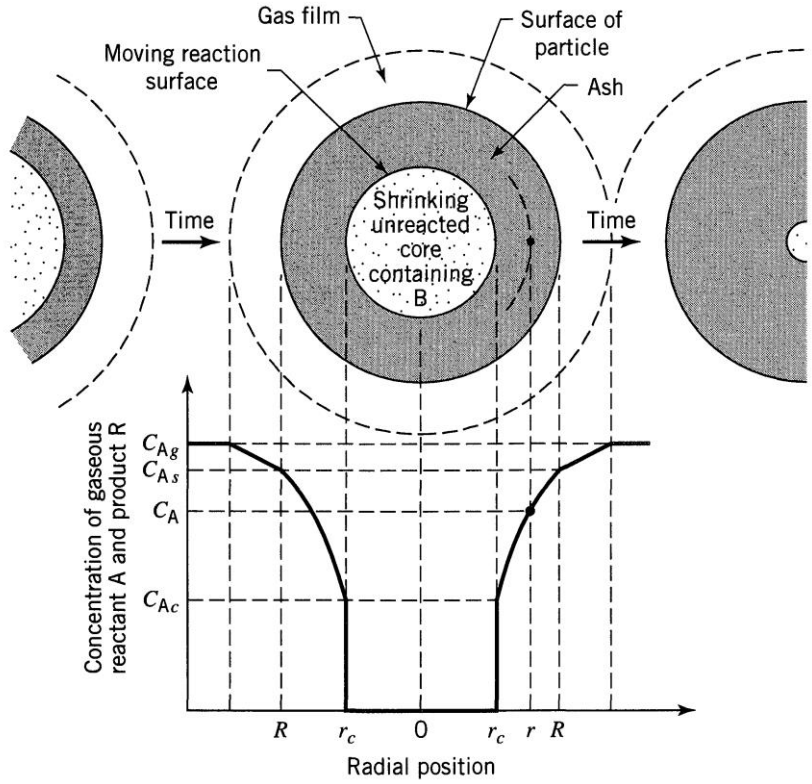

Figure2- 7: Representation of Shrinking Core Model (Levenspiel, 1999)

The reaction occurs first at the outer layer of the particle. The reaction zone then moves further into the solid, producing a solid product layer (Levenspiel, 1999). This model was first developed by (Yagi & Kunii, 1961), who visualised the steps occurring in succession during reaction.

- Diffusion of gaseous reactant A through the film surrounding the particle to the surface of the solid.
- Penetration and diffusion of A through the blanket of ash to the surface of the unreacted core.
- Reaction of gaseous A with solid at this reaction surface.
- Diffusion of gaseous products through the ash back to the exterior surface of the solid.
- Diffusion of gaseous products through the gas film back into the main body of fluid.

These individual resistances are combined producing the following rate expression.

$$-r_A = -\frac{1}{S_{ex}}\frac{dN_B}{dt} = \frac{C_A}{\frac{1}{k_g}+\frac{R(R-r_c)}{r_c D_e}+\frac{R^2}{r_c^2 k'}} \qquad \textit{Eq (41)}$$

Where C_A= Concentration of reactant gas A; k_g = mass transfer coefficient associated with diffusion through the gas film; D_e = effective diffusion coefficient of gaseous reactant in the product layer; k' = first-order intrinsic rate constant; R = radius of solid reactant particle; r_c = unreacted core radius;
The kinetic factor (K) is then derived as follows:

$$K = \frac{1}{\frac{1}{k_g} + \frac{R(R-r_c)}{r_c D_e} + \frac{R^2}{r_c^2 k'}} \qquad \textit{Eq (42)}$$

2.5.3) Effectiveness factor

The above model describes the ideal case of a gas-solid reaction. The physical structure of the solid material is an important factor with regards to the transport of gaseous material from the bulk gas to the reaction surface. The structure of a solid reactant can be classified non-porous and porous solids (Hayes & Kolaczkowski, 1998). Porous solids have micro-pores that have that creates micro tunnels within solid, which provide pathways for gas to pass through and exposes it to a larger surface area for reactions to occur (Hayes & Kolaczkowski, 1998). The diffusion of gas through these pores slows down the overall reaction rate (Hayes & Kolaczkowski, 1998). Depending on the structural properties of the solid, an effectiveness factor can be calculated to determine by what degree the reaction rate will be hampered (Hayes & Kolaczkowski, 1998). The effectiveness factor can be shown as a ratio (Hayes & Kolaczkowski, 1998);

$$\eta = \frac{overall\ rate\ of\ reaction}{ideal\ rate\ of\ reaction} \qquad \textit{Eq (43)}$$

It can also be defined as a function of Thiele modulus (ϕ);

$$\eta = \frac{3}{\phi^2}(\phi coth\phi - 1) \qquad \textit{Eq (44)}$$

For porous solids that are spherical, the Thiele modulus can be calculated from (Hayes & Kolaczkowski, 1998);

$$\phi = \frac{R_P}{3}\sqrt{\frac{k' S_g \rho_P}{D_e^*}} \qquad \textit{Eq (45)}$$

Where R_p is the particle radius; S_g = specific surface area of the sorbent particle; D_e^*= effective diffusion coefficient of gaseous reactant through micro-pores (Seader, et al., 2011). D_e^* can be approximated using the following equation

$$D_e^* = \varepsilon^2 \left[\frac{1}{(1/D_{AB}) + (1/D_K)}\right] \qquad \textit{Eq (46)}$$

Where

- ε = particle porosity;
- D_{AB} = molecular diffusivity of reactant gas A in bulk gas B (Seader, et al., 2011);

$$D_{AB} = \frac{0.00143T^{1.75}}{PMM_{AB}^{1/2}\left[(\sum v)_A^{1/3} + (\sum v)_B^{1/3}\right]^2} \qquad \textit{Eq (47)}$$

Where

- P = System pressure
- T = Temperature
- $MM_{AB} = \frac{2}{(1/MM_A)+(1/MM_B)}$ *Eq (48);*

  MM_A = Molar mass of reactant A, MM_B = Molar mass of bulk gas B

- $\sum v$ = summation of atomic and structural diffusion volumes and are taken from (Seader, et al., 2011)

- D_K = Knudsen diffusivity (Seader, et al., 2011)

$$D_K = 4.850 d_{pore}(T/MM_A)^{1/2} \qquad Eq\ (49)$$

Where

- d_{pore} = Diameter of the pore

CHAPTER 3: MODEL DEVELOPMENT AND SIMULATION STRATEGY

This chapter's aim was to present the development of design to simulate the performance of various basic industrial coal gas treatment plants as well develop a total annual cost (TAC) method to compare these technologies economically. A basic block flow diagram (BFD) of a coal gas treatment plant is shown on Figure 3-1, and served as the template for this work.

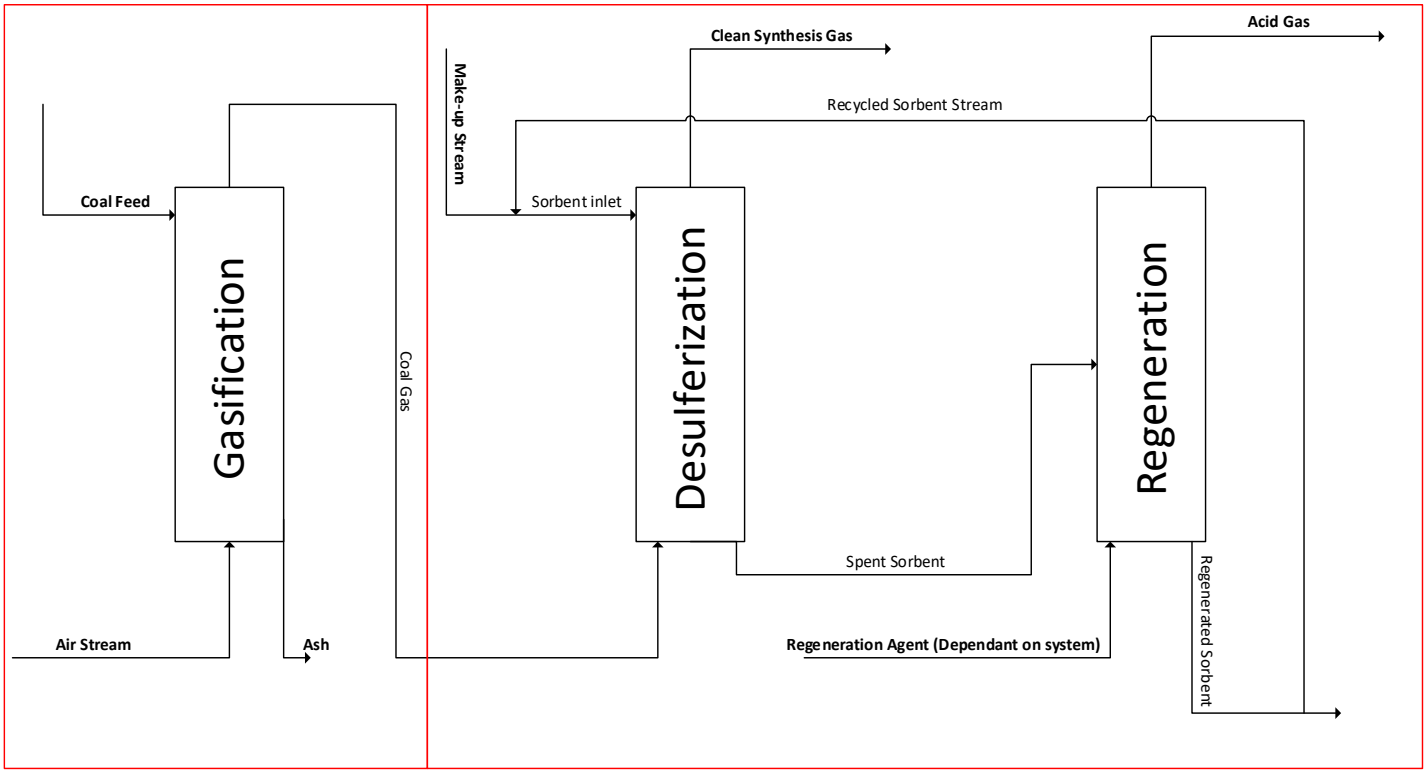

Figure 3-1: Block Flow Diagram of a Gas Treatment Process

Fresh coal is fed into a gasifier and undergoes gasification with air being used as the gasifying agent. Ash and unreacted carbon are collected at the bottom of the gasification process and is sent to a waste treatment plant. The gasified coal gas (sour gas) is then sent to a desulphurization process producing clean synthesis gas (sweet gas) which can then be used for electricity generation. A sorbent is used to rid the coal gas of the hydrogen sulphide (H_2S). The spent sorbent is then sent to a regeneration process, and with the use of a regeneration agent (if required), produces a stream of acid gas, which is then sent to a sulphur recovery plant, and regenerated sorbent. A portion of the regenerated agent is recycled to the desulphurization process and the remainder is purged from the system and sent to a waste treatment plant.

As shown in the BFD above, there were two major parts in this design, the first was the gasification of fresh coal and the second part was the treatment of the coal gas (desulfurization and regeneration processes). There are three methods of coal gas treatment that were considered for this work:

- Amine absorption (wet based process),

- Hot desulphurization with free metal-oxide (dry based process) and
- Hot desulphurization with a supported metal-oxide (dry based process), hence three coal gas treatment plants were designed.

Aspen Plus simulation package was used as the modelling tool. It is a process simulation software package that uses mathematical models to predict the performance of the process given the design and appropriate selection of thermodynamic models. The modelling is explained as follows:

3.1) Gasification

3.1.1) Gasification Method, Process Description and Process Flow Diagram

A fluidized bed coal gasifier was designed to achieve the gasification of coal and was chosen as the use of a fluidized bed gasifier to gasify coal, offers great control of temperature, which is important as the gasification process is highly exothermic, and is relatively cheaper than moving bed and entrained gasifiers.

Fluidized bed coal gasifiers are vertical counter-current reactors in which coal is fluidized by and reacts with air to produce a gas containing CO, H_2, CO_2, CH_4, and other hydrocarbons. Coal is fed to the top of the gasifier. A preheated stream of air is introduced at the bottom of the gasifier and flows upward fluidizing and reacting with the coal. As the coal descends in the gasifier, four processes take place in sequence: coal drying, coal pyrolysis, char gasification, and char combustion. Coal particles shrink and become denser forming the ash and unreacted carbon. These solids sink under gravity and are collected at the bottom and the coal gas leaves at the top. The process flow diagram shown on figure in Appendix A.1 was proposed as the model of the fluidized bed gasifier.

3.1.2) Assumptions

- Model is in steady state
- Model takes the processes of gasification into account (coal drying, coal pyrolysis, char gasification and char combustion)
- Coal drying and coal pyrolysis occurs instantaneously at the top of the gasifier
- The solid and gas temperatures are equal inside the gasifier
- All fine particles generated are assumed to be gasified, therefore elutriation of particles are negligible
- Pressure drop across the bed is assumed negligible

3.1.3) Simulation Properties

Table 3-2 lists the chemical species present in the process:

Component ID	Type	Component Name	Alias
O2	Conventional	OXYGEN	O_2
CO	Conventional	CARBON-MONOXIDE	CO
H2	Conventional	HYDROGEN	H_2

CO2	Conventional	CARBON-DIOXIDE	CO_2
H2O	Conventional	WATER	H_2O
CH4	Conventional	METHANE	CH_4
N2	Conventional	NITROGEN	N_2
H2S	Conventional	HYDROGEN-SULFIDE	H_2S
C6H6*	Conventional	BENZENE	C_6H_6
C	Solid	CARBON-GRAPHITE	C
S	Solid	SULFUR	S
COAL	Nonconventional		
DRY-COAL*	Nonconventional		
CHAR	Nonconventional		
ASH	Nonconventional		

*: C_6H_6 represents the tar and DRY-COAL represents the dried coal.

Table 3-2: Chemical species present in the gasification process

RK-SOAVE was the property method used to calculate the physical properties of mixed conventional components and conventional solid (CISOLID) components. HCOALGEN model is used to calculate the enthalpy of non-conventional components, respectively. The HCOALGEN model requires these three component attributes for nonconventional components: proximate analysis results (denoted as PROXANAL in Aspen Plus), ultimate analysis results (denoted as ULTANAL in Aspen Plus), and sulphur analysis results (denoted as SULFANAL in Aspen Plus). The proximate analysis gives the weight content of moisture, fixed carbon, volatile matter and ash. The ultimate analysis gives the weight composition of coal in terms of ash, carbon, hydrogen, nitrogen, chlorine, sulphur, and oxygen. The sulphur analysis divides the sulphur content into three types, pyritic, sulphate, and organic sulphur. The DCOALIGT model is used to calculate the density of non-conventional components. The DCOALIGT model requires only the two component attributes ULTANAL and SULFANAL. The enthalpy and density of coal are calculated by the HCOALGEN and DCOALIGT models, respectively. Table 3-3 shows the component attributes of coal used in our model, which are from (Wen & Onozaki, 1982). This sample was chosen due to its pyrolysis data being readily available.

Proximate analysis		**Ultimate analysis**		**Sulphur analysis**	
Element	**Value (wt.%)**	**Element**	**Value (wt.%, dry basis)**	**Element**	**Value (wt.%, dry basis)**
Moisture (wet basis)	4.58	C	77.76	Pyritic	0.87
Fixed carbon (dry basis)	39.16	H	5.24	Sulphate	0.87
Volatile matter (dry basis)	52.72	N	1.47	Organic	0.88
Ash (dry basis)	8.12	Cl	0		
		S	2.62		
		O	4.79		
		Ash	8.12		

Table 3-3: Component Attributes of Coal

3.1.4) Unit operations and Reaction Kinetics

3.1.4.1) Coal Drying

Coal drying was simulated using a RYield block, DRYING. The water present in the coal is assumed to be completely vapourized in this block. The water content in the proximate analysis of coal is used to determine the water vapour produced. The water content for the coal used in the study was 4.58wt.%, therefore the mass yield of the water vapours was set to 4.58%, therefore the mass yield of the dired coal produced was 100-4.85% = 95.42%. The products from this block was fed into a separator block, SEP-1, where the gases are separated from the solids. The water vapour mixes with the gas stream form the coal pyrolysis, char gasification, and char combustion processes. The heat duty required for the drying process was represented by a heat stream, Q-DRYING and is used to keep heat balance in the gasifier, showing that the heat required for drying is provided by the hot gases produced from char gasification and combustion

3.1.4.2) Coal Pyrolysis

A RYield block, PYROLYS, was used to simulate coal pyrolysis. In this block, the dried coal is broken into CO, H_2, CO_2, H_2O, H_2S, N_2, CH_4, C_6H_6, and char. The yield of each component is specified according to the results of the pyrolysis experiment (Wen & Onozaki, 1982). The heat required in the pyrolysis process, represented by the heat stream Q-PYROLYS in the model, is supplied by the heat exchange with the gas from char gasification and combustion. The pyrolysis products flow into a separator block SEP-2 where the gases flow upward into the coal drying process and the solid char flows downward into the char gasification and combustion processes.

3.1.4.3) Char gasification and combustion

Coal drying and pyrolysis is assumed to occur immediately upon entering the gasifier, therefore the total length of the gasifier is determined by the length of the char gasification and combustion process. RCSTR block, GASIF, is used. This provides a close representation of the temperature control characteristics of a fluidized bed gasifier.

Equation 2-5 are the solid-gas reactions with some of these rate being volume based and others being surface reactions. Gas readily diffuses into the particles for volumetric reactions with reactions taking place throughout the particle, whereas the gas is confined to the surface of the particle for the surface reactions. The volumetric reactions occur when diffusion rates are faster were as surface reactions occur when the intrinsic rate is faster. Equation 2 is relatively fast compared to the diffusion rates therefore the reaction occurs at the surface. Equations 3 to 5 are volumetric reactions due to the low operating temperature of the gasifier (typically 900°C (Levenspiel, 1999)).

Based on the above statements, the unreacted-core shrinking model is applied to describe the reaction rate of equation 2 (Wen & Onozaki, 1982):

$$R_{C-O_2} = \frac{P_{O_2}}{\frac{1}{k_{film}} + \frac{1}{k_s Y^2} + \frac{1}{k_{d,ash}}} \qquad \textit{Eq (50)}$$

Where:

- Rc-o_2 = reaction rate, mol/cm^3.s
- k_{film} = gas film diffusion coefficient
- k_s = chemical reaction constant
- $k_{d,ash}$ = ash diffusion coefficient
- Po_2 = partial pressure
- Y = (r_{core})/($r_{particle}$)
- $r_{particle}$ = radius of feed coal particles
- r_{core} = radius of unreacted core

In a fluidized bed gasifier, coal particle size is between the range of 1-10mm (Xu, et al., 2006), and in most cases, the gas film and ash diffusions are the rate-limiting steps, therefore the above rate is simplified as follows:

$$R_{C-O_2} = \frac{P_{O_2}}{\frac{1}{k_{film}} + \frac{1}{k_{d,ash}}} \qquad \textit{Eq (51)}$$

Where:

- $k_{film} = 0.292 \times 4.26 \times \frac{\frac{T}{1800}^{1.75}}{d_p T}$
- $k_{ash} = k_{film} \cdot \varepsilon_p^{2.5} \cdot \frac{Y}{1-Y}$
- dp = diameter of coal particle size
- Ep = porosity of ash (0.75)

The kinetic reaction rates for equations 3 to 7 are shown on Table 3-3.

Reaction Rate	Units
$R_{C-\mathrm{H_2O}} = 930e^{-\frac{45000}{1.987T}}.[C].\left(P_{H_2O} - P^*_{H_2O}\right)$; $P^*_{H_2O} = \frac{P_{H_2}.P_{CO}}{e^{17.29-\frac{16330}{T}}}$	mol/cm^3.s

$R_{C-CO_2} = 930e^{-\frac{45000}{1.987T}}.[C].(P_{CO_2} - P^*_{CO_2});$ $\quad P^*_{CO_2} = \frac{P^2_{CO}}{e^{20.92-\frac{20280}{T}}}$	mol/cm^3.s
$R_{C-H_2} = e^{-7.087-\frac{8078}{T}}.[C].(P_{H_2} - P^*_{H_2});$ $\quad P^*_{H_2} = \left(\frac{P_{CH_4}}{e^{-13.43+\frac{10100}{T}}}\right)^{0.5}$	mol/cm^3.s
$R_{CO-H_2O} = 2.877 \times 10^5.e^{-\frac{27760}{1.987T}}.\left(x_{CO}.x_{H_2O} - \frac{x_{CO_2}.x_{H_2}}{k_{wgs}}\right).P_t^{0.5-\frac{P_t}{250}}.e^{-8.91+\frac{5553}{T}};$ $\quad k_{wgs} = e^{-3.6890+\frac{7234}{1.8T}}$	mol/g(ash).s
$R_{H_2-O_2} = 8.83 \times 10^5.e^{-\frac{9.976\times10^4}{8.315T}}C_{H_2}C_{O_2}$	mol/m^3.s

Table 3-3: Kinetic rate expressions for char gasification and combustion (Wen & Onozaki, 1982)

Where:

- T = Temperature (K)
- Pi = Partial pressure of component i (atm)
- Pt = Total pressure (atm)
- Ci = Concentration of component i (mol/m3)
- [C] = Concentration of carbon i (mol/m3)

The kinetics of these reactions are provided in an external Fortran subroutine in the Aspen Plus. A RStoic block, CHAR-DEC was created to convert char into the following components: C, H_2, O_2, N_2, S, and ash to making it easier to simulate gas-solid reactions in Aspen Plus. This was done using the ultimate analysis of the coal and a calculator block, CHAR-DEC. The heat duty specified in this block was set to zero, in order to maintain the heat balance.

3.1.5) Inlet stream conditions and operating conditions

A coal flow rate of 84 tons/day (3.5 tons/hr) was selected and is a typical flowrate of coal processed in an industrial gasifier (Vamvuka, 1999). An operating pressure of 30 atm was selected. Gasification of up to 30 atm have been cited (Fermoso, et al., 2009). The gasification and combustion reaction rates are proportional to the partial pressure of oxygen present during operating, thus aiming to increase the mass conversion of coal (XCoal) by using a higher operating pressure. The air will act as a heat sink. This will reduce the temperature of the product gas stream, which would make subsequent cooling easier to achieve. Air temperature of 240°C was selected as this is just higher than the dew point temperature of water (234.5°C @ 30atm) minimizing the risk of condensing water vapours in the gasifier. This temperature is the steady state air temperature and a higher temperature would be required to initiate gasification. The bed temperature is kept at 900°C. A particle size of 1 mm was chosen. Smaller particle

sizes provide better conversion but fine particles (<1mm) could be carried with the gas stream resulting in slagging (Lv, et al., 2004).

3.1.6) Fluidization

In order for the RCSTR block, to better predict the performance of a fluidized bed, it is imperative to incorporate the fluidization behaviour. This is done via a pair of calculator blocks. The first block (AIR-FLOW) is used to determine the flowrate of air required to maintain fluidization. The algorithm for the AIR-FLOW block is shown on Figure 3-2.

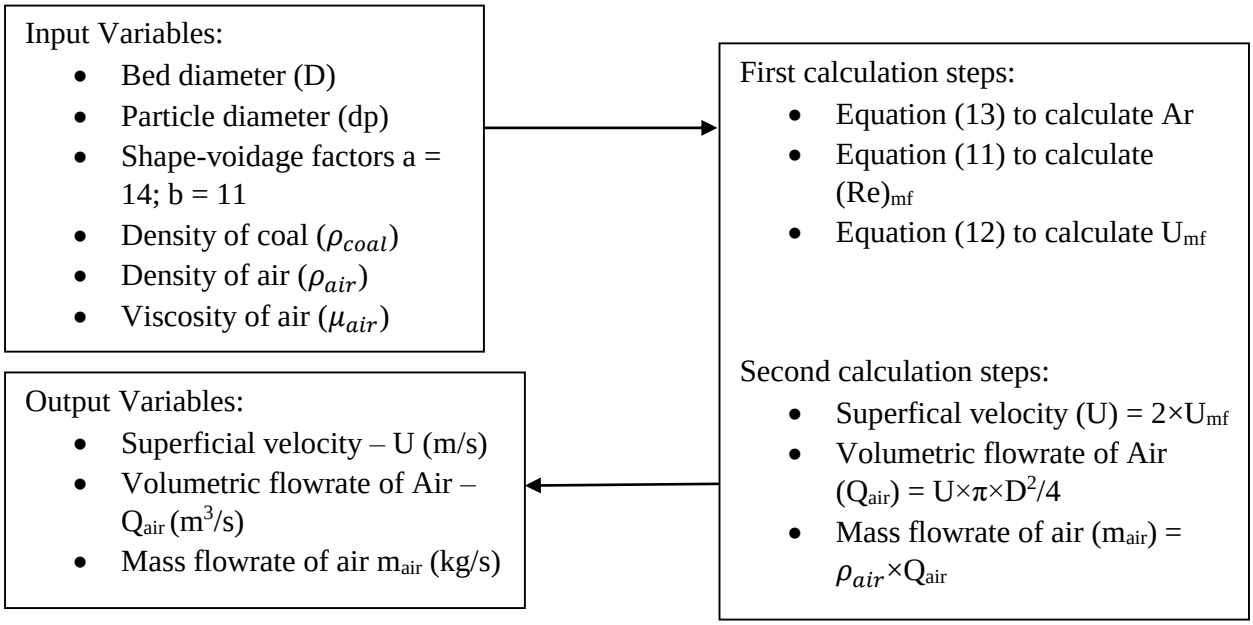

Figure 3-2: Air flowrate algorithm

The second calculator block (VOIDAGE), is used to determine the bed volume and bed voidage. The algorithm for the VOIDAGE block is shown on Figure 3-3.

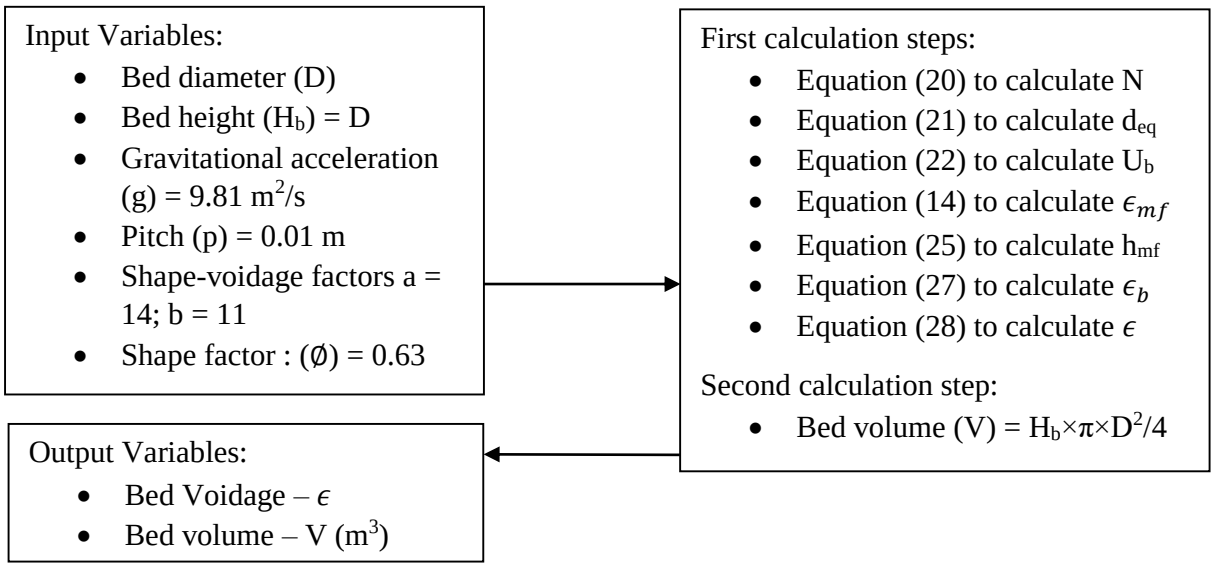

Figure 3-3: Fluidization algorithm for the gasifier

A bed height to diameter ratio of 1:1 was recommended as a precaution against slagging in gasifiers. The bubble diameter ($d_b \approx d_{eq}$) must be less than 1/3 of the bed diameter (D) (Dechsiri, 2004), and

serves as a check to avoid slagging. A fluidization velocity of twice the minimum fluidization velocity is chosen to establish bubbling fluidization of particles in a gasifier (Dechsiri, 2004). The density of air in the AIR-FLOW block, was taken at 900°C and 30 atm (8.89 kg/m^3) and not at the inlet conditions, as the air in gasifier are at the gasifiers operating conditions. The same applies with the viscosity of air (0.04828 mPa.s). A pitch of 1cm is chosen, anything bigger could result in jet penetration and inadequate particle movement (Geldart, 1985). The shape factor of coal is roughly around 0.63 (Wen & Onozaki, 1982). The calculation of the AIR-FLOW block is run before the MX-GASIN block is executed. This makes sure that the correct air flowrate is inputted before the GASIF block begins its calculation. The sequence step for the VOIDAGE block is run before the GASIF block is executed. This makes sure that the GASIF block has the bed volume and voidage before it begins its calculation. For a given bed height and diameter, these calculator blocks will calculate the superficial velocity, therefore the required air flowrate, a reactor bed volume and bed voidage. The GASIF block used these parameters together with the kinetics to assess the performance of the gasification model. This makes the bed height (H_b) and the bed diameter (D), the tuning parameters for this model, thus these parameters will be investigated in the optimization of the fluidized bed coal gasifier.

3.2) Amine Absorption

3.2.1) Amine selection and Simulation Properties

Methyldiethanolamine (MDEA) was chosen as the wet based gas treating agent. MDEA is very selective to H_2S and is the most widely used gas treating agent, which makes it the ideal choice for this design. Aspen Plus provides special data packages for amine systems. These packages allow for accurate modelling of amines for gas treating processes. These packages use the electrolyte capabilities, but also take into consideration kinetic reactions in the liquid phase. The modelling approach is fundamentally sound and has been validated through industrial applications. These data packages give more accurate results than those that do not consider kinetic reactions. ELELCNRTL is the property used. Henry's law is used for H_2S and CO_2. Enthalpy of solution data is used to develop this model. The applications include H_2S and CO_2 absorption/stripping with MDEA solutions. Table 3-4 lists the chemical species presented in the process:

Component ID	Type	Component Name	Alias
MDEA	Conventional	METHYL-DIETHANOLAMINE	$C_5H_{13}NO_2$
H2O	Conventional	WATER	H_2O
CO2	Conventional	CARBON-DIOXIDE	CO_2
H2S	Conventional	HYDROGEN-SULFIDE	H_2S
H3O+	Conventional	H3O+	H_3O^+
OH-	Conventional	OH-	OH^-
HCO3-	Conventional	HCO3-	HCO_3^-
CO3-2	Conventional	CO3--	CO_3^{2-}
HS-	Conventional	HS-	HS^-

S-2	Conventional	S--	S^{2-}
MDEAH+	Conventional	MDEA+	$C_5H_{14}NO_2^+$
CH4	Conventional	METHANE	CH_4
N2	Conventional	NITROGEN	N_2
O2	Conventional	OXYGEN	O_2
CO	Conventional	CARBON-MONOXIDE	CO
H2	Conventional	HYDROGEN	H_2
C6H6	Conventional	BENZENE	C_6H_6
NANO3	Conventional	SODIUM-NITRATE	$NANO_3$
KNO3	Conventional	POTASSIUM-NITRATE	KNO_3

Table 3-4: Chemical species used in the amine absorption process

3.2.2) Process Description and Process Flow Diagram

The process flow diagram on in Appendix A.2 was proposed as the model for the amine absorption process. The coal gas produced from gasification is sent into a pre-cooler, HX-1 where it is cooled until is a saturated vapour stream. The cooled gas is then sent to a tar removal tower, TAR-TOW. A stream of water is pumped by pump, P-101 and split into two streams, providing each stage an inlet of water, which is used to condense the tar molecules from the gas stream, before proceeding downstream. The product gas exits the top of the tower and is compressed in a compressor, C-101 and cooled in a heat exchanger, HX-2, to meet process conditions of downstream processes. The gas stream enters the bottom of an absorption column, ABSORBER, and a lean amine stream of (7 mol.% MDEA, 93 mol.% H_2O) enters at the top of the absorber, absorbing the H_2S present in the gas stream. The clean gas stream leaves at the top of the absorber and is heated by a heat exchanger HX-5 and decompressed by a turbine, T-101, to produce the final sweet gas product. The amine stream rich in sulphur exits the bottom of the absorber. It is then to a pressure relief valve, CV-1 and heated in a heat exchanger, HX-3, to meet process conditions of the regeneration process. The rich amine stream then enters a distillation column, REGEN. A stream of acid gases is produced at the top of the column, which is then sent to a sulphur recovery plant, and a lean amine stream is produced and exits the reboiler. 10% of the lean amine is purged and sent to water treatment plant, and the remainder is recycled with fresh make-up streams of MDEA and H_2O. The lean amine stream is pumped, using pump P-102, and cooled in a heat exchanger, HX-4, to process conditions before entering the absorber.

A stream of molten salts (60 wt.% $NaNO_3$, 40 wt.% KNO_3), is the utilities used for heat integration in this design. A heat stream, Q1, represents the cooling required from HX-1 and is sent to a dummy heat exchanger, HEX-1, which will simulate the heat transfer between the molten salts and hot coal gas. A hot stream of molten salts is produced from HEX-1 and is sent to another dummy heat exchanger, HEX-5. HEX-5 cools the molten salts to its inlet temperature and is recycled by pump, P-103, back to HEX-1, forming a closed loop. The remainder of the heat generated by HEX-5 is supplied to HX-5, by heat stream, Q2, representing that the heating of the final gas is progressed until the hot molten salts reaches its inlet conditions to be recycled. A purge stream is necessary in industrial processes as it allows for quality testing of regenerated material. There was insufficient literature of purge ratios for industrial

gas treatment processes, therefore this ratio was estimated. Amine solutions have greater structural stability than metal oxide sorbents due to the low operating temperatures. This means they have a larger multi-cycle capacity and would have a low purge ratio, therefore a purge ratio of 0.1 (10% purged) was selected.

There are two main approaches to modelling columns in process simulation software: rate-based and equilibrium-stage. Rate-based models utilize heat and mass-transfer correlations based on transfer properties and tray/packing geometry, while the equilibrium-stage models use empirical methods for simulation.

The design of this amine unit consists of the following sections:

- Tar removal
- Desulphurization (via an amine absorber)
- Regeneration (via distillation)
- Utilities, Auxiliary units and Heat integration

3.2.3) Tar removal

Tar removal is an essential part for this design, as desulphurization via an amine unit operate at temperature below the dew point of tar. Liquefied tar can compromise the operation of a process by clogging up equipment and must be removed from the coal gas before its sent downstream.

Before the coal gas can be treated for tar removal, it must be cooled. This pre-cooling stage is necessary as it will reduce the amount of water that is vaporized into the gas stream, during tar removal. This will also increase the effectiveness of the tar removal process as tar vapours at lower temperatures are easier to condense and provide most of the cooling required in this design. The cooling design is further explained in in section 3.2.6.

3.2.3.1) Tar column design

A spray tower was the choice of equipment for the tar removal process. This was modelled using A RadFrac Absorber block, TAR-TOW. The calculation type was set to equilibrium, because a spray tower has no trays or packing and would be incorrect to incorporate those factors into this design. The number of stages chosen was 2, this was found to be the minimum number of stages required to achieve effective tar removal and therefore, the cheapest design in terms of equipment cost. No Condenser or Reboiler type was selected, as a spray tower does not utilize either. A stream of water was split equally and added at each stage, to simulate water nozzles at various locations in a real spray column. The stage location of each water stream was placed above their respective stages and the gas stream was placed on its respective stage. Vapour is specified for the product stream leaving the top of the tower and a liquid for the product stream leaving the bottom. A tray diameter and spacing was specified, and the remaining column internals were automatically generated. The column was sized interactively with the

absorber block, TAR-TOW. This was done to determine appropriate column dimensions that are hydraulically operable but excluded the mass transfer effects of a tray column.

3.2.3.2) Inlet and Operating Conditions

The pressure of the gasification process upstream was 30 atm, therefore the operating pressure of the tar column was chosen to be 30 atm. This would mean that no additional investment would be needed on pressure changers. The water streams at each stage are at 25°C and 30 atm.

3.2.3.3) Design Specifications

The general industrial mass concentration limit of tar in process equipment, is less than 2.5mg/m^3 (*), therefore a design specification of 2.4mg/m^3 of tar was used for the gas product from the tar tower. The flowrate of water pumped into the system is varied in a design specification block, TAR-LIM, and determines the flowrate of water required to achieve the mass concentration of 2.4mg/m^3.

3.2.4) Desulphurization

3.2.4.1) Absorber column design

A RadFrac Absorber block, ABSORBER, was used to model the absorber column. The calculation type was set to rate-based. No Condenser or Reboiler type was selected, as the absorber did not require it. The location stage of the lean amine inlet is set above the first stage and the sour gas stream is set on the last stage. The number of stages is a tuning parameter and is used to optimize the column design, therefore an arbitrary number was selected, during preliminary design stages.

A sieve tray was chosen as the column internal, as it is the easiest to maintain and replace and would be needed due to the high corrosive nature of H_2S. A tray diameter and spacing was specified, and the remaining column internals were automatically generated. The correct tray specifications are required, to ensure that all stages of the column are hydraulically operable i.e. the prevention of entrainment, flooding and weeping.

3.2.4.2) Inlet and operating conditions

A column pressure of 55 atm was selected. The inlet temperature of the lean amine stream was set to 43°C with a composition of 7 mol% of MDEA with water, and the temperature of the inlet gas was set to 57°C. These design choices were made so that the column would operate under conditions of a typical amine absorber.

3.2.4.3) Design Specifications

The sales gas concentration limit of H_2S in gas streams is 4ppm, therefore a design specification of 3.9ppm of H_2S in the product gas was used. The flowrate of the lean amine stream entering the column is varied in a design specification tab in the ABSORBER block and determines the lean amine flowrate required to achieve the outlet concentration of 3.9ppm.

3.2.5) Regeneration

3.2.5.1) Regeneration column design

A distillation column was the choice of equipment for regeneration. It was chosen over a stripping column to avoid the investment of a stripping agent. A RadFrac Distillation block, REGEN, was used to model the distillation column. A partial condenser was selected as non-condensable gases are present and a vapour product stream is required to remove the captured H2S, and a kettle reboiler was selected. The number of stages chosen was 4. Two stages consisted of the partial condenser and the reboiler, and the remaining two stages where located in the column. This was the minimum number of stages required to produce an effective design and would be the cheapest option in terms of equipment cost. The feed location was set above the second stage (first column stage). A reflux ratio and boil-up ratio were specified to complete the specifications of the distillation column. A sieve tray was also chosen as the column internal for the regeneration process. A tray diameter and spacing were specified, and the remaining column internals were automatically generated.

3.2.5.2) Inlet and operating conditions

An operating pressure of 1.1 atm is selected. The pressure of the column needs to low enough to maintain low operating temperatures and reduce reboiler duties, but the risk of vacuum operation should also be avoided, therefore validating the pressure selection. The inlet temperature was another tuning parameter that was optimized for this column, as it will affect the duties required by the condenser and reboiler.

3.2.5.3) Design Specifications

The design specifications for this column were as follows:

1. The reflux ratio was varied to achieve the total sulphur recovery. This was done by a design specification tab in the REGEN block. The specification was the mass flowrate of H_2S exiting the REGEN block is equal to the mass flowrate of H_2S entering the ABSORBER block subtract the mass flowrate of H_2S exiting the ABSORBER block.
2. The corrosive ability of a sulphur-rich aqueous solution on steel can be limited at temperatures below 120°C (Mokatab, et al., 2019). This served as the second design specification required and was achieved by varying the boil-up ratio.

3.2.6) Auxiliary Units, Utilities and Heat Integration

3.2.6.1) Auxiliary Units

For the design of the amine unit, several auxiliary units are required to maintain operating conditions. A basic design for auxiliary units and utilities were conducted, as only major units were designed rigorously. The placement and functions of the auxiliary units were as follows:

- P-101 was used to discharge water to 30 atm, before it enters TAR-TOW.
- HX-1 was used to cool the hot coal gas down before entering TAR-TOW. HX-1 was set to cool until the gas was a stream of saturated vapours. This was the maximum cooling that could have been achieved, without condensation of tar molecules, thus making it the best inlet temperature for tar removal.
- C-101 was used to compress the gas product from TAR-TOW, to 55 atm, as this was the required pressure for the desulphurization process.
- HX-2 was used to cool the gas stream to 57°C, after it was compressed, as this was the required inlet gas temperature for the desulphurization process.
- CV-1 was used to relieve the pressure of the rich-amine stream to 1.1 atm, as this was the operating temperature required for the regeneration process
- HX-3 was used to heat the rich-amine stream, producing the inlet temperature required for the regeneration process. That temperature has a great impact on the duties required by the condenser and reboiler, therefore making it another tuning parameter that was used in the optimization for the regeneration process.
- P-102 was used to discharge the lean amine stream to 55 atm, as this was the operating pressure of the desulphurization process.
- HX-4 was used to cool the lean amine stream to 43°C, as this was the required inlet temperature for the desulphurization process.
- HX-5 was used to heat the sweet gas from the desulphurization process. The heating achieved was dictated by the heat recovery through heat integration.
- T-101 was used to decompress the gas product from ABSORBER, to 30 atm, as this was the pressure of the coal gas supplied to the amine unit.
- P-103 was used to circulate a molten salt stream.

3.2.6.2) Utilities

Utilities were used to maintain the operation of the auxiliary units. The utilities were defined in a utility tab in each block. The utility type was chosen from a list of available utilities, and the operating conditions for each utility was defined. The utilities used are as follows:

- Cooling water was used for HX-2, HX-4 and the condenser of the REGEN block. The water inlet conditions for HX-2 and HX-4 was set at 30 atm and 25°C, and an outlet temperature of 65°C (the outlet temperature of the water needed to be higher than the operating condition of the absorber). The water inlet conditions for the condenser was set at 1 atm and 25°C, and an outlet temperature of 90°C, to avoid the evaporation of cooling water
- Low pressure steam was used for the reboiler in the REGEN block and HX-3. The inlet conditions were set to 125°C and a vapour fraction of 1, and an outlet vapour fraction of 0, utilizing its heat of vapourization to achieve the heating required.

- A eutectic mixture of NaO_3 and KNO_3 (60 wt.% $NaNO_3$, 40 wt.% KNO_3) was used as the molten salt thermal fluid. This mixture is a common heat transfer fluid used in industrial heat exchanger (Reddy, 2011). The operating temperature of this mixture ranges between 200°C and 600°C (Reddy, 2011). The molten salts were only used for cooling in HX-1 and heating in HX-5, as the other heat exchangers operated below its temperature range. This utility was not defined under a utility tab, as it was not an option from the available list, and was designed as part of the heat integration of the amine unit.

3.2.6.2) Heat Integration

The purpose of the heat integration was to recover as much of the heat that was lost during the process. The heat that is recovered is supplied back to the sweet gas to increase its final temperature. A gas stream with a higher temperature is more valuable for electricity generation as more steam could be generated from it. The heat integration was set up as follows:

- Most of the heat loss occurred when the coal gas is cooled by HX-1. A stream of molten salts at 250°C was used as the thermal fluid to recover that heat, and was above the lower operating limit of this mixture, validating this choice. HEX-1 was used to simulate the heating of the molten salts passing through HX-1. A heat stream, Q1, was used to represent the amount of heat gain by the molten salts. A design specification, MOLTIN, was used to achieve an outlet temperature of 550°C, by varying the flowrate of the molten salts. This made sure that the molten salt stream was elevated close to but not above its temperature range.
- HEX-5 was used to simulate the heat transfer of the molten salts passing through HX-5. The block was set to achieve an outlet temperature of 250°C. This made sure that the molten salt stream would be returned to its original temperature so it can be recycled back to HX-1. A heat stream, Q2, was used to represent to heat generated from HX-1 by the molten salt stream and would be used to recover the heat of the final product gas in HX-5.

3.3) Hot Desulphurization (Free metal-oxide)

The process flow diagram shown on figure in Appendix A.3 was the model proposed for the hot desulphurization process. Zinc oxide was chosen as the sorbent to achieve gas treatment, as it has a great H_2S absorption capacity and is a common sorbent that is used. Characteristics of a typical zinc oxide sorbent were taken from (Gibson & Harrison, 1980), who studied desulphurization performance of free zinc oxide. The sorbent had a density of 1830 kg/m^3, a surface area of 17.9 m^2/g, a particle porosity of 0.67 and an average pore diameter of 10 nm.

Fluidized beds are used to carry out the as the main gas treatment units. It would provide great temperature control, as zinc oxide absorption processes are generally isothermal (Atimtay & Harrison, 1998). A fluidized bed is used to achieve the desulphurization via zinc oxide absorption, and

regeneration of zinc oxide sorbent. A feed of zinc oxide sorbent was fed into the first fluidized bed, FB1, as well as the coal gas, which undergoes desulphurization. The product gas enters a cyclone, CYC1, were elutriated solids were removed, producing a stream of sweet gas. The solids captured by CYC1 are mixed with the solids stream that exits the FB1. The solids stream then enters a second fluidized bed, FB2, and undergoes regeneration with the use of a pre-heated stream of air. Before the air enters the fluidized bed, it was compressed by C-101 and cooled/heated by HX-1. A stream of molten salts is used as the heat transfer fluid for HX-1, as air temperatures above 200°C. A dummy heat exchanger, HEX-1, was used to model the heat transfer of the molten salts in HX-1. The gas exiting FB2 was fed to a cyclone, CYC2, were elutriated solids were removed. A stream of acid gases was produced from CYC2 and sent to a sulphur recovery plant. The solids captured by CYC2 are mixed with the solids stream that exits the FB2, making up a stream of regenerated zinc oxide sorbent. 90% of this stream is purged and sent to a waste treatment plant. The remainder is recycled, with a fresh stream of zinc oxide, back for desulphurization.

The design fluidized bed was split into two divisions. At the bottom is a dense bed of solid and above that is the freeboard. A visual conception of this can be seen in chapter 2. The dense bed was simulated using a RCSTR block, (BED1 and BED2), and the principles of fluidization. It was assumed that majority of the reaction occurs in this section as most of the solids are present there, therefore the freeboard height was not included in the reaction volume. A reactor volume (bed volume) and vapour fraction (bed voidage) were required inputs. No attrition or agglomeration of particles were assumed; therefore, the particle size distribution throughout the fluidized beds were kept constant. The mass of elutriated solids is split from the solids stream exiting the RCSTR blocks, and mixed with the gas stream exiting the RCSTR blocks. The split fraction calculation is shown in section 3.3.1.1. This setup for each fluidized bed is highlighted by red boarders in the process flow diagram.

The design of this unit can be divided into the following sections:

- Desulphurization
- Regeneration
- Solid Separation
- Auxiliary Units and Utilities

A basic design was conducted for solid separation and auxiliary units, as only major units (Desulphurization and Regeneration) were designed rigorously. Table 3-5 lists the chemical species presented in the process:

Component ID	Type	Component Name	Alias
H2O	Conventional	WATER	H_2O
CO2	Conventional	CARBON-DIOXIDE	CO_2

H2S	Conventional	HYDROGEN-SULFIDE	H_2S
CH4	Conventional	METHANE	CH_4
N2	Conventional	NITROGEN	N_2
O2	Conventional	OXYGEN	O_2
CO	Conventional	CARBON-MONOXIDE	CO
H2	Conventional	HYDROGEN	H_2
C6H6	Conventional	BENZENE	C_6H_6
SO2	Conventional	SULFUR-DIOXIDE	O_2S
NANO3	Conventional	SODIUM-NITRATE	$NANO_3$
KNO3	Conventional	POTASSIUM-NITRATE	KNO_3
ZNO	Solid	ZINC-OXIDE	ZnO
ZNS	Solid	ZINC-SULFIDE-WURTZITE	ZnS

Table 3-5: Chemical species used in the hot desulphurization process

3.3.1) Desulphurization

3.3.1.1) Fluidization, TDH and Elutriation

The fluidization behaviour of the first fluidized bed, FB1 was incorporated using a calculator block, VOID1. The calculation algorithm was as follows:

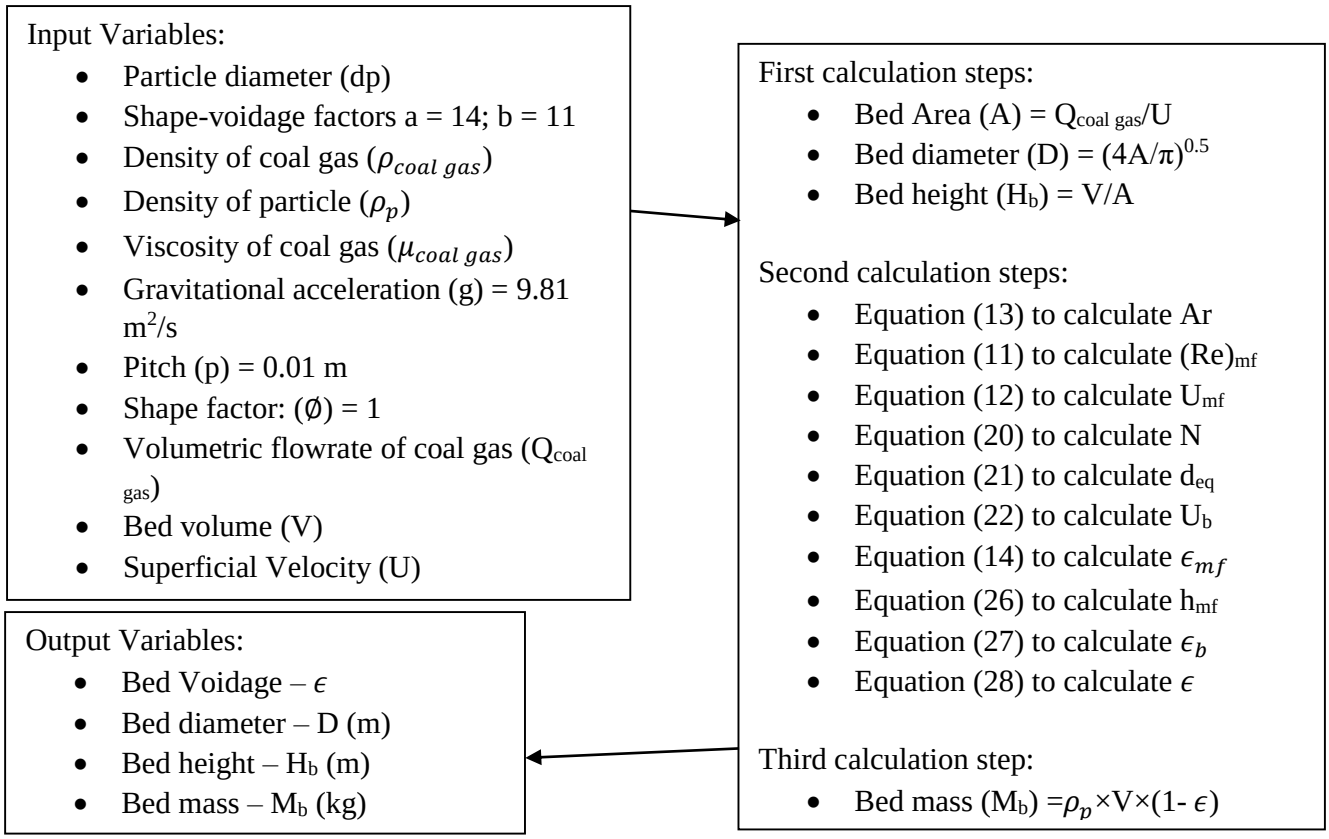

Figure 3-4: Fluidization algorithm for FB1

The effects of elutriation and TDH of the first fluidized bed was incorporated in the same calculator block as above. The calculation algorithm was as follows:

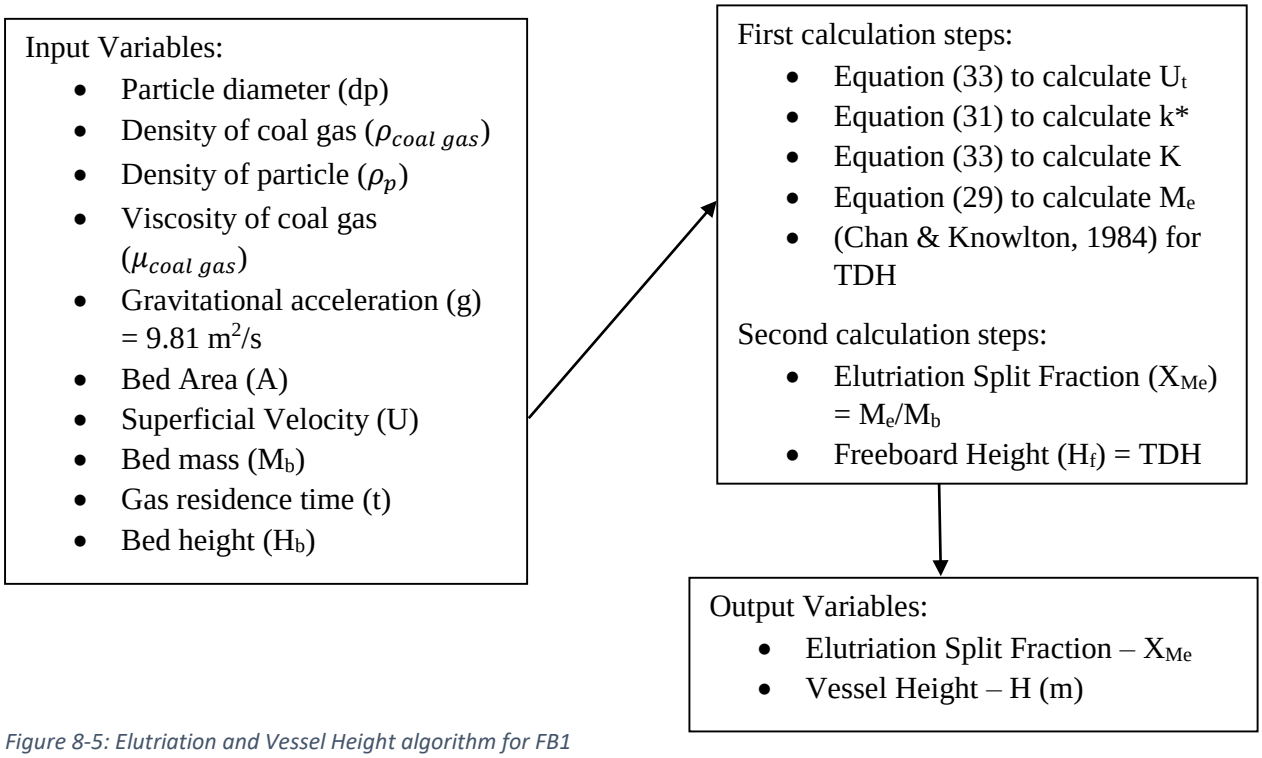

Figure 8-5: Elutriation and Vessel Height algorithm for FB1

A pitch (the distance between the center of holes on a distributor plate) of 1cm is chosen, anything bigger could result in jet penetration and inadequate particle movement (Geldart, 1985). Zinc oxide particles were assumed spherical for this design, therefore a shape factor of 1 was chosen. The superficial velocity was a tuning parameter, which was investigated in the optimization of the fluidized bed. The gas residence time was used in equation 32, as it represents the residence time of the solids present at the interface between the dense bed and the freeboard. The calculator blocks used these parameters together with the kinetics to assess the performance of the fluidized bed. The results from these calculations included, the bed voidage, bed height (H_b), bed diameter (D), the vessel height (H) and the elutriation split fraction.

3.3.1.2) Reactions and Kinetics

The reaction kinetics were inputted via a reaction block R-1. The reaction between H_2S and zinc oxide is shown below:

$$ZnO(s) + H_2S(g) \leftrightarrow ZnS(s) + H_2O(g) \qquad Eq\ (52)$$

The reaction rate was assumed first order reaction with respect to the concentration dependency of H_2S. The overall kinetic factor was calculated via a calculator block, RXN1. The calculation algorithm was as follows:

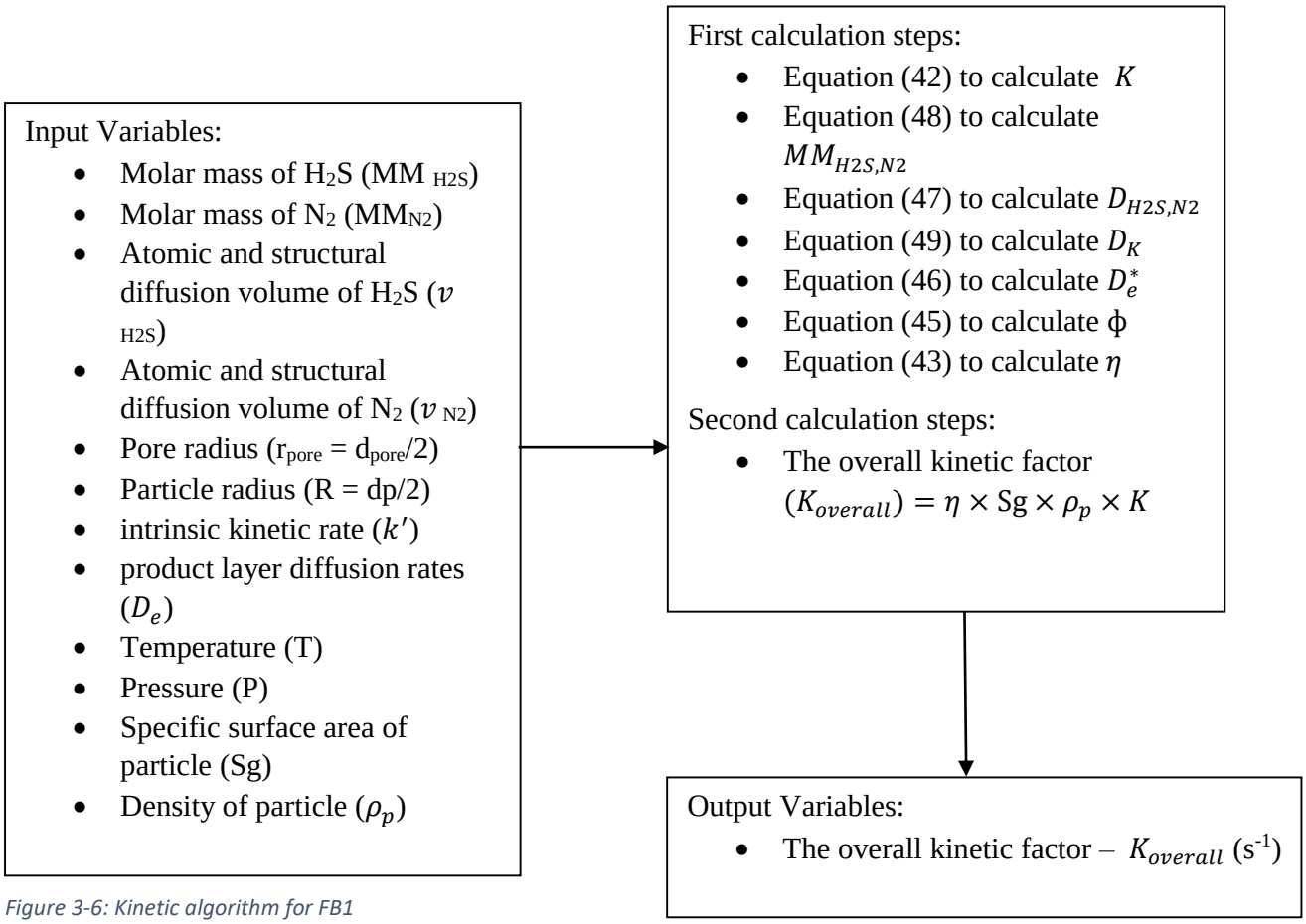

Figure 3-6: Kinetic algorithm for FB1

The shrinking-core model was chosen for the kinetic modelling of zinc oxide, therefore equation 35 was used. Mixing in the fluidized bed is inherently turbulent; therefore, gas film diffusion was assumed negligible. Equation 35 was then read as follows:

$$K = \frac{1}{\frac{R(R-r_c)}{r_c D_e} + \frac{R^2}{r_c^2 k'}} \qquad Eq\ (53)$$

A visual representation of the reacted spherical zinc particle is shown below:

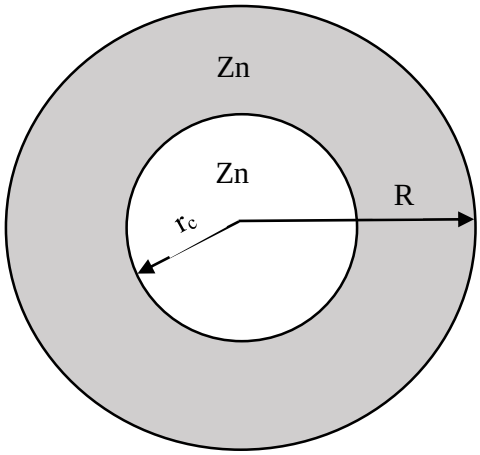

Figure 3-7: Visual representation of a reacted zinc oxide particle

The unreacted core radius (r_c) was calculated from the conversion (X_{ZnO}) of solid zinc oxide using the following equation:

$$X_{ZnO} = 1 - \left(\frac{r_c}{R}\right)^3 \qquad Eq\ (54)$$

The conversion was expressed in terms of molar flowrates as follows:

$$X_{ZnO} = \frac{n_{ZnO,in} - n_{ZnO,out}}{n_{ZnO,in}} \qquad Eq\ (55)$$

Where:

- $n_{ZnO,in}$ = molar flowrate of zinc oxide entering the fluidized bed
- $n_{ZnO,out}$= molar flowrate of zinc oxide exiting the fluidized bed

Using an outlet condition ($n_{ZnO,out}$), meant that calculator block, RXN1 was an iterative calculation. The simulation was reinitialized with previous results until convergence was reached. The intrinsic kinetics (k') and product layer diffusion rates (D_e) were extracted from (Atimtay & Harrison, 1998). The operating range of their work was 400-600°C. The rates were as follows:

$$k' = 0.0131 e^{\left[-\frac{43095.2}{RT}\right]} \qquad Eq\ (56)$$

$$D_e = 9.8 \times 10^{-6} e^{\left[-\frac{110457.6}{RT}\right]} \qquad Eq\ (57)$$

Where:

- R = universal gas constant (8.314 J/mol.K)
- T = temperature (K)

The zinc oxide sorbent is a porous particle; therefore, the effectiveness factor was incorporated in the second calculation step. The specific surface area and particle density were multiplied to the kinetic factor to convert it from an area-based expression into a volumetric-based expression, as ASPEN Plus only operates with volumetric or catalyst weight-based kinetics.

3.3.1.4) Inlet and operating conditions

The operating pressure of the fluidized bed was set to 30 atm, which was the same pressure of the gasification process, therefore pressure changers were not needed. The operating temperature was set to 550°C. This was chosen as lower temperatures produced a slow reaction rate and unrealistic vessel sizes. The flowrate of sorbent had no effect on the performance of the fluidized bed, therefore a feedrate of 2 kmols/hr (162.78 kg/hr) (consisting of make-up sorbent and recycled sorbent) of zinc oxide sorbent is fed to the fluidized bed, as this was the lowest amount required for the simulation and would result in the lowest operating cost in terms of sorbent requirements. A zinc oxide particle size of 50 µm was chosen, to produce fluidization behavior akin to Geldart Group A powder, this can be shown on Figure 3 in section 2.2.2). This was the smallest Geldart Classification that could be fluidized. The smaller the particle the greater the reaction rate as diffusion and kinetic resistances are reduced, therefore rationalizing the choice. Free metal-oxide sorbents are structurally unstable, therefore its ability to be used continuously is lower. A large purge ratio would be required to ensure high quality sorbent was continuously present in the process, therefore a purge ratio of 0.9 (90% purged) was selected.

3.3.1.4) Design Specifications

The sales gas concentration limit of H_2S in gas streams is 4ppm, therefore a design specification of 3.9ppm of H_2S in the product gas was used. The bed volume of the fluidized bed is varied in a design specification block, H2SOUT, and determines the bed dimensions required to achieve the outlet concentration of 3.9ppm.

3.3.2) Regeneration

3.3.2.1) Fluidization, TDH and Elutriation

The fluidization behaviour of the second fluidized bed, FB2 was incorporated using a calculator block, VOID2. The calculation algorithm was as follows:

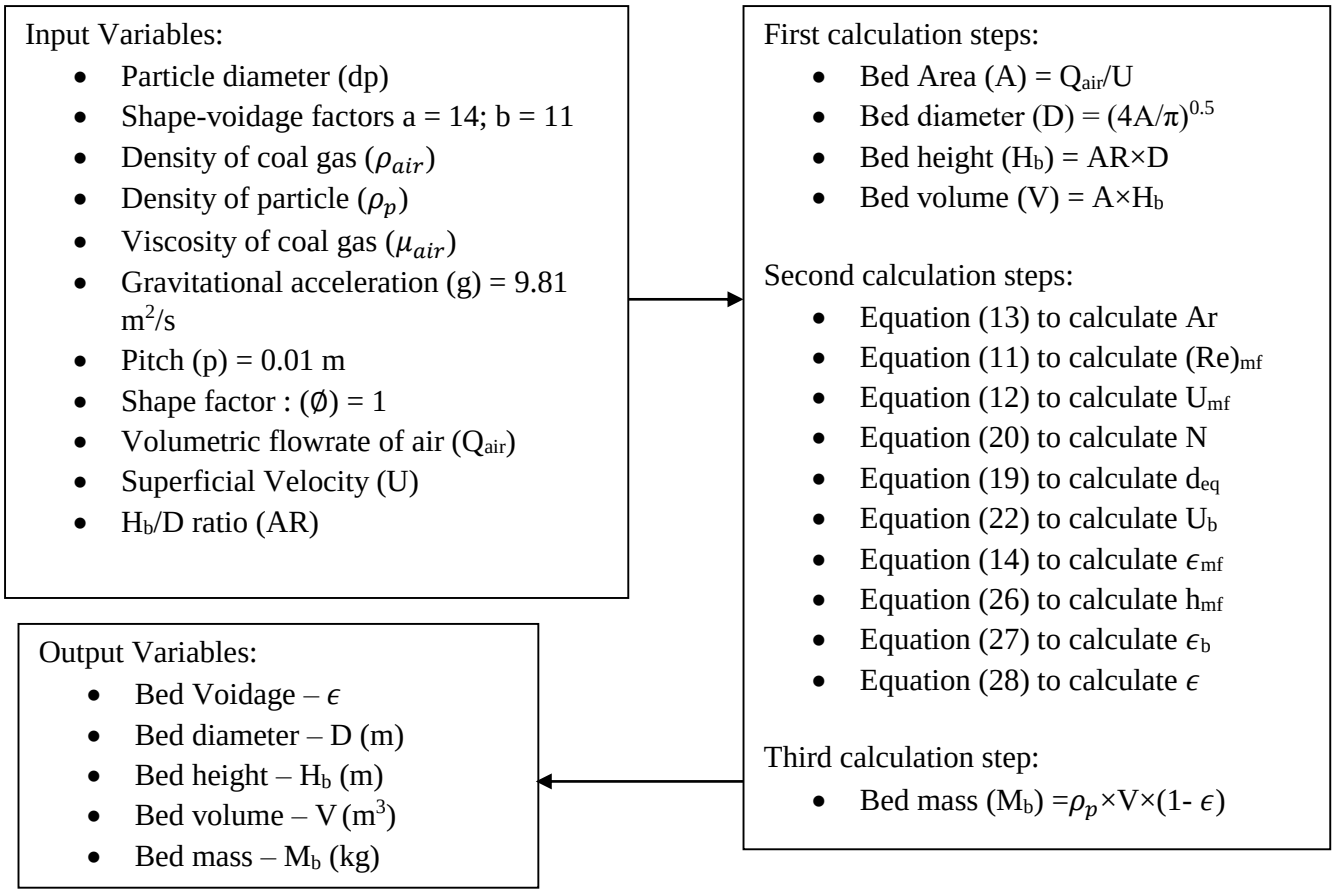

Figure 9: Fluidization algorithm for FB2

The effects of elutriation and TDH of the second fluidized bed was incorporated in the same calculator block as above. The calculation algorithm was as follows:

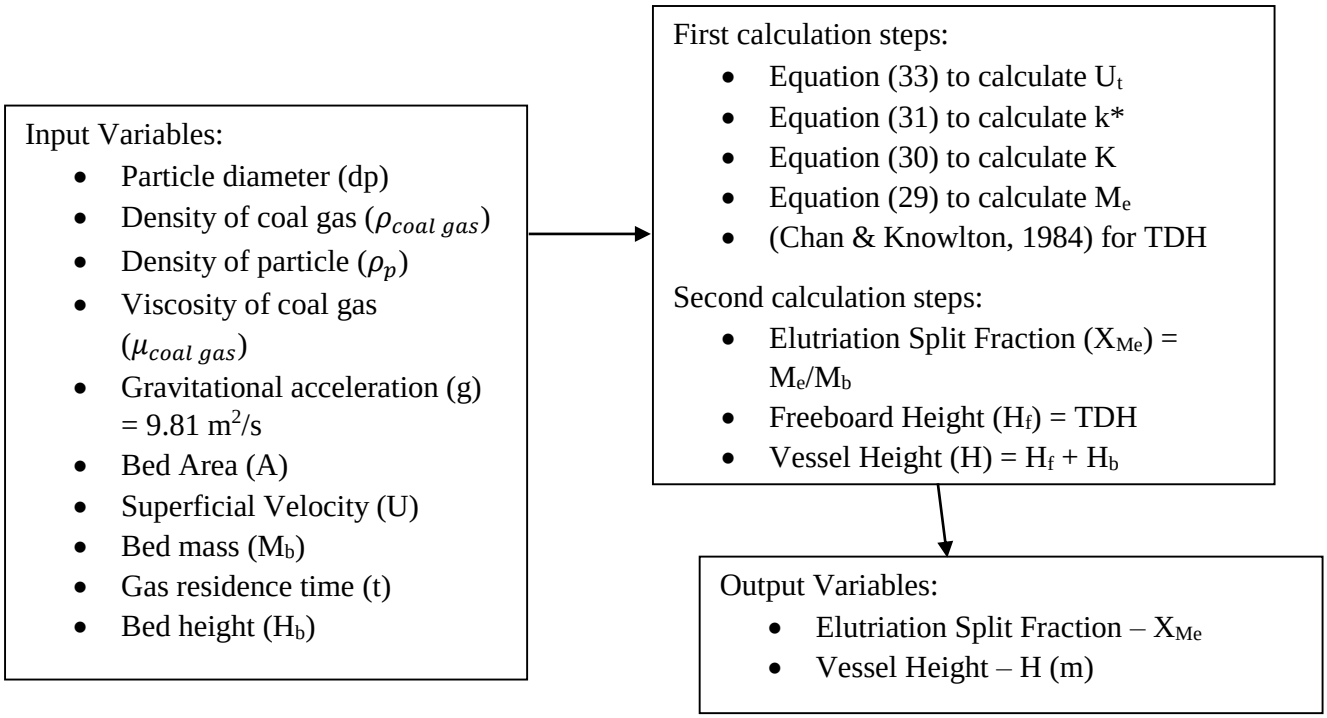

Figure 3-9: Elutriation and Vessel Height algorithm for FB2

A pitch of 1cm is chosen, anything bigger could result in jet penetration and inadequate particle movement (Geldart, 1985). Zinc oxide particles were assumed spherical for this design, therefore a shape factor of 1 was chosen. The superficial velocity and bed height to bed diameters were tuning parameters, which were investigated in the optimization of the fluidized bed. The gas residence time was used in equation 32, as it represents the residence time of the solids present at the interface between the dense bed and the freeboard. The calculator blocks used these parameters together with the kinetics to assess the performance of the fluidized bed. The results from these calculations included, the bed voidage, bed height (H_b), bed diameter (D), the vessel height (H) and the elutriation split fraction.

3.3.2.2) Reactions and Kinetics

The reaction kinetics were inputted via a reaction block R-2. The reaction between O_2 and zinc sulphide is shown below:

$$ZnS(s) + 1.5O_2(g) \leftrightarrow ZnO(s) + SO_2(g) \qquad Eq\ (58)$$

The reaction rate was assumed first order reaction with respect to the concentration dependency of O_2. The overall kinetic factor was calculated via a calculator block, RXN2. The calculation algorithm was as follows:

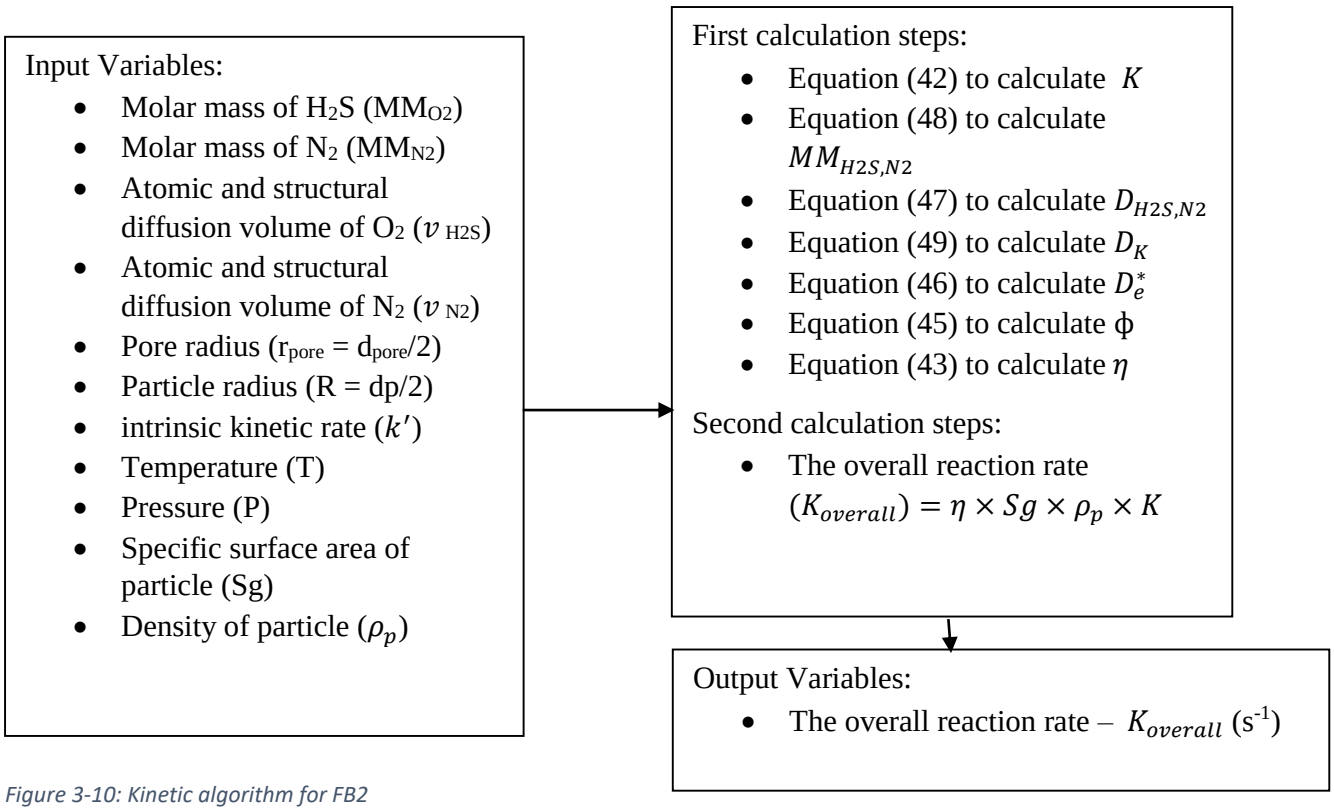

Figure 3-10: Kinetic algorithm for FB2

The shrinking-core model was chosen for the kinetic modelling of zinc oxide, therefore equation 35 was used. Turbulent operation was assumed; therefore, gas film diffusion was assumed negligible. For temperatures below 830°C the reaction rate is largely independent of the thickness of the product layer

of zinc oxide (*); therefore, product layer diffusion was assumed negligible. Equation 35 was then read as follows:

$$K = \frac{r_c'^2}{R'^2} k' \qquad \textit{Eq (59)}$$

A visual representation of the reacted particle in the regeneration process is shown on Figure 3-11:

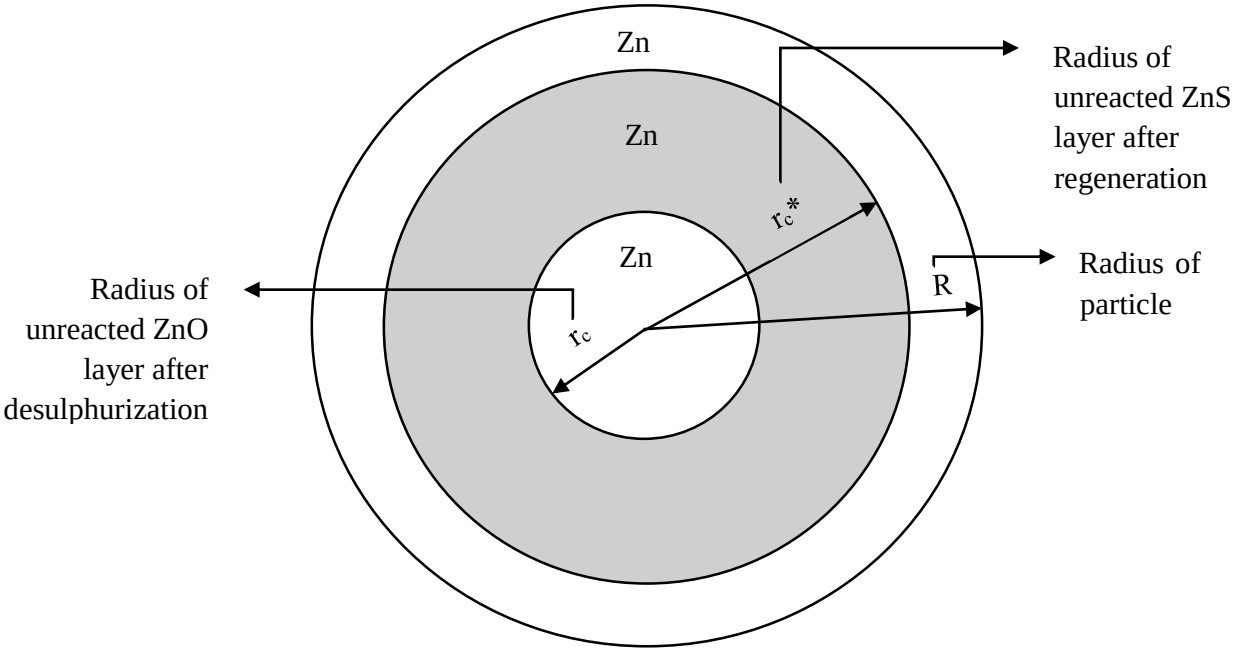

Figure 3-11: Visual representation of a reacted particle in the regeneration process

R' is the thickness of the zinc sulphide layer before regeneration. r_c' is the thickness of the unreacted zinc sulphide layer. From the figure above the follow applies:

- $R' = R - r_c$
- $r_c' = r_c^* - r_c$

r_c was used from the previous the desulphurization process. r_c* was calculated from the conversion (X_{ZnO}) of solid zinc sulphide layer using the following equation:

$$X_{ZnS} = 1 - \frac{R^3 - r_c^3}{r_c^{*3} - r_c^3} \qquad \textit{Eq (60)}$$

The conversion was expressed in terms of molar flowrates as follows:

$$X_{ZnS} = \frac{n_{ZnS,in} - n_{ZnS,out}}{n_{ZnS,in}} \qquad \textit{Eq (61)}$$

Where:

- $n_{ZnS,in}$ = molar flowrate of zinc sulphide entering the fluidized bed
- $n_{ZnS,out}$= molar flowrate of zinc sulphide exiting the fluidized bed

Using an outlet condition ($n_{ZnS,out}$), meant that calculator block, RXN1 was an iterative calculation. The simulation was reinitialized with previous results until convergence was reached. The intrinsic

kinetics (k') was extracted from (Prabhu, et al., 1984). The operating range of their work was 400-600°C. The rate was as follows:

$$k' = 1.12 \times 10^{17} e^{\left[-\frac{353000}{RT}\right]} \qquad \textit{Eq (62)}$$

Where:

- R = universal gas constant (8.314 J/mol.K)
- T = temperature (K)

3.3.2.3) Inlet and operating conditions

The operating conditions of the fluidized bed was set to 30 atm and 550°C, which was the same conditions of the inlet solids stream, therefore saving on auxiliary cost for the solids stream. A stream of air was fed in at 30 atm and 550°C, which was the operating conditions of the process.

3.3.2.4) Design Specifications

The flowrate of air was varied to achieve total sulphur recovery. The was done using a design specification block, ZNSOUT. The specification was the mass flowrate of ZnO exiting the FB2 is equal to the mass flowrate of ZnO entering the FB1. This ensure that all zinc sulphide is converted to zinc oxide.

3.3.3) Solid Separation

3.3.3.1) Solid Separator

A cyclone was the choice of solid separator used to remove the solid particles present in the gas effluent from the fluidized bed. This was modelled using cyclone blocks, CYC1 and CYC2. The gas stream out of the fluidized beds containing elutriated solids was fed into the cyclones. Gas streams exited the top of each cyclone and the solids at the bottom. The default calculation method of Leith-Licht was selected as it predicts the separation fairly accurate for the give particle size (50μm). This method uses experimental data to calculate the separation of solids in the cyclone. The cyclone can be characterized by eight dimensions that are often expressed as their ratio to the cyclone body diameter, D (Dirgo & Leith, 2007), as shown by the Figure 20.

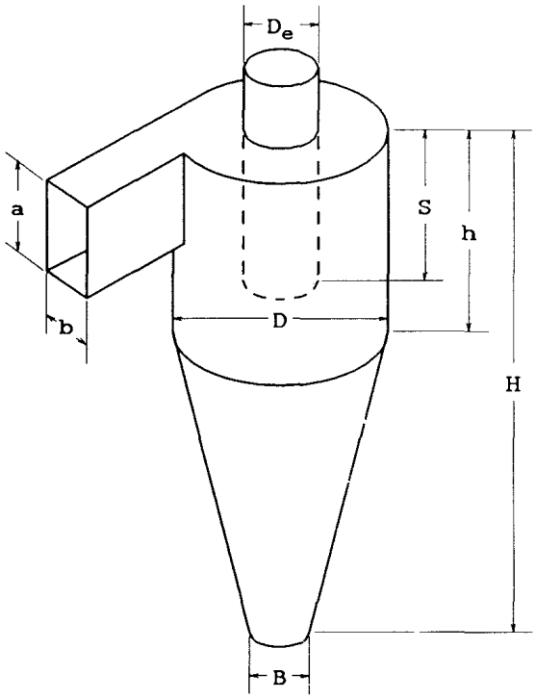

Figure 3-12: Cyclone dimensions

Table 3-6 below shows the dimension ratios for a Stairmand high-efficiency cyclone design (Stairmand, 1951) used in this design and dimensions were added to each of the cyclone blocks.

Dimensions	Dimension ratio (dimension/D)
Cyclone diameter, D	1
Gas outlet diameter, D_e	0.5
Inlet height, a	0.5
Inlet width, h	0.2
Outlet duct length, S	0.5
Cyclone height, H	4
Cylinder height, h	1.5
Dust outlet diameter, B	0.375

Table 3-6: Dimension Ratios of Stairmand High-Efficiency Cyclone

The cyclone diameter, D, was varied to achieve a separation efficiency fraction very close to 1 (0.9999; 1 = total solid separation). The was done using design specification blocks, CYCD-1 and CYCD-2 for cyclone blocks CYC1 and CYC2 respectively.

3.3.4) Auxiliary Units and Utilities

The only auxiliary units required for this design were a compressor, C-101, that discharges the air stream at 30 atm. The air temperature was found to be 663°C after compression, therefore a heat exchanger HX-1 was used to cool the air feed down to 550°C, before entering the second fluidized bed, FB2.

A eutectic mixture of NaO_3 and KNO_3 (60 wt.% $NaNO_3$, 40 wt.% KNO_3) was used as the heat transfer fluid. Its temperature range is close to the operating temperature of HX-1, and chosen against cooling

water, as cooling water would vaporize at these conditions. HEX-1 was used to simulate the heating of the molten salts passing through HX-1. A heat stream, Q, was used to represent the amount of heat gain by the molten salts. A design specification, MOLTIN, was used to achieve an outlet temperature of 575°C, by varying the flowrate of the molten salts flowrate. This made sure that the molten salt stream was not elevated close to or above its temperature range.

3.4) Hot Desulphurization (Supported metal-oxide)

Silica (SiO_2) was used as the support for zinc oxide sorbents in various desulphurization studies. The supported sorbent was produced by means of wet impregnation using a metal precursor. The properties of a supported sorbent prepared by (Govender, 2017) are shown below:

- Particle composition: 20 wt.% of ZnO and 80 wt.% SiO_2
- Particle density = 1046 kg/m^3
- Particle size = 100 µm
- Specific surface area of particle = 300 m^2/g
- Pore diameter = 12 nm
- Particle porosity = 0.717

3.4.1) Simulation set-up

The design of the supported zinc oxide process was conducted in the same manner as the free zinc oxide process. The mass flowrate of the supported zinc oxide sorbent was 5 times greater than the free zinc oxide. This was done to ensure that the mass flowrate of zinc oxide entering the desulphurization process was the same, as the weight percent of ZnO in the support was 20%. The difference in particle density was due to the difference in their composition. The particle size used for the supported sorbent process was the particle size produced by (Govender, 2017). The supported zinc oxide sorbent was less dense than the free zinc oxide sorbent. Supported metal-oxide sorbents have greater stability than free metal-oxide sorbents, but are not well-developed on an industrial scale, therefore a purge ratio of 0.5 was selected. The changes are listed on Table 3-7:

Sorbent flowrate and composition	
Free zinc oxide system	**Supported zinc oxide system**
163 kg/hr. (ZnO wt.% = 100)	815 kg/hr. (ZnO wt.% = 20; SiO_2 wt.% = 80)
Fluidization Blocks VOID1 and VOID2	
Parameters	**Free zinc oxide system** / **Supported zinc oxide system**
Density of particle - ρ_p (kg/m^3)	1830 / 1046
Particle size- d_p (µm)	50 / 100
Reaction Kinetic Blocks RXN1 and RXN2	
Parameters	**Free zinc oxide system** / **Supported zinc oxide system**
Pore diameter - d_{pore} (nm)	10 / 12
Density of particle - ρ_p (kg/m^3)	1830 / 1046

Particle porosity - ε	0.67	0.717
Specific surface area of particle – Sg (m^2/g)	17.9	300
Purge ratio	0.9	0.5

Table 3-7: Parameter changes for supported sorbent process

The structure of a supported sorbent was defined by (Govender, 2017) as a mesoporous solid that has small agglomerates (typically less than 1µm) of active species dispersed over the surface of the support and within its pores. Due to the small particle sizes of these agglomerates, they assumed that the reaction occurred at the surface of the agglomerate, therefore diffusion through the product layer and shrinking of unreacted core of agglomerates was assumed negligible. Equation 35 in both calculator blocks RXN1 and RXN2 was then read as follows:

$$K = k' \qquad Eq\ (63)$$

Supported sorbents are porous solids, therefore an effectiveness factor was incorporated. The specific surface area and particle density were multiplied to the kinetic factor to convert it from an area-based expression into a volumetric-based expression

3.5) Total Annual Cost (TAC) Analysis

A simple equation was described by (Luyben, 2010) to evaluate the total annual cost (TAC) of a new plant. This was the economic tool used to compare the economic requirements of each design. The equation was as follows:

$$TAC\ \left(\frac{R}{yr}\right) = \frac{Capital\ Cost\ (R)}{Payback\ period(yr)} + Operating\ Cost\left(\frac{R}{yr}\right) \qquad Eq\ (64)$$

The payback period is defined as the time required to pay back the initial investment of a plant and is generally between 3 and 5 years. A payback period of 3 years was selected for this design.

The capital and operating costs are broken down in the following sections:

3.5.1) Operating Cost

Since the costing method was developed as a comparative design, only the process materials and utilities were considered for the operating costs. The unit prices of theses process materials and utilities for each process are shown below:

Process Material (PM)	Unit Price
MDEA	1 $/ton
Water	33.3 R/ton
ZnO	2 $/kg
$ZnCl_2$	1 $/kg
SiO_2	130 $/ton
Utilities (UT)	**Unit Price**
Cooling water	33.3 R/ton
LP steam	4.16 $/ton
Molten Salts	1000 $/ton

Table 3-8 :Unit cost of process materials and utilities (Alibaba, n.d.)

The unit prices are multiplied by the required flowrate of the process materials and utilities to make up the operating costs and can be expressed as follows:

$$Operating\ Cost\left(\frac{R}{yr}\right) = \sum_{PM}\left[\text{Unit Price}\left(\frac{R}{kg}\right) \times Flowrate\left(\frac{kg}{yr}\right)\right] + \sum_{UT}\left[\text{Unit Price}\left(\frac{R}{kg}\right) \times Flowrate\left(\frac{kg}{yr}\right)\right]$$

Eq (65)

Molten salts are recyclable, provided the heat gained from the process fluid is removed and the molten salts is returned to its original condition. The heat generated by the molten salts can be used to generate steam or provide heating requirements for other process streams, therefore making it a capital cost. It is assumed that all three processes have the same molten salts capital costs, therefore the cost of molten salts was excluded from the total annual cost (TAC). Heating and pumping equipment for the utilities were not designed and also not incorporated in the total annual cost (TAC) of the amine process.

3.5.2) Capital cost

The capital cost of the process consists of the direct costs associated with each unit. Aspen Process Economic Analyzer (APEA) was used in tandem with Aspen Plus to determine the direct cost of each unit. There were two steps in using APEA to determine direct costs. The first was the mapping of each unit operation to determine the relevant pieces of equipment needed. Some unit operations may contain more than one piece of equipment. The mapping of the unit operations for each process were as follows:

Amine Unit Mapping

Unit Operation	Equipment Tag	Equipment Type	Description
TAR-TOW	TAR-TOW-tower	DTW TRAYED	Trayed tower
ABSORBER	ABSORBER-tower	DTW TRAYED	Trayed tower
REGEN	REGEN-tower	DTW TRAYED	Trayed tower
	REGEN-cond	DHE TEMA EXCH	TEMA shell and tube exchanger
	REGEN-cond acc	DHT HORIZ DRUM	Horizontal drum
	REGEN-reflux pump	DCP CENTRIF	Centrifugal pump
	REGEN-bottoms pump	DCP CENTRIF	Centrifugal pump
	REGEN-reb	DRB KETTLE	Kettle reboiler
HX-1	HX-1	DHE TEMA EXCH	TEMA shell and tube exchanger
HX-2	HX-2	DHE TEMA EXCH	TEMA shell and tube exchanger
HX-3	HX-3	DHE TEMA EXCH	TEMA shell and tube exchanger
HX-4	HX-4	DHE TEMA EXCH	TEMA shell and tube exchanger
HX-5	HX-5	DHE TEMA EXCH	TEMA shell and tube exchanger
P-101	P-101	DCP CENTRIF	Centrifugal pump
P-102	P-102	DCP CENTRIF	Centrifugal pump
C-101	C-101	DGC CENTRIF	Centrifugal compressor
T-101	T-101	DTURTURBOEXP	Turboexpander

Hot Desulphurization (Free and Supported metal-oxide) Mapping

Unit Operation	Equipment Tag	Equipment Type	Description
FB1	FB1	DTW PACKED	Packed tower
FB2	FB2	DTW PACKED	Packed tower
CYC1	CYC1	EDC CYCLONE	Cyclone dust collector
CYC2	CYC2	EDC CYCLONE	Cyclone dust collector
HX-1	HX-1	DHE TEMA EXCH	TEMA shell and tube exchanger
C-101	C-101	DGC CENTRIF	Centrifugal compressor

Table 3-9: Mapping of process equipment on APEA

For the hot desulphurization processes, dummy simulations were set up, similar to the process designed in chapter 3.3. The fluidized bed units are replaced by a RPLUG block. RPLUG block is used in the design of fixed bed reactors. A fluidized bed reactor is similar to a fixed bed reactor in terms of construction, the difference is in the bed characteristics and operating conditions, therefore it was used to determine the direct cost of the reactor vessel. Unit dimensions and material of construction specifications were added for the main units to get a more accurate prediction of their respective costs. The material of construction used throughout the design was stainless steel 316L, as conventional carbon steel would corrode under an H_2S present environment. Stainless steel 316L was shown to have a great corrosion resistance to H_2S therefore validating the choice.

The second part of the APEA process was the project evaluation. The engineering location was set to Johannesburg, South Africa. This was to ensure that cost indices relevant to South Africa were used and that the cost was estimated on a Rand [R] bases. APEA has a list of current vendors and their associated prices. For this design the default vendors were used. The direct cost of each unit operation comprised of the following costs:

- Equipment
- Piping
- Concrete
- Grout
- Piling
- Instrumentation
- Electrical wiring
- Equipment insulation
- Piping insulation
- Paint

The direct cost for each piece of equipment was extracted from the project evaluation. The capital cost for each plant design was then calculated as follows:

$$Capital\ Cost\ (R) = \sum_{i=Equipment}[Direct\ Cost_i(R)] \qquad Eq\ (66)$$

CHAPTER 4: MODELLING AND REGRESSION OF DESULPHURIZATION KINETICS

4.1) Data Extraction

The intrinsic kinetics (k') used in the desulphurization simulations were based on free zinc-oxide particles. This chapter aims to develop a model in order to regress for intrinsic kinetics of supported zinc oxide sorbent. The sorbent in question was the one produced in studies by (Neelan). A silica supported zinc oxide sorbent was prepared by means of wet impregnation, using $ZnCl_2$ as the metal precursor. The properties of the sorbent are shown on table 4-1.

Supported Sorbent Properties	
Particle composition	20 wt.% of ZnO and 80 wt.% SiO_2
Particle density	1046 kg/m^3
Specific surface area of particle	300 m^2/g
Pore diameter	12 nm
Particle porosity	0.717
Particle radius	50 µm

Table 4-1: Supported Sorbent properties

The desulphurization performance of the sorbent was tested in a packed bed reactor. A gas containing 1 mol% of H_2S was fed into the reactor. The procedure was carried out at 350°C and 550°C. Table 4-2 shows the characteristics of the system used by (Govender, 2017).

System Characteristics	
Bed diameter	2.1 cm
Bed length	2.3 cm
Bed voidage	0.373
Inlet gas velocity	0.05 m/s
Inlet molar concentration at 350°C	0.195 mol/m^3
Inlet molar concentration at 550°C	0.148 mol/m^3

Table 4-2: System characteristics of supported sorbent

Ratios of the inlet H_2S concentration to the outlet H_2S concentration were recorded over the duration of his runs in the form of break through curves. The data was extracted for 350°C and 550°C as shown in Appendix B. This provided experimental data on the performance of a silica supported zinc oxide sorbents to fit our model results.

4.2) Modelling

A model proposed by (Dasgupta, et al., 2003) was used to describe this system. In this model, a supported particle is assumed to consist of spherical grains of uniform size separated by pores through which the reacting gases diffuse. The reaction proceeds at the surface of the grain. Figure 4-1 is a visual representation of the sorption process in a supported porous sorbent.

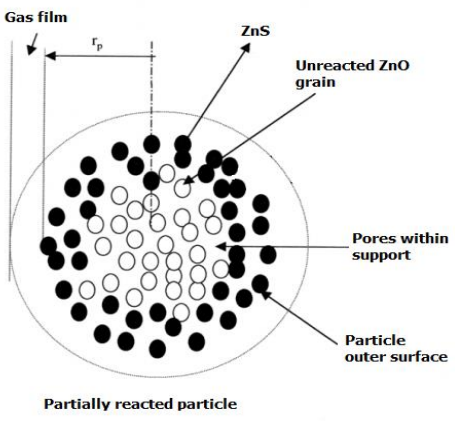

Figure 10:Visual representation of a supported sorbent

4.2.1) Mass balance in the packed bed reactor

Consider an isothermal plug flow system in a packed bed of spherical particles, in which pressure drop is negligible and there is no variation in the gas velocity along the length of the bed. By making a species balance in the gaseous phase in the packed bed the following equation is obtained:

$$\frac{\partial C_b}{\partial t} + \frac{U}{\epsilon}\frac{\partial C_b}{\partial z} = D_z \frac{\partial^2 C_b}{\partial z^2} - \frac{1-\epsilon}{\epsilon} K_m a \left(C_b - C_P|_{r\,=\,r_p}\right) \qquad \textit{Eq (67)}$$

Where:

- t = time, (s)
- z = axial position in the bed
- C_b = concentration of gas reactant in the bed, (mol/m^3)
- C_p = concentration of gas reactant within the pores of particle, (mol/m^3)
- U = superficial gas velocity, (m/s)
- ϵ = bed voidage
- D_z = axial diffusion co-efficient of reactant gas, (m^2/s)
- K_m = average mass transfer coefficient
- a = external surface area per unit volume of the particle, (m^2/m^3)
- r = radius, (m)
- r_p = radius of particle, (m)

An efficient method for the numerical solution of this system is the method of lines. In this method the spatial derivatives are discretized, while the time derivative is not. This reduced equation 67 to an ordinary differential equation (ODE), which will simplify the numerical computations and reduce the CPU time further, therefore the mass balance was read as:

$$\frac{dC_{bi}}{dt} + \frac{U}{\epsilon}\frac{C_{bi+1} - C_{bi-1}}{2\Delta z} = D_z \frac{C_{bi-1} - 2C_{bi} + C_{bi+1}}{\Delta z^2} - \frac{1-\epsilon}{\epsilon} K_m a \left(\frac{C_{bi} - C_{Pi}|_{r\,=\,r_p}}{1}\right) \qquad \textit{Eq (68)}$$

The terms on the left-hand side of the above equation are the unsteady-state and convection terms, while those on the right-hand side are the axial dispersion and flux, respectively. The boundary conditions for equation 68 are:

$$C_{bi} = C_{b0} \;\; at\ z = 0;\ \frac{C_{bi+1} - C_{bi-1}}{2\Delta z} = 0\ at\ i = N; \qquad Eq\ (69)$$

Where i represents the position along the reactor bed and N is the number spatial positions along the reactor bed.

4.2.2) Balance within pores of a particle located at distance z in the reactor:

The mass balance of diffusing reactant gas inside the pores of the spherical particle at an axial location z in the bed is given as:

$$\varepsilon \frac{\partial C_p}{\partial t} + \frac{1}{r^2}\frac{\partial}{\partial r}(r^2 N_r) + a f_p(r) = 0 \qquad Eq\ (70)$$

Where:

- N_r = molar diffusion flux in the radial direction of the grain
- f_p = flux owing to the chemical reaction at the solid reactant surface

Equation 70 is a partial differential equation (time and radial directions being independent variables), therefore an approach was adopted to simplify numerical computations and significantly reduce the CPU time further. In this approach, radial concentration profiles within the solid pores were averaged and the average surface and gas phase concentrations within the pores of the particles were determined as follows:

$$\frac{d\bar{C}_{pi}}{dt} - \frac{3}{r_p} K_m \left(C_{bi} - C_{Pi}|_{r = r_p} \right) + \frac{3(1-\epsilon)}{r_p \epsilon} k' \bar{C}_{pi} = 0 \qquad Eq\ (71)$$

Where the concentration of gas reactant within the pores at the periphery of the spherical particle was determined as:

$$C_{Pi}|_{r = r_p} = \frac{\left(K_m C_{bi} + \frac{5D_e}{r_p} \bar{C}_{pi} \right)}{\left(K_m + \frac{5D_e}{r_p} \right)} \qquad Eq\ (72)$$

Where D_e is the effective diffusion co-efficient of reactant gas(m^2/s). The boundary condition for equation 71 was:

$$\bar{C}_{pi} = 0 \;\; at\ t = 0\ along\ the\ length\ of\ the\ bed \qquad Eq\ (73)$$

The original partial differential equation 70, was reduced to an ordinary differential equation 71 with only z dependence by the aforementioned assumptions. Together with equation 68, the model describes the sorbent behaviour in a packed bed of porous supported solid sorbents in a gas flow under isothermal conditions. This resulted in a system of ordinary differential equations as a function of time, containing dependent variables C_{bi} and $\bar{C}_{pi}$. The ODE system was implemented in MATLAB (shown in Appendix C.1) with the ODE system reading as follows:

$$
\begin{vmatrix}
\left(\frac{dC_b}{dt}\right)_{i=0} \\
\left(\frac{dC_b}{dt}\right)_{i=1} \\
\vdots \\
\left(\frac{dC_b}{dt}\right)_{i=N} \\
\left(\frac{d\bar{C}_p}{dt}\right)_{i=0} \\
\vdots \\
\left(\frac{d\bar{C}_p}{dt}\right)_{i=N}
\end{vmatrix}
=
\begin{vmatrix}
0 \\
D_z \frac{C_{b0} - 2C_{b1} + C_{b2}}{\Delta z^2} - \frac{1-\epsilon}{\epsilon} K_m a \left(C_{b1} - \frac{\left(K_m C_{b1} + \frac{5D_e}{r_p}\bar{C}_{p1}\right)}{\left(K_m + \frac{5D_e}{r_p}\right)} \right) - \frac{U}{\epsilon}\frac{C_{b2} - C_{b0}}{2\Delta z} \\
D_z \frac{C_{bN-1} - 2C_{bN} + C_{bN+1}}{\Delta z^2} - \frac{1-\epsilon}{\epsilon} K_m a \left(C_{bN} - \frac{\left(K_m C_{bN} + \frac{5D_e}{r_p}\bar{C}_{pN}\right)}{\left(K_m + \frac{5D_e}{r_p}\right)} \right) \\
\frac{3}{r_p} K_m \left(C_{b0} - \frac{\left(K_m C_{b0} + \frac{5D_e}{r_p}\bar{C}_{p0}\right)}{\left(K_m + \frac{5D_e}{r_p}\right)} \right) + \frac{3(1-\epsilon)}{r_p \epsilon} k' \bar{C}_{p0} \\
\frac{3}{r_p} K_m \left(C_{b0} - \frac{\left(K_m C_{bN} + \frac{5D_e}{r_p}\bar{C}_{pN}\right)}{\left(K_m + \frac{5D_e}{r_p}\right)} \right) + \frac{3(1-\epsilon)}{r_p \epsilon} k' \bar{C}_{pN}
\end{vmatrix}
$$

The external surface area per unit volume of the particle (a) was calculated as follows:

$$a = Sg \times \rho_p \qquad \textit{Eq (74)}$$

The pore structures of the supported sorbent are well defined, therefore D_e was estimated using equation 40. The solution of the model was insensitive to K_m , therefore the Chilton and Colburn analogy for mass transfer was used as follows:

$$j_M = j_D \equiv \frac{K_m}{U}(N_{Sc})^{2/3};\ N_{Sc} = \frac{\mu}{\rho D_{AB}} \qquad \textit{Eq (75)}$$

The average transport coefficient, j_D, for flow through beds packed with spherical particles of size D_p $(2r_p)$ is as follows:

$$j_D = 1.17(N_{Re})^{-0.415};\ N_{Re} = \frac{D_p.\rho.U}{\mu} \qquad \textit{Eq (76)}$$

Where, ρ is the density of the gas stream and μ is the viscosity of the gas stream. These properties were estimated using Aspen Plus. The number of spatial points (N) was set to 201 and was varied correct any mathematical instabilities. The spatial increment (Δz) was then calculated as follows:

$$\Delta z = \frac{Bed\ length}{N-1} \qquad \textit{Eq (77)}$$

4.3) Regression and Results

The solution of the ODE system was implemented on MATLAB (shown in Appendix C.2). This system was stiff therefore, ode15s solver was used to solve the differential equations and subsequently plot the concentration vs time data. A brute force approach was adopted for this regression, using D_z and k'as the tuning parameters. Multiple combinations of D_z and k' were tested until the model fitted the experimental data.

At 350°C, K_m and D_e were calculated to be 7.8 x10^{-3} [m/s] and 1.2 x10^{-9} [m^2/s] respectively. A fit was obtained using D_z and k'values of 1x10^{-5} [m^2/s] and 2x10^{-11} [m/s] respectively. The fit can be seen on Figure 4-2.

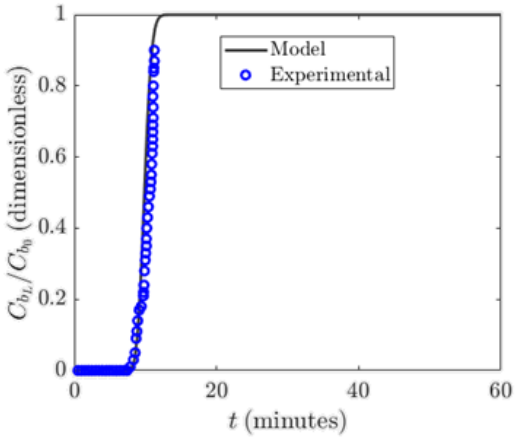

Figure 11: Model fit against experimental data at 350°C extracted from MATLAB

The change in concentration along the length of the bed can be seen on the Figure 4-3. It can be seen that the concentration of reactant gas decreased along the length of the bed. As time increased the concentration decreased further along the bed as the sorbent began to saturate. Once saturation of the sorbent was reached the concentration of the reactant remain constant throughout the bed. These results represent typical concentration behaviour in a packed bed reactor, placing greater confidence in the regressed values

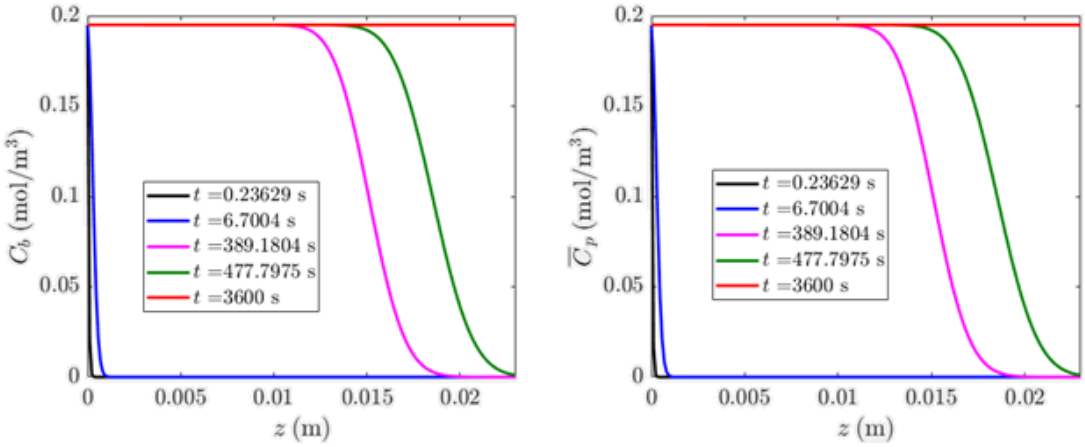

Figure 12: Gas concentration along the length of the bed at 350°C extracted from MATLAB

At 550°C, K_m and D_e were calculated to be 0.0109 [m/s] and 1.5 x10^{-9} [m^2/s] respectively. The fit was obtained using D_z and k'values of 5x10^{-5} [m^2/s] and 1x10^{-10} [m/s] respectively. The fit can be seen on Figure 4-5. The deviation of during initial part of the experimental data from the model could be a result of gas channeling or bypass of reactant gas through the bed.

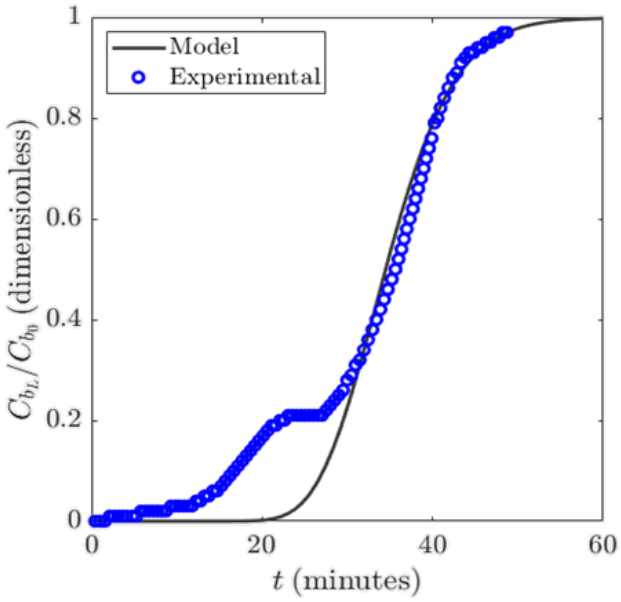

Figure 13-5: Model fit against experimental data at 550°C extracted from MATLAB

The change in concentration along the length of the bed can be seen on the Figure 4-6. It can be seen that the concentration of reactant gas decreased along the length of the bed. As time increased the concentration decreased further along the bed as the sorbent began to saturate. Once saturation of the sorbent was reached the concentration of the reactant remain constant throughout the bed.

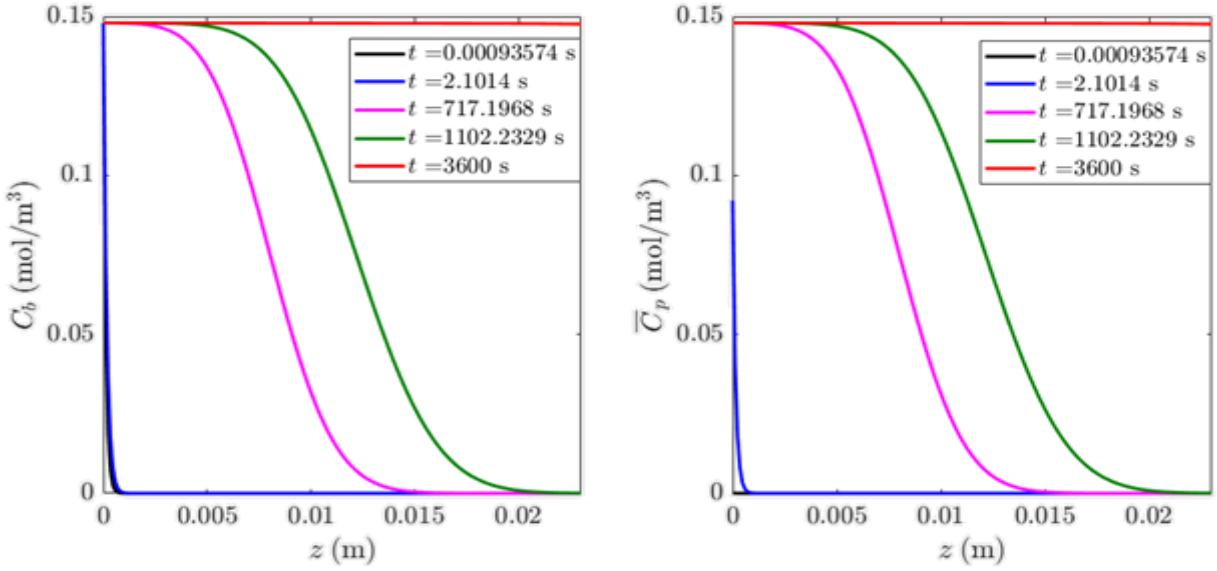

Figure 4-6: Gas concentration along the length of the bed at 550°C extracted from MATLAB

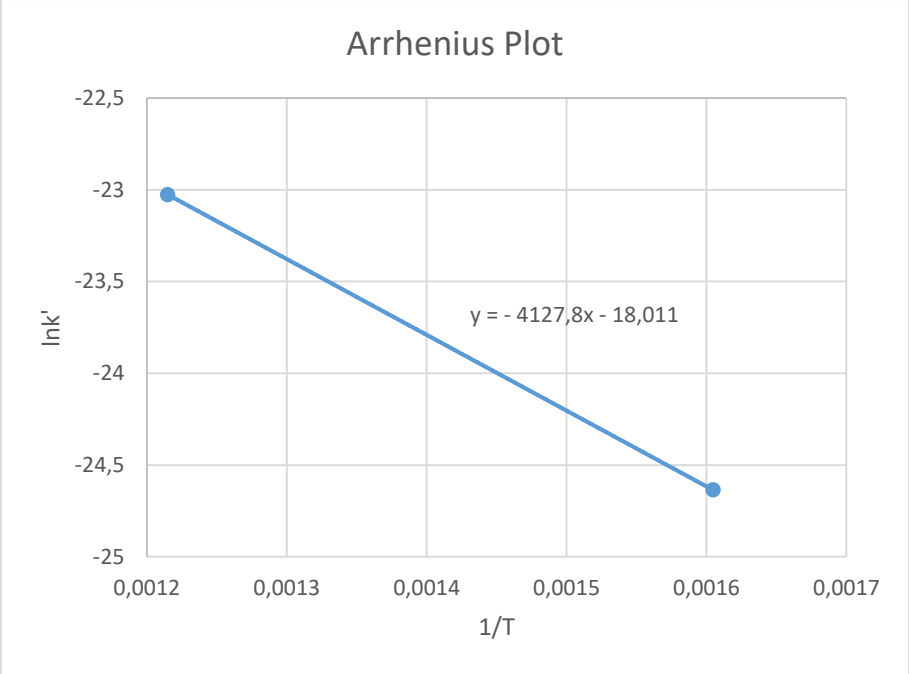

Figure 4-7: Arrhenius Plot

An Arrhenius plot was drawn up for this system and is shown on Figure 4-7 along with the equation of the plot. From the equation of the plot, the pre-exponential factor can be determined from the y-intercept and the activation energy from the gradient. The activation energy (Ea), pre-exponential factor ($k_0{}'$) and the intrinsic rate expression (k') were determined as follows:

$$-\frac{Ea}{R} = -4127.8 \quad ; \quad Ea = 34319\, J/mol \qquad \textit{Eq (78)}$$

$$ln(k_0{}') = -18.011 \; ; \; k_0{}' = 1.51 \times 10^{-8} \qquad \textit{Eq (79)}$$

$$k' = 1.51 \times 10^{-8} e^{-\frac{34319}{RT}} \qquad \textit{Eq (80)}$$

CHAPTER 5: RESULTS AND DISCUSSION

5.1) Gasification

For the gasification process, reactor bed volume was the key optimization variable. The dimensions of the bed i.e. bed diameter and bed height, are varied in a sensitivity analysis to determine the optimal bed volume. From the figure below it can be seen that the mass conversion of coal to coal gas remains constant at 92% for bed dimensions greater than 2m. This was the maximum conversion that could be achieved as the reaming 8 wt% of the coal consisted of and inert ash product. The smaller the bed the smaller the reactor vessel, which reduces material and installation costs.

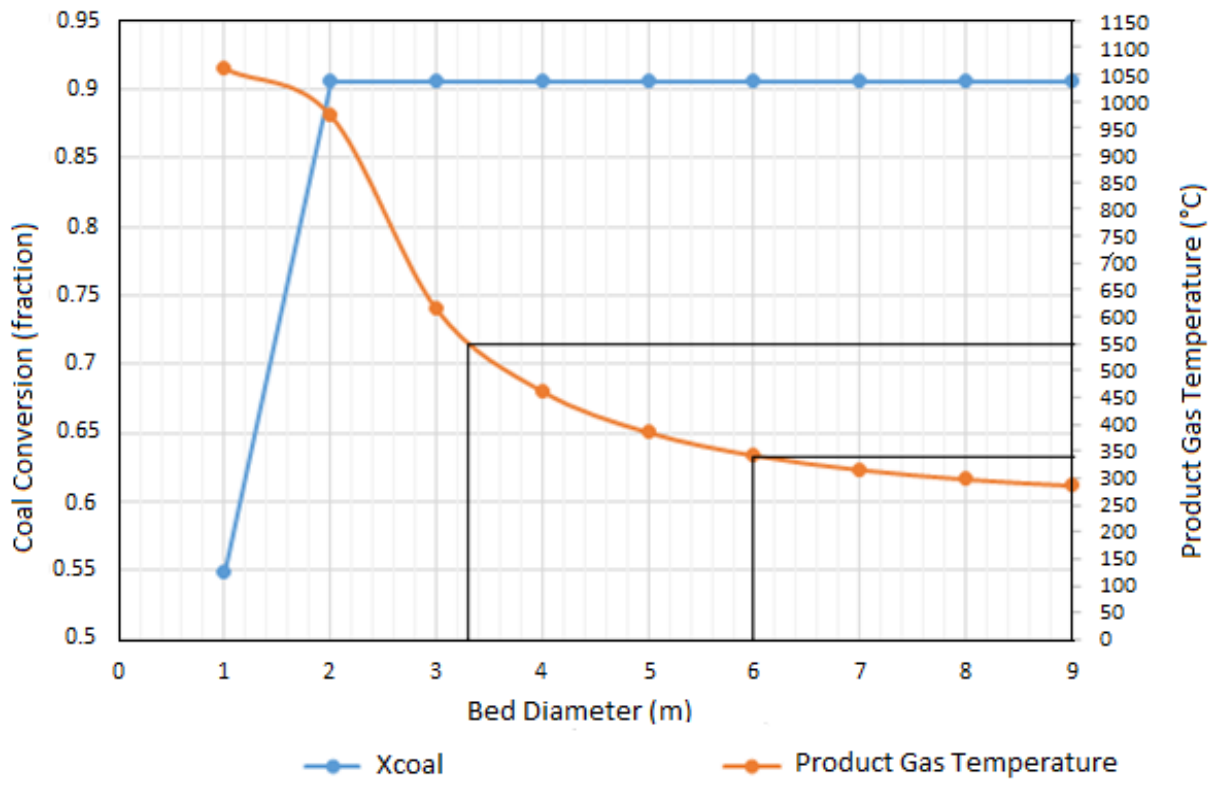

Figure 5-1: Coal Conversion and Product Gas Temperature versus Bed diameter

The product temperature decreases as the bed diameter increases. Lower product temperature means less cooling required for downstream processes, which operate at much lower temperatures. There were two designs considered for the gasifier. The first gasifier has a bed diameter of 6m for the amine absorption process, as the degree of cooling of the product gas decreases drastically after dimensions were increased from this point. The second gasifier has a bed diameter of 3.3 m for the hot desulphurization processes, as this produced a coal gas temperature of 550°C, required for the downstream processes. Figure 5-2 plots the bubble diameter (Db) against the bed diameter (D) and

a third of the bed diameter (D/3). The bubble diameter ($d_b \approx d_{eq}$) must be less than a 1/3 of the bed diameter (Dechsiri, 2004) to avoid slagging operation. The bubble diameter (denoted by the gray line) is less than a third of the bed diameter (denoted by the red line), which means all data points taken from this sensitivity consider operation without significant slagging.

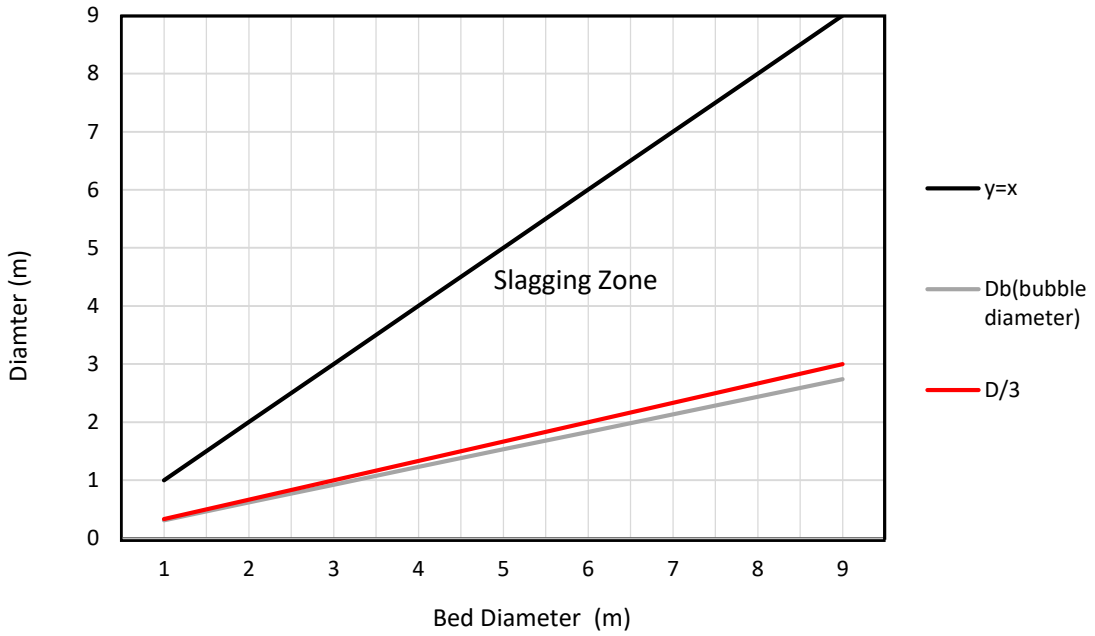

Figure 5-2: bubble diameter versus bed diameter

5.2) Amine Absorption

5.2.1) Tar removal

A column height and diameter of 1.3 m and 2.5 m respectively was used to achieve hydraulic operability. The spacing between each stage was set to 0.65 m. The water flowrate of 148 135 kg/hr was required and was split evenly into two streams (74 067.5 kg/hr each). One stream entered the first stage and other was supplied to the second stage.

5.2.2) Desulphurization

In the sensitivity analysis the number of stages is varied to determine the number of stages that uses the least amount of amine solution to meet the desired design composition of 3.9 ppm (less than the limit of 4ppm) of H2S in the sweetened product gas. Lower amine solution means lower operating costs and should be minimized. Lower solution feed also means less solvent carried over into the stripper, therefore lowering the duties required for regeneration.

From Figure 5-3 it can be seen that as the number of stages increases, the amount of feed solvent required decreases until stage 13 and starts to increase thereafter. This makes 13 tray stages the optimal number of stages, with a solvent feed rate of 450.37 kmol/hr. Tray diameters and tray spacing of 2.2m and 0.45m was used to achieve hydraulic operability throughout the sensitivity.

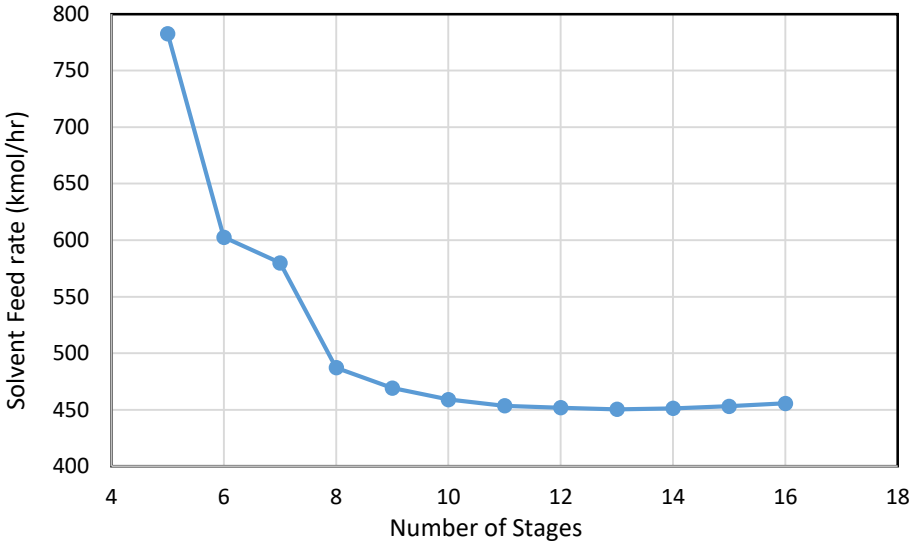

Figure 5-3: Solvent Feed rate versus Number of Stages

5.2.3) Regeneration

For the stripper, feed temperature was the optimization variable. The feed temperature was varied from 60°C to 110°C. For feed temperatures above 110°C, reboiler temperature exceeded 120°C, violating the temperature constraint on the design. From Figure 5-4 it can be seen that a higher feed temperature will reduce the duty required for regeneration. This is at the cost of preheating the feed. This make 110°C the optimal feed temperature as this requires the lowest duties for operation, having a reflux ratio and boilup ratio were found to be 0,0964656 and 0,990794 respectively, while maintaining a reboiler temperature (118,24°C) of less than 120°C.

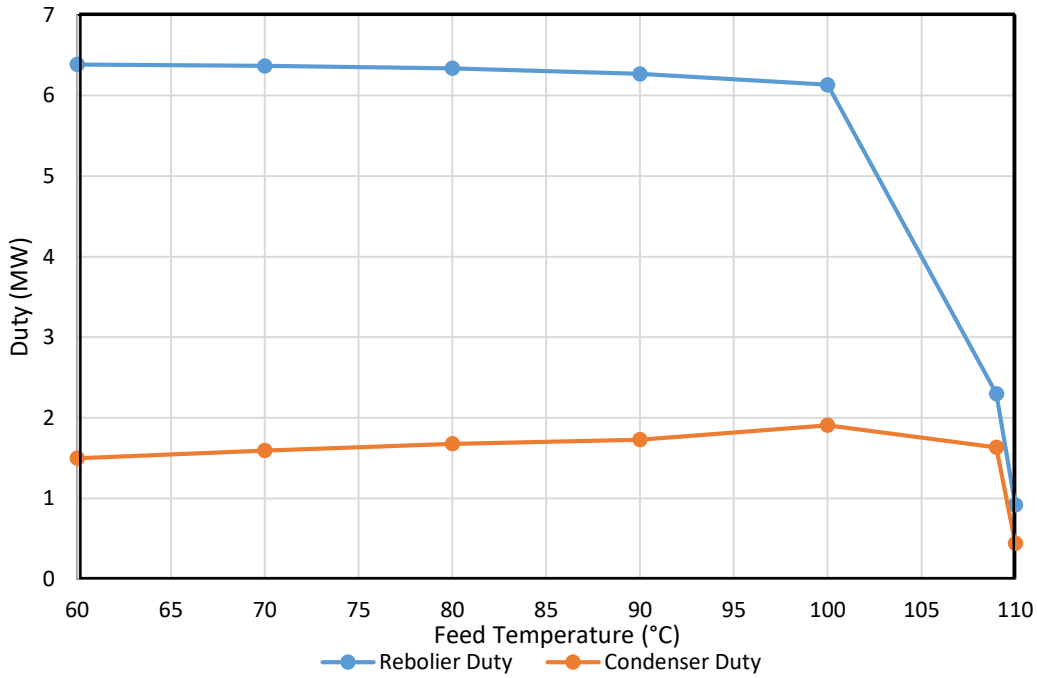

Figure 5-4: Regenerator column duties versus feed temperature

Hydraulic operability was slightly more difficult to achieve as compared to the absorber. With changing reflux and boilup ratios, vapour and liquid levels varied, requiring a change in column internals across the sensitivity analysis. A tray spacing of 0.61m was chosen along with the various tray diameter on the table below, to satisfy the hydraulic checks.

Feed Temperature (°C)	Column Diameter (m)
60	1.33
70	1.32
80	1.32
90	1.31
100	1.3
109	1.2
110	0.65

Table 5-1: Column Diameter required at feed temperature for regeneration

5.2.4) Utilities

A molten salts flowrate of 119 203 kg/hr was required for the cooling of coal gas in HX-1 and heating of sweet gas in HX-5. Cooling water flowrates of 34 461.6 kg/hr, 7364.3 kg/hr and 5828 kg/hr were required for cooling in HX-2, HX-4 and the regenerator condenser respectively. Low pressure steam flowrates of 7259.3 kg/hr and 1501.84 kg/hr were required for heating in HX-3 and the regenerator reboiler.

5.3) Hot Desulphurization (Free metal-oxide)

The main objective in the optimization of the fluidized beds was to choose the least expensive design that meets all design specifications. (Luyben, 2010) uses the vessel height and diameter to calculate the capital cost of a column vessel as follows:

$$Column\ capital\ cost = 17640(D)^{1.066}(H)^{0.802} \qquad Eq\ (81)$$

This equation serves as an estimated vessel cost for the optimization of the fluidized beds, as integrating APEA in the optimization process on ASPEN PLUS became too tedious.

5.3.1) Desulphurization

The superficial velocity was the variable investigated for the optimization of FB1. The superficial velocity determined the vessel dimensions required to achieve the desired design composition of 3.9 ppm of H_2S in the sweetened product gas, and a cost estimate for FB1. The superficial velocity was varied in a sensitivity from 0.1 to 1.5 m/s and the cost estimates for FB1 are shown on the figure below.

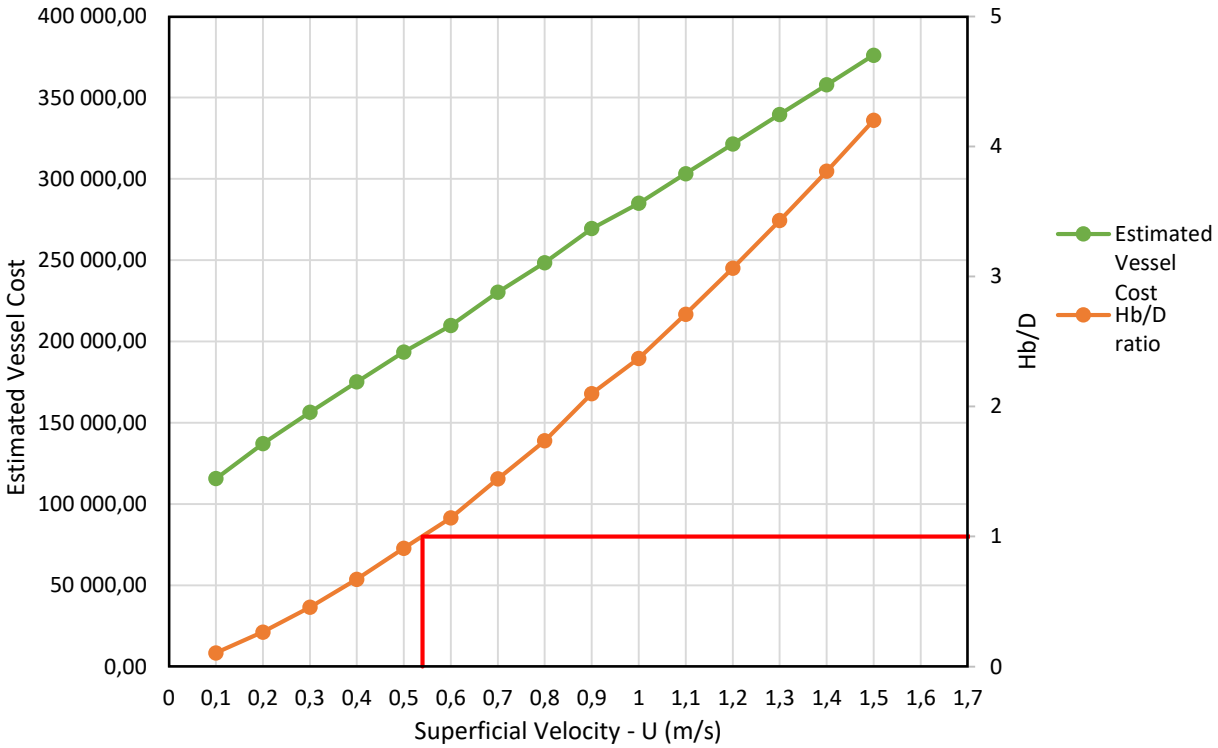

Figure 5-5: Estimated Vessel Cost and bed height to bed diameter ratio of (FB1-free sorbent) versus Superficial gas velocity

It can be seen the cost of the vessel (denoted by the green line) increased with superficial velocity, therefore a lower velocity would produce a cheaper design. The bed height to diameter ratio (H_b/D) was an important design consideration used for the optimization of FB1. If the H_b/D ratio is too small, it could lead to insufficient gas-solid contact time and if the H_b/D ratio is too large then the vessel could suffer from excessive structural stress. Typical (H_b/D) ratios of fluidized bed reactors

range from 1-5:1 (*). The H_b/D ratios for each design are denoted by the orange line on the figure above. It can be seen that the H_b/D ratio increased with superficial velocity. A superficial velocity of 0.54 m/s as this produced a H_b/D ratio of 1:1, which is the minimum ratio of range for typical fluidized bed reactors.

5.3.2) Regeneration

A bed height (H_b) was required in order to produce the bed volume necessary to carry out the regeneration. A bed height to diameter ratio (H_b/D) was investigated along the superficial velocity for the optimization of FB2. H_b/D ratios of 1:1, 3:1 and 5:1 were used for this design as it considered values throughout the range. The superficial velocity was varied from 0.1 to 0.5 m/s for each of the H_b/D ratios and the cost estimates for FB2 are shown on the figure below.

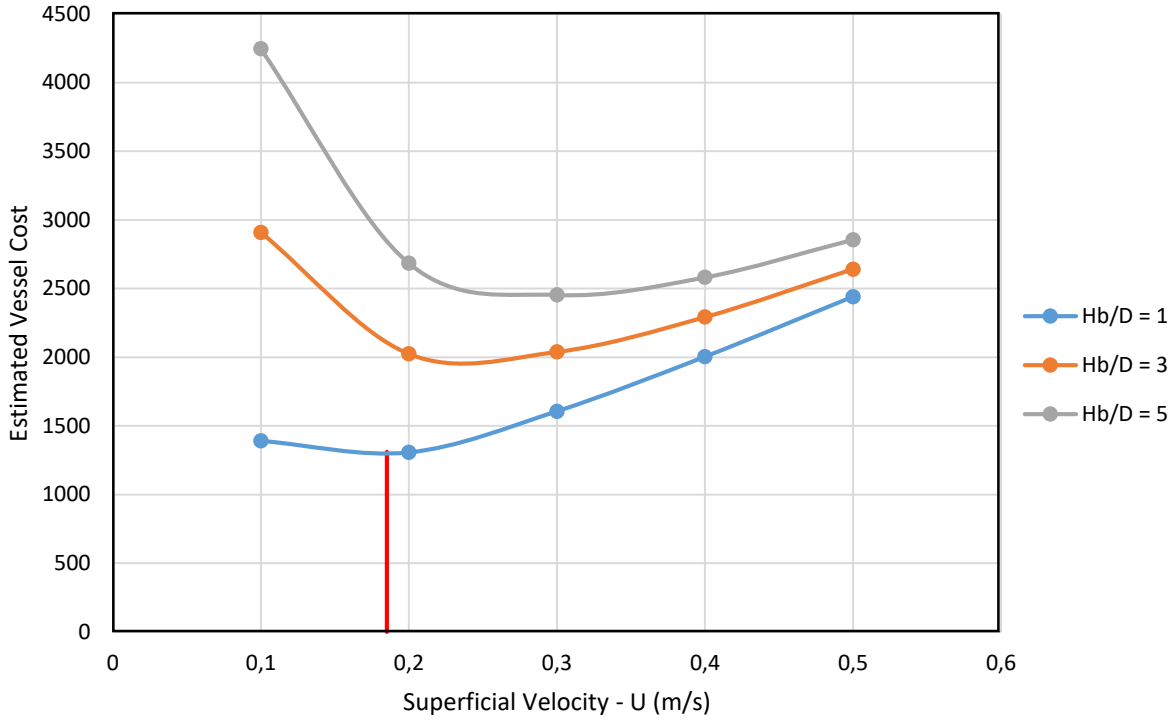

Figure 5-6: Estimated Vessel Cost of (FB2-free sorbent) at various bed height to bed diameter ratios versus Superficial gas velocity

It can be seen from the figure above that lower H_b/D ratios result in lower costs, therefore a H_b/D ratio of 1:1 was chosen. The lowest cost (denoted by the black line) was achieved with a superficial velocity of 0.185 m/s and was selected.

5.3.3) Solid separation and Utilities

Diameters of 1.43m and 0.08m were required for the first and second cyclone respectively, to achieve a solid separation efficiency close to 100%. The flowrate of 59 kg/her of molten salts was used to achieve the cooling in HX-1.

5.4) Hot Desulphurization (Supported metal-oxide)

5.5.1) Desulphurization

The simulation of the regressed kinetics resulted in a superficial gas velocity of 0.00712 m/s in order to achieve an H_b/D ratio of 1. This produced a bed diameter (D) and bed height (H_b) of 25.8 m which are unrealistic for a fluidized bed reactor. The model used for the regression did not consider product layer diffusion as an inhibiting factor. The intrinsic kinetics obtained from the regression compared to literature kinetics was found to be 6 orders of magnitude lower. The low intrinsic rate constant extracted from the regression may not be a true reflection of the reaction behaviour, if mass transfer limitations through the product layer diffusion were significant. It was decided that the intrinsic rate constant and product layer diffusion rate constant from literature would be incorporated in the kinetics for the supported sorbent, therefore equation 35 in the kinetic calculator block, RXN1, was read as:

$$K = \frac{1}{\frac{R_{agg}(R_{agg}-r_c)}{r_c D_e} + \frac{{R_{agg}}^2}{r_c^2 k'}} \qquad \textit{Eq (82)}$$

Where R_{agg} is the particle size of an agglomerate and was found to be 50 nm (Govender, 2017). The superficial velocity was the variable investigated for the optimization of FB1. The superficial velocity determined the vessel dimensions required to achieve the desired design composition of 3.9 ppm of H_2S in the sweetened product gas, and a cost estimate for FB1. The superficial velocity was varied in a sensitivity from 1 to 8 m/s and the cost estimates for FB1 are shown on the figure below.

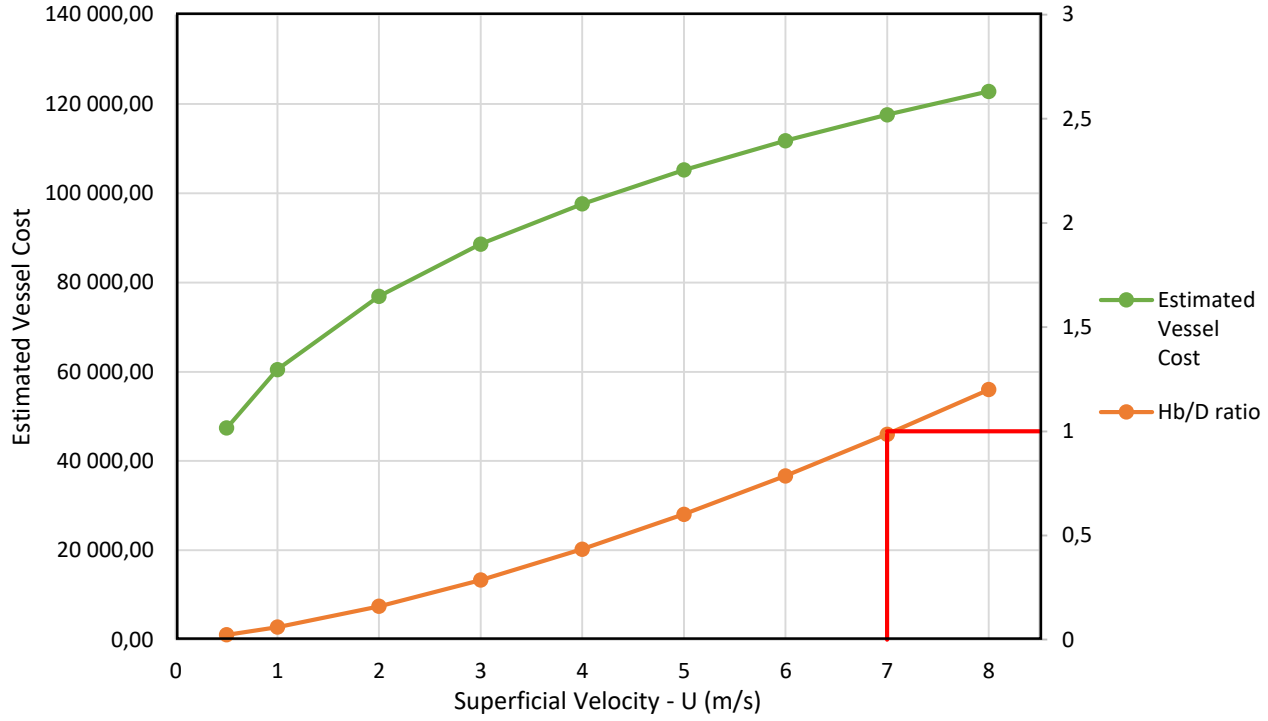

Figure 5-7: Estimated Vessel Cost and bed height to bed diameter ratio of (FB1-supported sorbent) versus Superficial gas velocity

It can be seen the cost of the vessel (denoted by the green line) increased with superficial velocity, therefore a lower velocity would produce a cheaper design. The H_b/D ratios for each design are denoted by the orange line on the figure above. It can be seen that the H_b/D ratio increased with superficial velocity. A superficial velocity of 7m/s was chosen as this produced a H_b/D ratio of 1:1, which is the minimum ratio of range for typical fluidized bed reactors. This produced a vessel height to diameter (H/D) of 16.7:1 which falls in the range of 1.7-20:1 for typical fluidized bed reactors (*)

5.3.2) Regeneration

A bed height (H_b) was required in order to produce the bed volume necessary to carry out the regeneration. A bed height to diameter ratio (H_b/D) was investigated along the superficial velocity for the optimization of FB2. H_b/D ratios of 1:1, 3:1 and 5:1 were used for this. The superficial velocity of air was varied from 0.1 to 0.9 m/s for each of the H_b/D ratios and the cost estimates for FB2 are shown on the figure below.

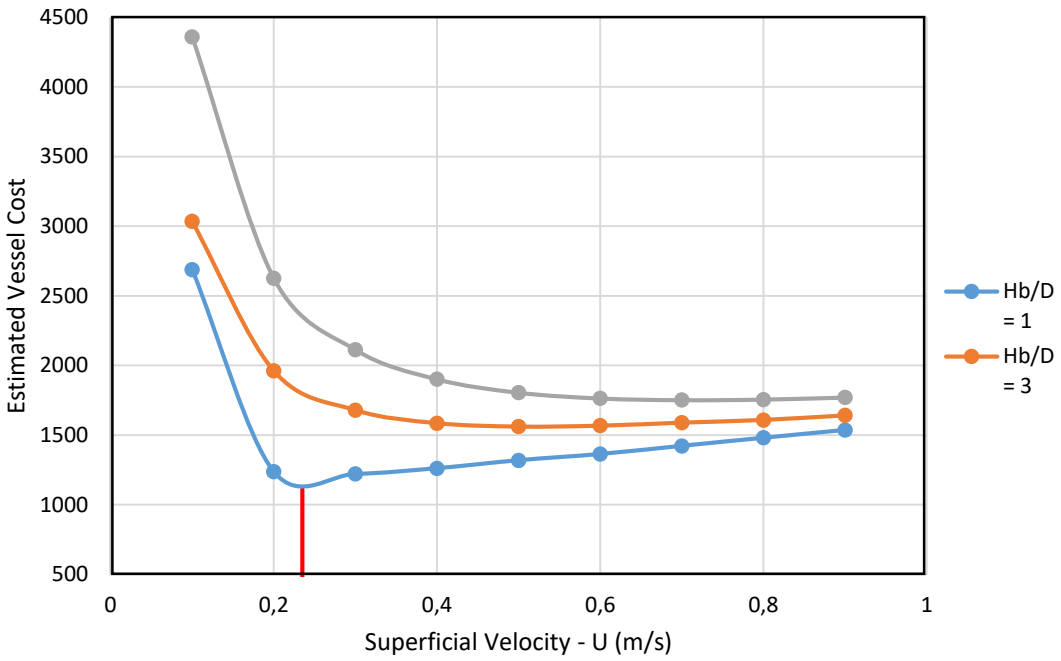

Figure 5-8: Estimated Vessel Cost of (FB2-supported sorbent) at various bed height to bed diameter ratios versus Superficial gas velocity

It can be seen from the figure above that lower H_b/D ratios result in lower costs, therefore a H_b/D ratio of 1:1 was chosen. The lowest cost (denoted by the black line) was achieved with a superficial velocity of 0.235 m/s and was selected.

5.3.3) Solid separation and Utilities

Diameters of 1.5m and 0.11m were required for the first and second cyclone respectively, to achieve a solid separation efficiency close to 100%. The flowrate of 59 kg/her of molten salts was used to achieve the cooling in HX-1.

5.5) Process summaries

This section contains the summaries for each process. The summaries show the sequence of process equipment and auxiliary units, optimised vessel dimensions of process equipment and operating conditions of all units for each process. The amine absorption process summary is shown of Figure 5-9. The process summary for the hot desulphurization process using free sorbent and supported sorbent are shown of Figure 5-10 and 5-11 respectively.

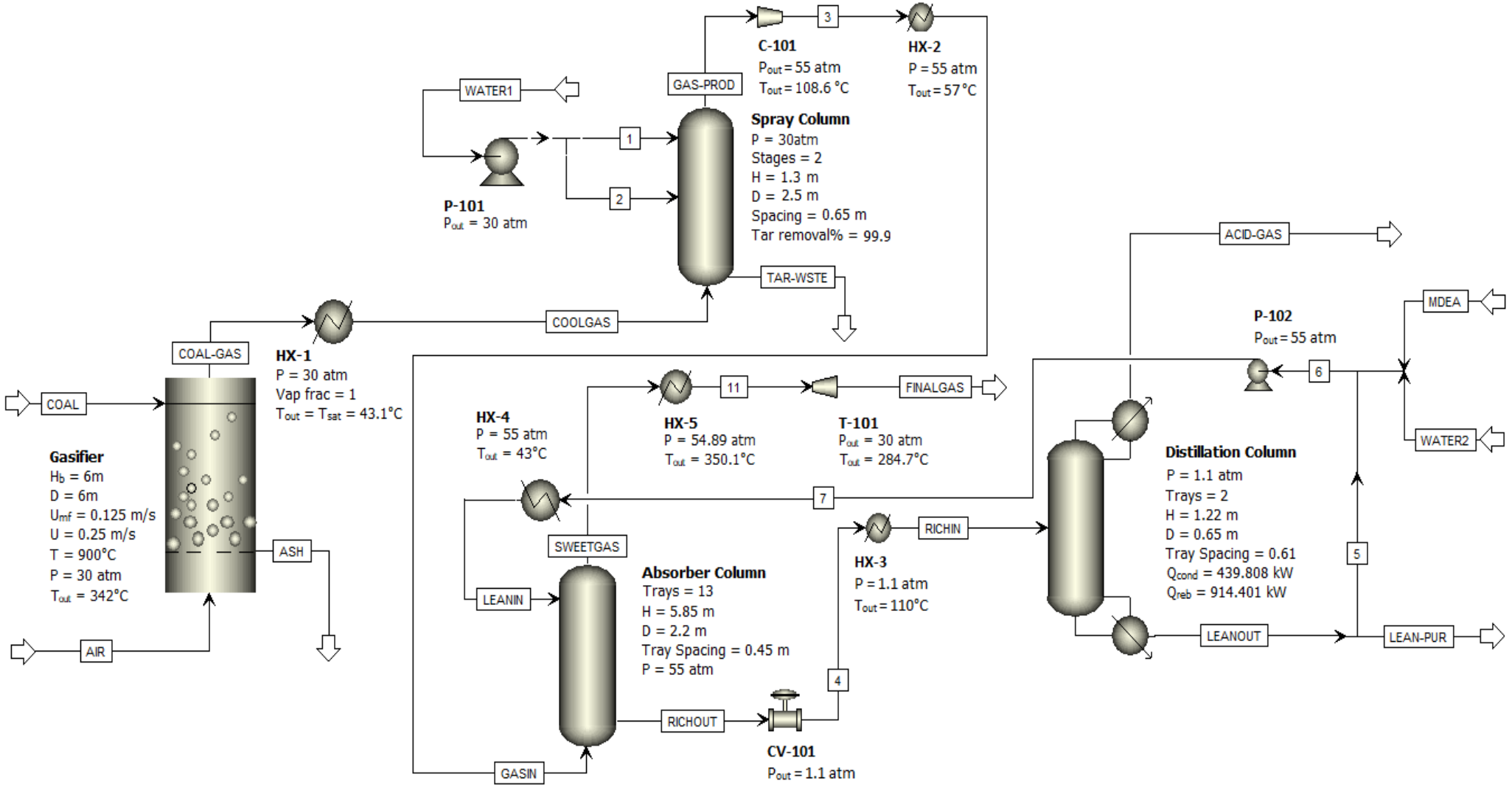

Figure 14-9: Process summary of the amine absorption process

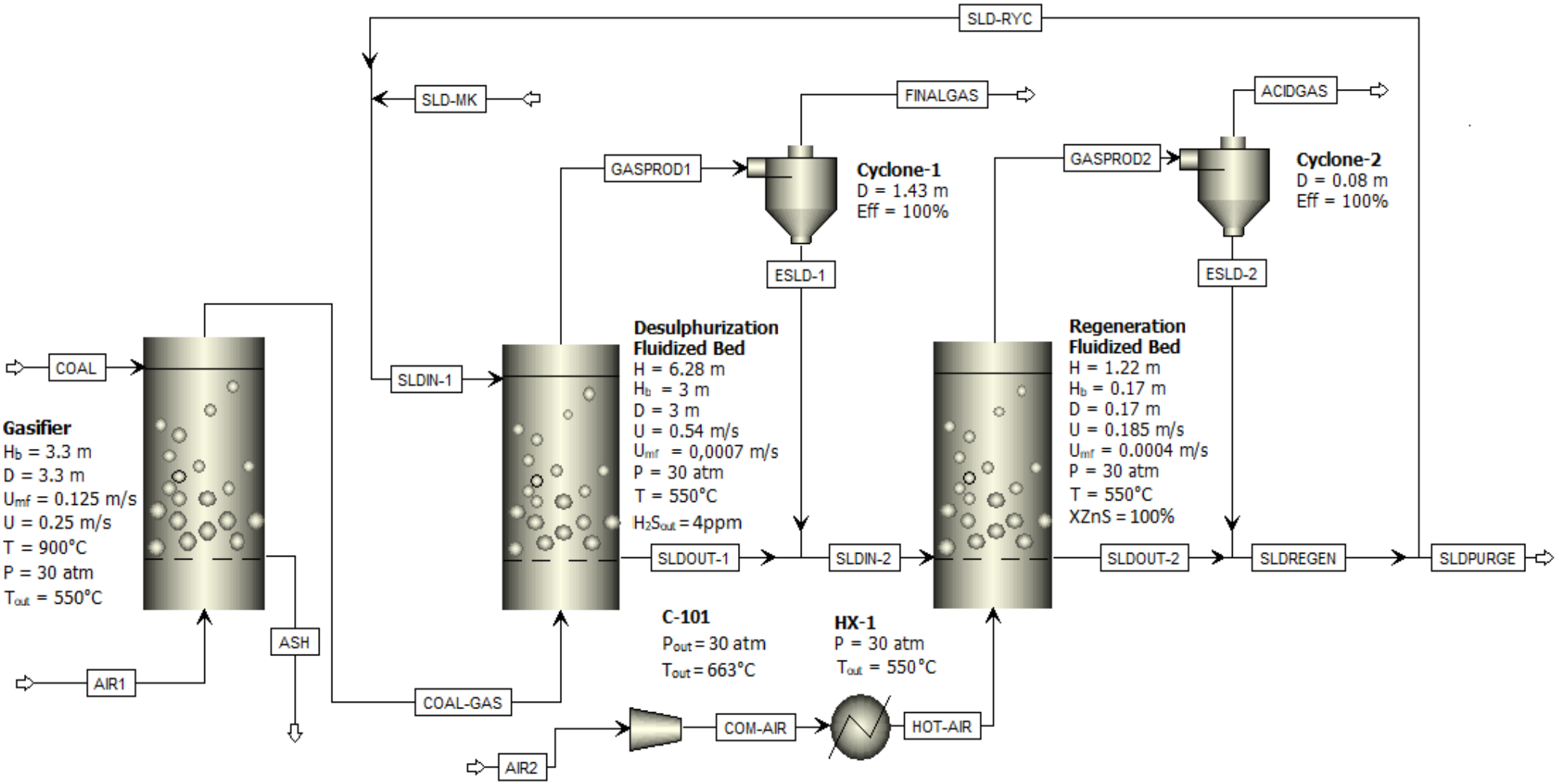

Figure 5-10: Process summary of the hot desulphurization process using free sorbent

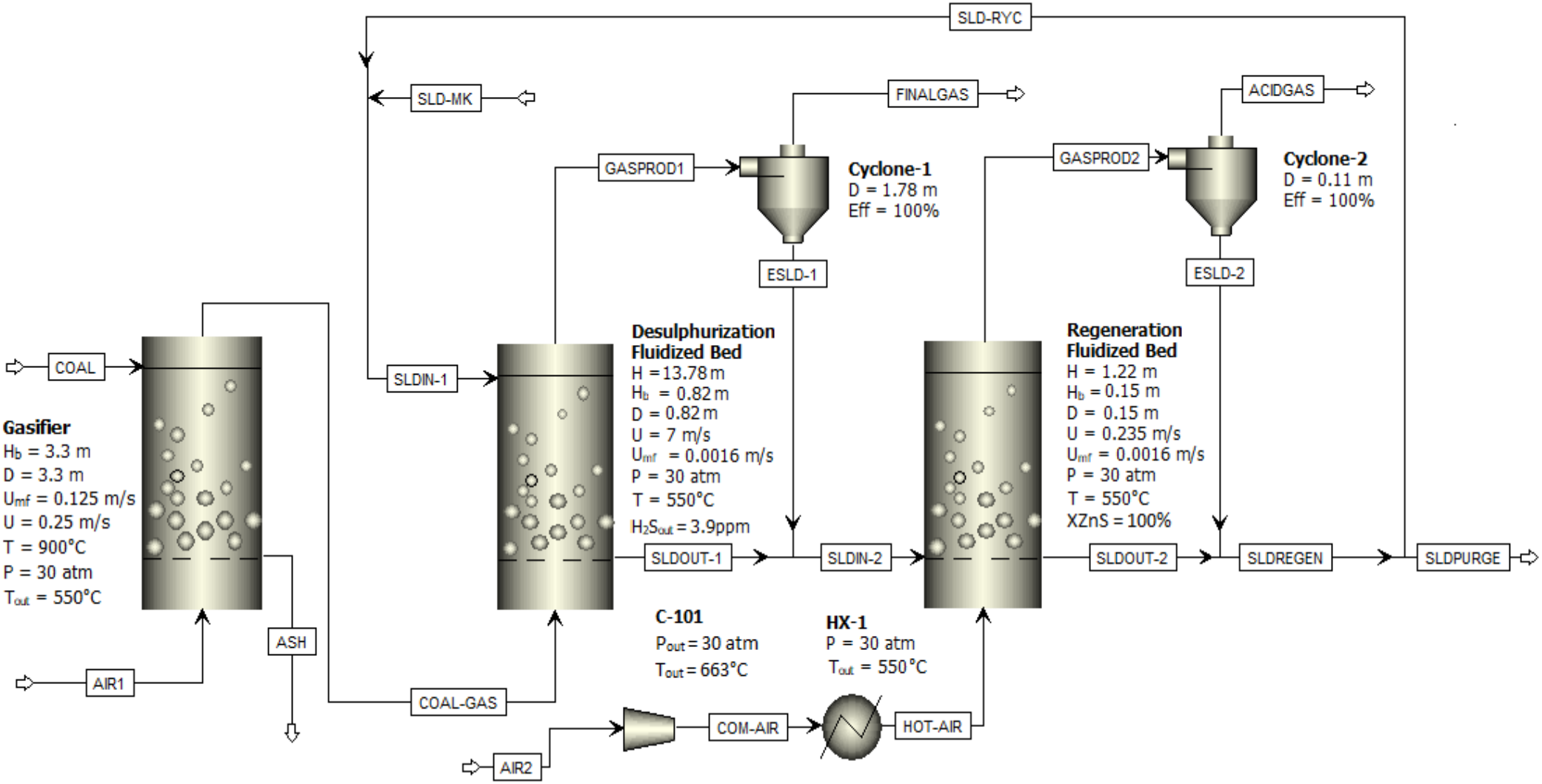

Figure 5-11: Process summary of the hot desulphurization process using supported sorbent

5.6) Total Annual Cost (TAC) Analysis

A costing summary for each process is shown on Table 5-2 with the detailed analyses for each process shown in Appendix D. From Table 5-2, it can be seen that the amine absorption process produced a greater capital cost than the hot desulphurization processes. This was as a result of the auxiliary units and larger number of process equipment required for the process. The operating cost was also greater for the amine absorption process as the use of utilities were required. This meant that the TAC for an amine absorption process exceeded the TAC for the hot desulphurization processes, therefore making the use of hot desulphurization processes economically more favourable than the amine absorption process.

Process	Capital Cost [R]	Operating Cost [R/yr]	Total Annual Cost [R/yr]
Amine absorption	105 657 900	63 943 698	99 162 998
Hot desulphurization (Free sorbent)	32 633 000	38 038 852	48 916 519
Hot desulphurization (Supported sorbent)	22 403 500	24 991 419	32 459 252

Table 5-2: Total Annual Cost Summary for each process

The capital cost for the supported sorbent process was less than the capital cost of the free sorbent process. This was due to the reduced size of FB1 produced by using the supported sorbent, resulting in a cheaper direct cost for FB1. The operating cost was also lower for the supported sorbent process. This was due to the metal precursor ($ZnCl_2$) and the silica support being collectively cheaper than the free sorbent and the lower sorbent purge rate used in the supported sorbent process, which resulted in less fresh sorbent being used. This meant that the TAC for the supported sorbent process was less than the free sorbent process, therefore making the use of supported sorbents economically more favourable.

CHAPTER 6: CONCLUSIONS AND RECOMMENDATIONS

6.1) Conclusions

Desulphurization is an integral step in any coal gas treatment process, as sulphur compounds are corrosive to process equipment and harmful to the environment. The removal sulphur compounds from synthesis gas is imperative for electricity generation processes, making gas treatment technologies very important. This was a comparative study on the performance and total annual cost (TAC) between an amine absorption process (wet-based), a hot desulphurization process with free metal-oxide (dry based process) and a hot desulphurization process with a supported metal-oxide (dry based process).

Operability and Process Costs

- Due to the low temperature operation of the amine absorption process, a large amount of pre-cooling of the coal gas was required after gasification, therefore an additional heat exchanger was required to achieve that cooling.
- Condensation of tar (represented by C_6H_6) present in the coal gas would also occur at these conditions, therefore a tar removal step using a water spray tower was required prior to desulphurization.
- The desulphurization process for the amine absorption process operated at pressures around 55 atm and temperatures below 60°C, and regeneration process for the amine absorption process operated at pressures around 1 atm and temperatures above 110°C, therefore multiple auxiliary units were added in order for processes streams to meet operating conditions.
- Utilities were a major requirement due to the number of heat exchangers present in the amine absorption process.
- The percentage of sorbent purged for the amine absorption process was 10%. The percentage of sorbent purged for the hot desulphurization process using a free sorbent, was 90%. This was due to free zinc oxide sorbent being very unstable and subject to sintering at these high operating temperatures. The percentage of sorbent purged for the hot desulphurization process using a supported sorbent, was 50%. This was due to supported sorbents having greater stability than free sorbents
- The waste products from the amine absorption process consisted of tar trapped in water that was removed from the spray tower, and the amine solution that was purged from the system. The flowrate of the tar waste stream was 148 630 kg/hr and the flowrate of purged amine solution was 454.87 kg/hr, therefore the total waste production of this system was 149 084.87 kg/hr (1 305 983.46 tons/yr). The waste product from the hot desulphurization processes was the fraction of the regenerated sorbent that was purged. The flowrate of the purged free sorbent stream was 146.5 kg/hr (1283.3 tons/year) and the flowrate of the purged supported sorbent was 407.5 kg/hr (3 569.7 tons/year) and

- The capital cost of the amine absorption process was calculated to be R 105 657 900 operating cost was 63 943 698 R/yr and the TAC was R99 162 998 R/yr. The capital cost of the hot desulphurization process using a free sorbent was calculated to be R32 633 000, operating cost was 38 038 852 R/yr and the TAC was R48 916 519 R/yr. The capital cost of the hot desulphurization process using a supported sorbent was calculated to be R22 403 500 operating cost was 24 991 419 R/yr and the TAC was 32 459 252 R/yr

Operation of the hot desulphurization processes occurred at 550°C and 30 atm. This was the conditions of the coal gas exiting the gasifier, therefore no pre-cooling was required for the hot desulphurization processes. Condensation of tar was avoided due to the high operating temperature of the hot desulphurization processes; therefore, the use of a tar removal unit was avoided. The operating conditions throughout the hot desulphurization processes were 550°C and 30 atm, therefore only two auxiliary units were required for this process i.e. a compressor to discharge air at 30 atm and a heat exchanger to cool the air stream to 550°C before entering FB2, with molten salts being the only utility required. This meant that the hot desulphurization processes were more thermally efficient than amine absorption. The purge rate of the amine absorption process was the lowest, due to the amine solution having a good stability due to low operating temperatures. This low purge rate meant that the amine solution regenerated was effectively utilized, making this process a more effective option than hot desulphurization. The waste produced from the amine absorption process is greater than that of the hot desulphurization processes, but the waste material from the amine absorption process is trapped in water, which is an advantage as water treatment technologies are well developed and disposal of a solid waste streams being limited to landfill sites. The supported sorbent process produced more waste than the free sorbent process, however, 81.5 kg/hr of the 407.5 kg/hr was the active ZnO therefore more of the ZnO was utilized with the supported sorbent. The capital cost of the amine absorption process was greater than that of the hot desulphurization process and this due to the larger amounts of process and auxiliary units required. The operating cost of the amine absorption process was greater than that of the hot desulphurization process and this was use to the greater requirements of utilities. The direct cost of FB1 using the supported sorbent was less than that of the free sorbent. The TAC for the amine absorption process was greater than that of the hot desulphurization processes and the supported sorbent produced a lower TAC than that of the free sorbent, therefore hot desulphurization processes are economically less intensive than amine absorption processes with lower waste production, and supported sorbents provide cheaper and more effective operation than free metal oxide sorbents.

6.2) Recommendations

The following recommendations should be considered to further improve the magnitude and the validity of this study:

- Rigorous design over auxiliary units should be conducted in order to estimate equipment sizes. Incorporating these sizes in APEA would provide more accurate direct costs of auxiliary units.
- Auxiliary units required for the utilities to meet operating conditions should be designed. This will provide a better estimate of the number of process equipment required by each process and subsequently a more accurate estimate of the capital costs.
- Incorporate attrition and agglomeration of particles in the fluidization behaviour of the hot desulphurization processes. This will better predict the realistic operation of a fluidized bed by considering the interaction between particles.
- Reactions in the freeboard should be considered. This will provide a better prediction of the reaction capabilities of the fluidized beds.

A model that incorporates the effects of product layer diffusion should be developed and applied to regress for the intrinsic kinetics of the supported sorbent. This will result in better predictions of the intrinsic rate for the supported sorbent.

6.3) Significance of the study

This study proved that dry desulphurization technologies are a viable and economically less intensive alternative to wet desulphurization technologies and showed that product layer diffusion may have a significant effect on the reaction rate of supported sorbents.

References

Atimtay, A. & Harrison, D., 1998. *Desulfurization of Hot Coal Gas.* Berlin: Springer-Verlag.

Bailie, J., Hutchings, G. & O'Leary, S., 2001. *Supported Catalysts.* s.l.:Elsevier.

Basu, P., 2006. *Combustion and Gasification in Fluidized Beds.* 1st ed. Halifax: CRC Press.

Bergman, P., Paasen, S. & Boerrigter, H., 2002. *The novel "OLGA" technology for complete tar removal from biomass producer gas.* Strasbourg: ECN.

Chan, I. & Knowlton, T., 1984. The effect of pressure on entrainment from bubbling gas fluidized beds. *Fluidization. New York: Engineering Foundation,* pp. 283-290.

Cheremisinoff, N., 2002. *Handbook of Water and Wastewater Treatment Technologies.* Woburn: Butterworth-Heinemann .

Dasgupta, K., Rai, K. & Verma, N., 2003. Breakthrough and Sulfate Conversion Analysis during Removal of Sulfur Dioxide by Calcium Oxide Sorbents. *The Canadian Journal of Chemical Engineering,* Volume 81, pp. 53-62.

Davidson, J. F. & Harrison, D., 1963. *Fluidized Particles.* Cambridge: Cambridge University Press.

Dechsiri, C., 2004. *Particle transport in fluidized beds: experiments and stochastic models,* Groningen: s.n.

Dirgo, J. & Leith, D., 2007. Cyclone Collection Efficiency: Comparison of Experimental Results with Theoretical Predictions. *Aerosol Science and Technology,* 4(4), pp. 401-415.

Fermoso, J. et al., 2009. High-pressure gasification reactivity of biomass chars produced at different temperatures. *Journal of Analytical and Applied Pyrolysis,* Volume 85, pp. 287-293.

Fournol, A., Bergougnou, M. & Baker, C., 1973. Solids entrainment in a large gas fluidized beds. *Canadian Journal of Chemical Engineering,* Volume 51, pp. 401-404.

Fung, A. & Hamdullahpur, F., 1993. Effect of bubble coalescence on entrainment in gas fluidized beds. *Powder Technology,* Volume 34, pp. 251-265.

Geldart, D., 1985. The Design of Distributors for Gas-Fluidized-Beds. *Powder Technology,* Volume 42, pp. 67-78.

George, S. & Grace, J., 1978. Entrainment of particles from aggregative fluidized beds. *AIChEJ,* Volume 74, pp. 67-74.

Gibson, J. & Harrison, D., 1980. The Reaction between Hydrogen Sulfide and Spherical Pellets of Zinc Oxide. *Ind. Eng. Chem. Process Des. Dev,* Volume 19, pp. 231-236.

Govender, N., 2017. *HIGHLY DISPERSED ZINC-BASED SORBENTS FOR DESULPHURISATION: SYNTHESIS AND APPLICATION,* Durban: University of Kwa-Zulu Natal.

Hayes, R. & Kolaczkowski, 1998. *Introduction to Catalytic Combustion.* Alberta: CRC Press.

Higman, C. & van der Burgt, M., 2011. *Gasification.* 2nd ed. Johannesburg: Elsevier.

Levenspiel, O., 1999. *Chemical Reaction Engineering.* New York: John Wiley & Sons.

Luyben, W., 2010. Design and Control of a Methanol Reactor/Column Process. *Ind. Eng. Chem. Res,* Volume 49, pp. 6150-6163.

Lv, P., Xiong, Z. & Chang, J., 2004. An experimental study on biomass air-steam gasification in a fluidized bed. *Bioresource Technology,* Volume 95, pp. 95-101.

Mokatab, S., Poe, W. & Mak, J., 2019. *Handbook of Natural Gas Transmission and Processing.* 4th ed. Cambridge: Elsevier.

Nicolaou, P., 2016. *Removal, Utilization and Separation of Tars from Syngas,* Delft: Delft University of Technology.

Prabhu, G., ULrichson, D. & Pulsifer, A., 1984. Kinetics of the Oxidation of Zinc Sulfide. *Ind. Eng. Chem. Fundam,* Volume 23, pp. 271-273.

Reddy, R., 2011. Editorial: Molten Salts. *Journal of Phase Equilibria and Diffusion,* 32(4), pp. 269-270.

Seader, J., Henly, E. & Roper, D., 2011. *SEPARATION PROCESS PRINCIPLES: Chemical and Biochemical Operations.* New York: John Wiley & Sons, Inc.

Stairmand, C., 1951. High-efficiency cyclone design. *Trans. Inst. Chem. Eng,* Volume 29, p. 365.

Svarovsky, L., 1981. *Solid-Gas Seperation.* Bradford: Elsevier.

Toomey, R. D. & Johnstone, H. F., 1952. Gaseous fluidization of solid particles. *Chem.Eng.Progr.,* Volume 48, p. 200.

Vamvuka, D., 1999. Coal Gasification. *SAGE Journals,* pp. 515-576.

Wen, C. & Onozaki, M., 1982. *User's manual for computer simulation and design of the moving bed coal gasifier,* s.l.: Department of Chemical Engineering West Virginia.

Wen, C. Y. & Yu, Y. H., 1966. A Generalized Methodology for Estimating Minimum Fluidization Velocity. *AIChE ,* Volume 12, p. 610.

Xu, S., Zhang, D. & Ren, Y., 2006. *Large-scale coal gasification technology,* Beijing: Beijing: Chemical Industry Press.

Yagi, S. & Kunii, D., 1961. Chemical Reactor Omnibook. *Chemical Engineering Science,* Volume 16, pp. 364-380.

Yang, W.-C., 2003. *Handbook of Fluidization and Fluid-Particle Systems.* 1st ed. Pittsburgh: CRC Press.

APPENDIX A: PROCESS FLOW DIAGRAMS

A.1) Gasification:

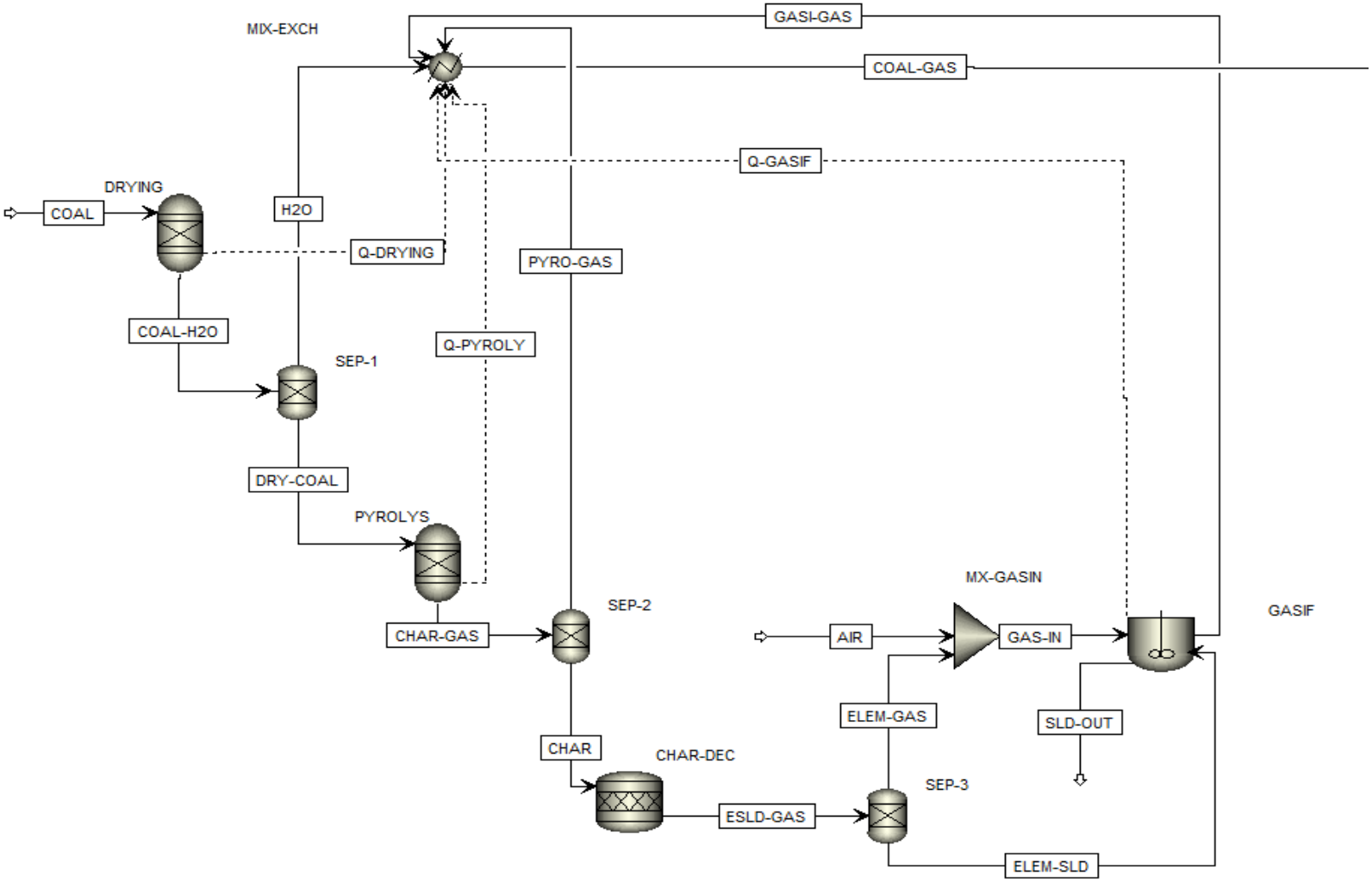

A.2) Amine absorption process

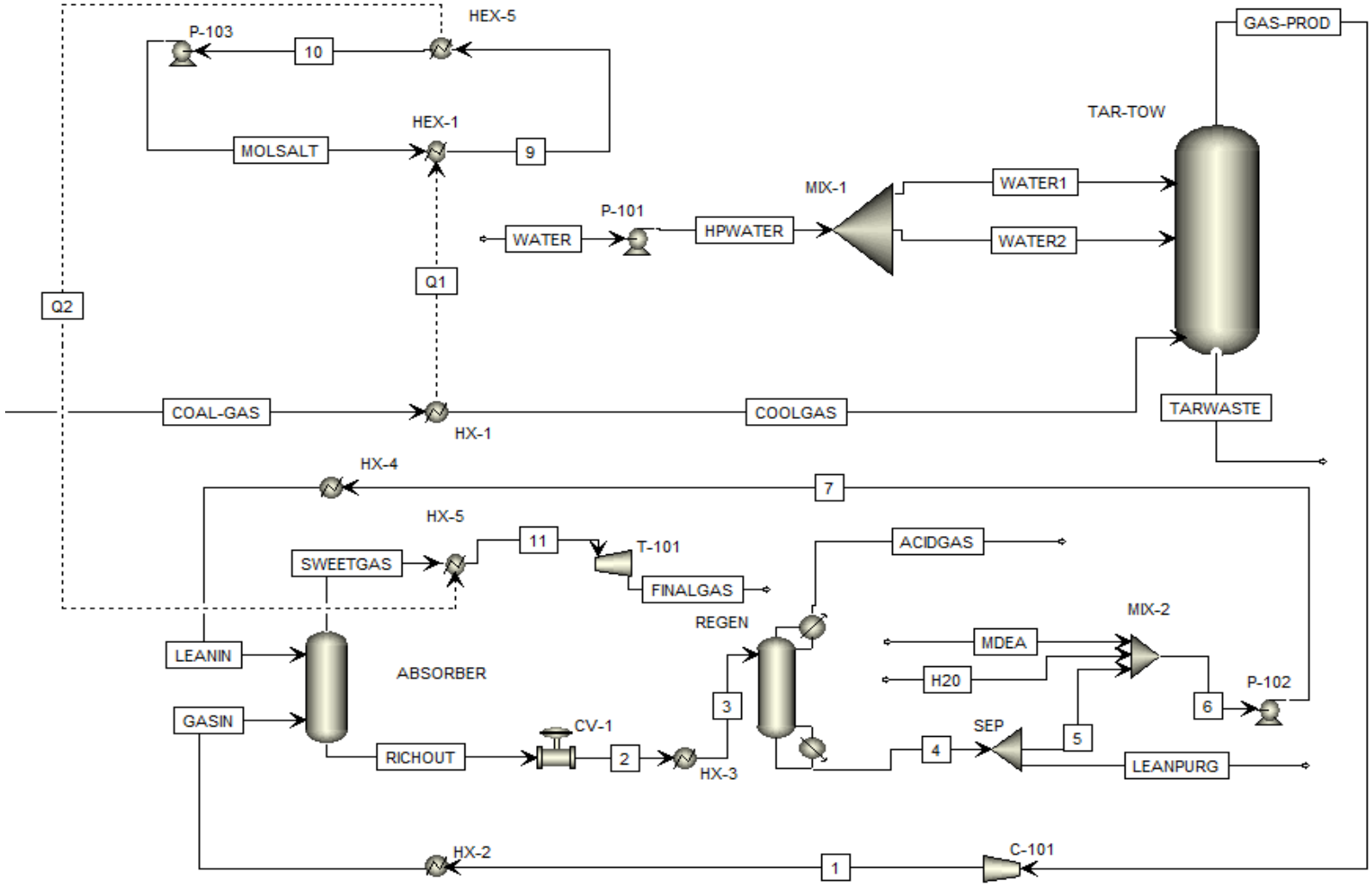

A.3) Hot Desulphurization Process:

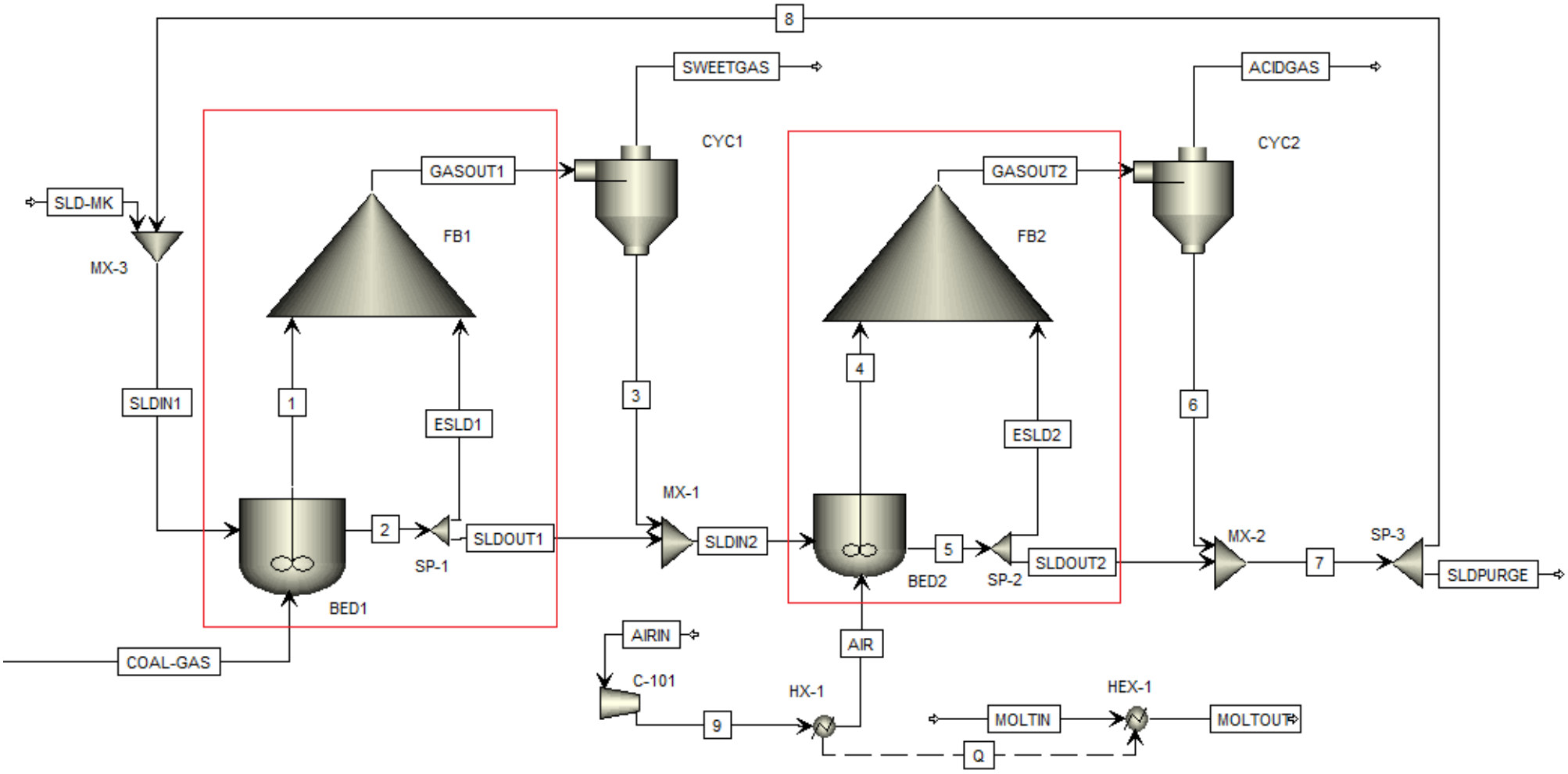

APPENDIX B: DATA EXTRACTION AND BREAKTHROUGH CURVES

350°C			
t (min)	C_b/C_{bo}	t (min)	C_b/C_{bo}
0,52	0	9,86	0,28
1,02	0	9,97	0,31
1,51	0	10,04	0,33
2	0	10,13	0,35
2,49	0	10,13	0,37
2,98	0	10,18	0,4
3,47	0	10,29	0,43
3,96	0	10,42	0,46
4,46	0	10,56	0,49
4,95	0	10,69	0,51
5,44	0	10,77	0,53
5,93	0	10,83	0,55
6,42	0	10,88	0,58
6,91	0	10,95	0,61
7,4	0	11,01	0,63
7,86	0,01	11,02	0,65
8,32	0,03	11,04	0,67
8,55	0,05	11,04	0,69
8,69	0,09	11,05	0,77
8,8	0,11	11,09	0,71
8,91	0,14	11,09	0,74
9,13	0,17	11,11	0,8
9,41	0,18	11,16	0,84
9,72	0,21	11,18	0,85
9,74	0,22	11,25	0,87
9,79	0,24	11,25	1

Table 4-1: Breakthrough data extracted at 350°C (Govender, 2017)

550°C							
t (min)	C_b/C_{bo}	t (min)	C_b/C_{bo}	t (min)	C_b/C_{bo}	t (min)	C_b/C_{bo}
0,43	0	15,23	0,07	29,49	0,26	40,93	0,82
0,98	0	15,72	0,08	29,98	0,28	41,36	0,84
1,55	0	16,21	0,09	30,47	0,29	41,85	0,86
2,13	0,01	16,7	0,1	30,97	0,31	42,35	0,88
2,63	0,01	17,19	0,11	31,46	0,32	42,84	0,89
3,12	0,01	17,69	0,12	31,95	0,34	43,33	0,91
3,61	0,01	18,18	0,13	32,44	0,36	43,82	0,92
4,09	0,01	18,67	0,14	32,94	0,38	44,31	0,93
4,76	0,01	19,16	0,15	33,41	0,4	44,81	0,93
5,27	0,01	19,65	0,16	33,88	0,42	45,3	0,94
5,8	0,02	20,15	0,17	34,32	0,44	45,79	0,94
6,29	0,02	20,64	0,18	34,75	0,46	46,28	0,95
6,78	0,02	21,13	0,19	35,22	0,48	46,77	0,95
7,27	0,02	21,62	0,19	35,64	0,5	47,26	0,96
7,76	0,02	22,11	0,2	36	0,52	47,76	0,96
8,25	0,02	22,61	0,2	36,34	0,54	48,25	0,97
8,74	0,02	23,1	0,21	36,65	0,56	48,72	0,97
9,33	0,03	23,59	0,21	36,97	0,58		
9,84	0,03	24,08	0,21	37,33	0,6		
10,31	0,03	24,57	0,21	37,68	0,62		
10,8	0,03	25,06	0,21	38	0,64		
11,29	0,03	25,55	0,21	38,31	0,66		
11,78	0,03	26,05	0,21	38,65	0,68		
12,28	0,04	26,54	0,21	38,96	0,7		
12,77	0,04	27,03	0,21	39,25	0,72		
13,26	0,05	27,52	0,22	39,57	0,74		
13,75	0,05	28,01	0,23	39,88	0,76		
14,24	0,06	28,5	0,24	40,22	0,79		
14,73	0,06	29	0,25	40,58	0,8		

Table B-2: Breakthrough data extracted at 550°C (Govender, 2017)

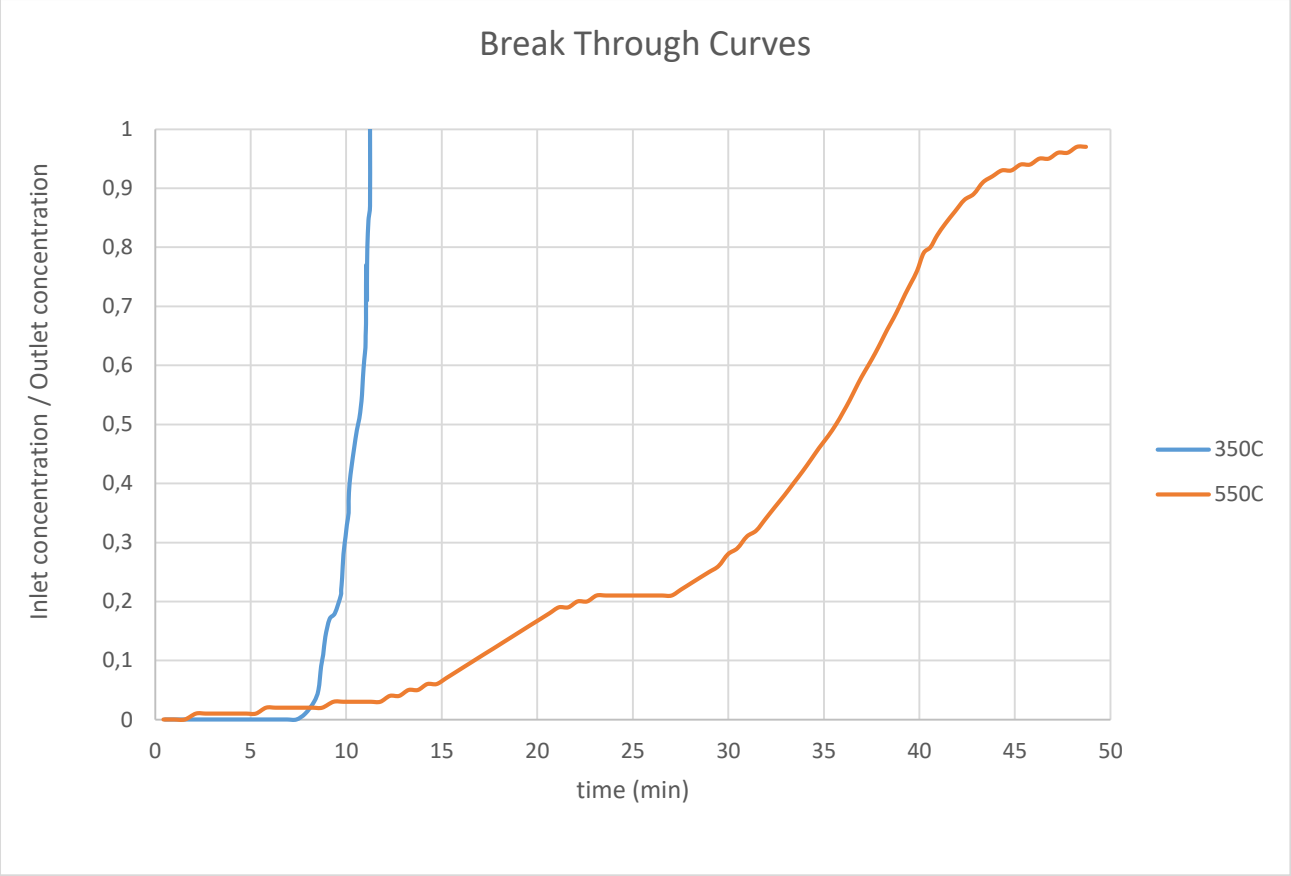

Figure B-1: Plot of the Breakthrough Curves extracted from (Govender, 2017)

APPENDIX C: MATLAB SCRIPTS

C.1) coupled_transfer22.m

```
function dydt = coupled_transfer22(t,y)

% load parameters
global Dz a Ep U EB Rp De Km nx delta_x K
t
T = y(1:nx);
c = y(nx+1:2*nx);

dTdx2=zeros(1,nx);
dCdx2=zeros(1,nx);

% dTdx2(1) = 0;
%
% dCdx2(1) = (3*Km/Rp)*(T(1)-(Km*T(1) + 5*De*c(1)/Rp)/(Km + 5*De/Rp))...
%     - 3*(1-Ep)*K*c(1)/(Rp*Ep);

for j=1:nx
    if (j==1)
        dTdx2(j) = 0;

        dCdx2(j)    =    (3*Km/Rp)*(T(j)-(Km*T(j)    +    5*De*c(j)/Rp)/(Km    +
5*De/Rp))...
    - 3*(1-Ep)*K*c(j)/(Rp*Ep);

    elseif (j==nx)
        dTdx2(j) = Dz*(2*T(j-1) - 2*T(j))/(delta_x^2) - ...
            ((1-EB)*Km*a/EB)*(T(j) - (Km*T(j) + 5*De*c(j)/Rp)/...
            (Km + 5*De/Rp));

        dCdx2(j) = (3*Km/Rp)*(T(j)-(Km*T(j) + 5*De*c(j)/Rp)/...
            (Km + 5*De/Rp))- 3*(1-Ep)*K*c(j)/(Rp*Ep);

    else
%         dTdx2(j) = Dz*(T(j+1)+T(j-1) - 2*T(j))/(delta_x^2) - ...
%             (U/EB)*(T(j+1)-T(j-1))/(2*delta_x) - ...
%             ((1-EB)*Km*a/EB)*(T(j) - (Km*T(j) + 5*De*c(j)/Rp)/...
%             (Km + 5*De/Rp));

        dTdx2(j) = Dz*(T(j+1)+T(j-1) - 2*T(j))/(delta_x^2) - ...
            (U/EB)*(T(j+1)-T(j-1))/(2*delta_x) - ...
            ((1-EB)*Km*a/EB)*(T(j) - (Km*T(j) + 5*De*c(j)/Rp)/...
            (Km + 5*De/Rp));


        dCdx2(j) = (3*Km/Rp)*(T(j) - (Km*T(j) + 5*De*c(j)/Rp)/...
            (Km + 5*De/Rp))- 3*(1-Ep)*K*c(j)/(Rp*Ep);
    end
end

dCdt=dCdx2';

dTdt=dTdx2';

dydt=[dTdt; dCdt];
```

C.2) caller.m (at 350°C)

```
global Dz a Ep U EB Rp De Km nx delta_x K

% Adjustable parameters:
Dz = 1e-5;                    % m/s
K = 2e-11;                    % m/s


% Constants:
a = 123425200.8;                % m^2/m^3
Ep = .717;                  % [-]; intra-particle porosity
U = 0.05;                    % m/s
EB = .373;                   % [-]; bed porosity
Rp = 50e-6;                  % particle radius; metres
Temperature = 350+273.15;    % Kelvin
R = 8.314;                   % J/(mol. K)
ReactorLength=2.3/100;       % metres
Nspace=201;
tmax=60*60;                      % s

Km = 7.8e-3;                  % m/s
De = 1.2e-9;                   % m^2/s

c0 = zeros(Nspace,1);
T0 = zeros(Nspace,1);
T0(1) = 0.195;                % mol/m^3

y0 = [T0; c0];

t=[0 tmax];

nx=length(c0);

delta_x = ReactorLength/(nx-1);

pos = 0:delta_x:ReactorLength;

options = odeset('RelTol',1e-5,'AbsTol',1e-5);

[t, y]=ode15s(@coupled_transfer22,t,y0,options);

vv=size(y);
vvv=vv(1);

figure(1)
subplot(1,3,1)
plot(pos,y(floor(vvv/5),1:nx),'k-','LineWidth',2)
hold on
plot(pos,y(floor(vvv/3),1:nx),'b-','LineWidth',2)
hold on
plot(pos,y(floor(3*vvv/4),1:nx),'m-','LineWidth',2)
hold on
plot(pos,y(floor(80*vvv/100),1:nx),'-','color',[0 .5 0],'LineWidth',2)
hold on
plot(pos,y(vvv,1:nx),'r-','LineWidth',2)
xlabel('$z\:\mathrm{(m)}$','interpreter','latex','FontSize',16)
set(gca,'TickLabelInterpreter','latex','FontSize',16)
xlim([0 ReactorLength])
ylabel('$C_b\:\mathrm{(mol/m^3)}$','interpreter','latex','FontSize',16)
```

```
set(gca,'TickLabelInterpreter','latex','FontSize',16)
lgd=legend(strcat('$t$ = ',num2str(t(floor(vvv/5))),' s'), ...
    strcat('$t$ = ',num2str(t(floor(vvv/3))),' s'),...
    strcat('$t$ = ',num2str(t(floor(3*vvv/4))),' s'),...
    strcat('$t$ = ',num2str(t(floor(80*vvv/100))),' s'),...
    strcat('$t$ = ',num2str(t(floor(vvv))),' s'),'Location','southeast');
set(lgd,'Interpreter','latex')

% figure(2)
subplot(1,3,2)
plot(pos,y(floor(vvv/5),nx+1:2*nx),'k-','LineWidth',2)
hold on
plot(pos,y(floor(vvv/3),nx+1:2*nx),'b-','LineWidth',2)
hold on
plot(pos,y(floor(3*vvv/4),nx+1:2*nx),'m-','LineWidth',2)
hold on
plot(pos,y(floor(80*vvv/100),nx+1:2*nx),'-','color',[0 .5 0],'LineWidth',2)
hold on
plot(pos,y(vvv,nx+1:2*nx),'r-','LineWidth',2)
xlabel('$z\:\mathrm{(m)}$','interpreter','latex','FontSize',16)
set(gca,'TickLabelInterpreter','latex','FontSize',16)
xlim([0 ReactorLength])
ylabel('$\overline{C}_p\:\mathrm{(mol/m^3)}$','interpreter','latex','FontSi
ze',16)
set(gca,'TickLabelInterpreter','latex','FontSize',16)
lgd=legend(strcat('$t$ = ',num2str(t(floor(vvv/5))),' s'), ...
    strcat('$t$ = ',num2str(t(floor(vvv/3))),' s'),...
    strcat('$t$ = ',num2str(t(floor(3*vvv/4))),' s'),...
    strcat('$t$ = ',num2str(t(floor(80*vvv/100))),' s'),...
    strcat('$t$ = ',num2str(t(floor(vvv))),' s'),'Location','southeast');
set(lgd,'Interpreter','latex')

% figure(3)
subplot(1,3,3)
plot(t/60,y(:,nx)./T0(1),'-','color',[0.23 0.23 0.23],'LineWidth',2)
xlim([0 tmax/60])
hold on
% plot experimental breakthrough curve
timeExp=[0.52 1.02 1.51 2 2.49 2.98 3.47 3.96 4.46 4.95 5.44 5.93 6.42 6.91
7.4 7.86 8.32 8.55 8.69 8.8 8.91 9.13 9.41 9.72 9.74 9.79 9.86 9.97 10.04
10.13 10.13 10.18 10.29 10.42 10.56 10.69 10.77 10.83 10.88 10.95 11.01 11.02
11.04 11.04 11.05 11.09 11.09 11.11 11.16 11.18 11.25 11.25];

CdivC0exp = [0 0 0 0 0 0 0 0 0 0 0 0 0 0 0 0.01 0.03 0.05 0.09 0.11 0.14
0.17 0.18 0.21 0.22 0.24 0.28 0.31 0.33 0.35 0.37 0.4 0.43 0.46 0.49 0.51
0.53 0.55 0.58 0.61 0.63 0.65 0.67 0.69 0.77 0.71 0.74 0.8 0.84 0.85 0.87
0.9];

plot(timeExp,CdivC0exp,'o','color',[0 0 1],'LineWidth',2)
xlabel('$t\:\mathrm{(minutes)}$','interpreter','latex','FontSize',16)
set(gca,'TickLabelInterpreter','latex','FontSize',16)
% set(gca,'XScale','log')
ylabel('$C_{b_L}/C_{b_0}\:\mathrm{(dimensionless)}$','interpreter','latex',
'FontSize',16)
ylim([0 1])
yticks([0 0.2 0.4 0.6 0.8 1])
lgd=legend(strcat('Porous model'), ...
    strcat('Experiment'),'Location','northwest');
set(lgd,'Interpreter','latex')
set(gca,'TickLabelInterpreter','latex','FontSize',16)
toc
```

APPENDIX D: TAC DATA

D.1) Amine Absorption Process

Capital Cost

Major Units	Direct Cost [R]	Auxiliary Units	Direct Cost [R]
REGEN-cond	1 088 500,00	C-101	22 307 800,00
REGEN-cond acc	1 528 700,00	HX-1	7 976 600,00
REGEN-reb	1 687 500,00	HX-2	7 944 800,00
REGEN-reflux pump	389 200,00	HX-3	1 955 000,00
REGEN-tower	2 559 100,00	HX-4	2 268 800,00
ABSORBER-tower	11 837 400,00	HX-5	11 636 800,00
TAR-TOW-tower	6 750 000,00	T-101	21 072 300,00
		P-101	2 613 400,00
		P-102	2 042 000,00
Capital Cost TOTAL		**R 105 657 900,00**	

Operating Cost

Raw material Cost

Material	Unit	kg/hr	$/kg	R/kg	R/yr
Water	TAR-TOW	148 135,20		0,0333	43 241 819,98
	ABSORBER	6 887,34		0,0333	2 010 467,01
MDEA	ABSORBER	379,27	0,001	0,01481	49 239,13
				TOTAL	45 301 526,12

Utility Cost

Utilities	Units	kg/hr	$/kg	R/kg	R/yr
LP Steam	HX-3	7 259,30	0,00416	0,0616096	3 920 528,36
	REGEN-reb	1 501,84	0,00416	0,0616096	811 098,36
Water	HX-2	34 461,60		0,0333	10 059 609,84
	HX-4	7 364,30		0,0333	2 149 696,61
	REGEN-cond	5 828,00		0,0333	1 701 238,66
				TOTAL	18 642 171,83

Operating Cost TOTAL [R]/year	63 943 697,95
Payback Period (years)	**Currency Conversion R/$**
3	14,81

Total Annual Cost (TAC)
99 162 997,95 R/yr

D.2) Hot Desulphurization (Free metal-oxide)

Capital Cost					
Major Units				Direct Cost [R]	
FB1				14 921 200,00	
CYC1				1 149 800,00	
FB2				1 073 700,00	
CYC2				129 100,00	
C-101				14 558 100,00	
HX-1				801 100,00	
Capital Cost TOTAL [R]				R 32 633 000,00	
Operating Cost					
Raw material Cost					
Material	kg/hr	$/kg		R/kg	R/yr
ZnO	146,50	2		29,62	38 038 852,39
Operating Cost TOTAL [R]/year				38 038 852,39	
Payback Period (years)				Currency Conversion R/$	
3				14,81	
Total Annual Cost (TAC) 48 916 519,06 R/yr					

D.3) Hot Desulphurization (Supported metal-oxide)

Capital Cost					
Major Units				Direct Cost [R]	
FB1				4 688 900,00	
CYC1				1 162 800,00	
FB2				1 058 300,00	
CYC2				134 300,00	
C-101				14 558 100,00	
HX-1				801 100,00	
Capital Cost TOTAL [R]				22 403 500,00	
Operating Cost					
Raw material Cost					
Material	kg/hr	$/kg		R/kg	R/yr
ZnO	81,5				
$ZnCl_2$	136,4742	1,1		16,291	19 489 458,01
SiO_2	326,00	0,13		1,9253	5 501 960,61
Operating Cost TOTAL [R]/year				24 991 418,62	
Payback Period (years)				Currency Conversion R/$	
3				14,81	
Total Annual Cost (TAC) 32 459 251,96 R/yr					